Resistivity Modelling of Fracture Zones and Horizontal Layers in Bedrock

Reiser, Fabienne; Dalsegg, Einar; Dahlin, Torleif; Ganerød, Guri V.; Rønning, Jan S.

2009

NGU Report 2009.070

Resistivity Modelling of Fracture Zones and Horizontal Layers in Bedrock.

Geological Survey of Norway
NO-7491 Trondheim, Norway
Tel.: 47 73 90 40 00
Telefax 47 73 92 16 20

REPORT

Report no.: 2009.070 | ISSN 0800-3416 | Grading: Open

Title:
Resistivity Modelling of Fracture Zones and Horizontal Layers in Bedrock

Authors:
Fabienne Reiser, Einar Dalsegg, Torleif Dahlin, Guri V. Ganerød and Jan S. Rønning

Client:
Statens vegvesen, Vegdirektoratet / NGU

County:

Commune:

Map-sheet name (M=1:250.000)

Map-sheet no. and -name (M=1:50.000)

Deposit name and grid-reference:

Number of pages: 120 Price (NOK): 520,-
Map enclosures:

Fieldwork carried out:

Date of report: 20.12.2009

Project no.: 329500

Person responsible:

Summary:

2D resistivity modelling was done in order to examine the imaging resolution of 4 different configurations for mapping of fracture zones in bedrock. The studied arrays include Dipole-dipole, Gradient, Pole-dipole and Wenner. A variety of geological models were tested and the imaging possibilities and limitations of the different arrays were analysed. Apart from imaging fracture zones with various depth, width, contrast and dip, some models for horizontal layers were also examined. The forward modelling was done with the program RES2DMOD whereas the inversion was carried out with RES2DINV. The protocol files simulate the measuring procedure with an ABEM Lund system which is based on a layout of 4 cables with total 81 electrode positions.

Generally it can be noted that the best results were achieved with Gradient and Dipole-dipole, especially for mapping fracture zones with various depth and width. The Gradient configuration gives the best response for mapping steeply dipping structures and different contrasts, whereas Wenner is good at illustrating horizontal layers. Dipole-dipole and Pole-dipole show the most accurate results for situations where a low resistivity top layer is present.

All in all it can be said that the vertical/horizontal filter value 2 clearly improves the image of vertical structures whereas a filter value of 0.5 increases the image quality of horizontal layers.

Keywords: Geophysics (Geofysikk)	Fracture zones (Sprekkesoner)	Bedrock (Berggrunn)
Resistivity (Resistivitet)	Syntethic models (Syntetiske modeller)	Modelling (Modellering)
		Scientific report (Fagrapport)

CONTENTS

FIGURES

1. INTRODUCTION

2D resistivity imaging is widely used in engineering and environmental applications, and the Geological Survey of Norway (NGU) has used the method since 2000 for characterization of fracture zones in bedrock (Rønning 2003, Rønning et al. 2003, Rønning et al. 2009, Ganerød et al. 2006). For mapping the subsurface, different electrode configurations can be used whereas each one of them has its own advantages and drawbacks. In this work, Dipole-dipole, Gradient, Pole-dipole and Wenner were examined. The different configurations can be seen in figure 2.1. A current is applied and the potential difference between two electrodes can be measured. The altered electrode positions give rise to different current flow and hence lead to different responses. To get information about deeper regions, the distance between the electrodes is increased to force the current to flow deeper.

It is of highly important to choose the right array for a survey, since they can all have fairly different responses depending on the feature present in the subsurface. To save labour costs in the field, it is a good alternative to create synthetic data, do the inversion and analyses the results. In this way, it is possible to become more confident in choosing the optimal array in different geological situations, and to learn more about the possibilities and the limitations connected to the 2D resistivity method.

The forward modeling was done using the program RES2DMOD version 3.01.52 (Loke 2002) for creating synthetic data. To simulate measured data, 5 % random noise was added and these data were subsequently inverted using RES2DINV version 3.57.37 (Loke 2008). The electrode spacing was chosen to be 10 m and the length of the 2D line was 800 m. For the inversion the standard least-squares constraint was used which minimises the square of the difference between the measured and calculated apparent resistivity. We have also tried "Robuste Inversion" (L1-type inversion). This inversion code tends to give sharp interface between different regions, and the resistivity within each region is almost constant (Loke 2008). We do not think that this is the situation in nature. On the contrary, fracture zones consists often of a core zone with breccias, a distal part with 3 - 8 fractures per meter and a transmission zone with even less fractures (Braathen & Gabrielsen 2000). Since the two inversion techniques gave small deviations in details and the main responses from the different structures were common, we decided in this project to do only standard least square inversion. The effect of choosing different values for the vertical/horizontal filter was also examined.

The NGU has earlier performed 2D resistivity modeling for the Wenner and Dipole-dipole configuration (Rønning et al. 2009). In this modeling, the standard electrode configuration which is a part of the program RES2DMOD (Loke 2002), was used. However, these do not agree with the electrode configuration used in the field. To avoid overestimation of the possibilities with the method, it was necessary to do the modeling with the same electrode configurations as used in the field measurements. New protocol files for Dipole-dipole, Gradient, Pole-dipole and Wenner were created. In the central part of our models, the modeled electrode configuration simulate exactly the measuring procedure used with an ABEM Lund System (Dahlin 1993), which is based on a layout of 4 cables with total 81 electrode positions. To cover an extended 2D line the first cable can be moved to the end and lateral profiling can be achieved. The measuring procedure can be seen in figure 2.2.

The aim of the project is to find possibilities and limitations of the resistivity method and learn which electrode configuration is most suitable for different models.

2. ELECTRODE CONFIGURATIONS

Every single electrode configuration has its own advantages and disadvantages (Reynold 1997). The different way of measuring leads to dissimilar responses depending also on the feature present in the subsurface. The electrode configurations discussed in this project can be seen in figure 2.1.

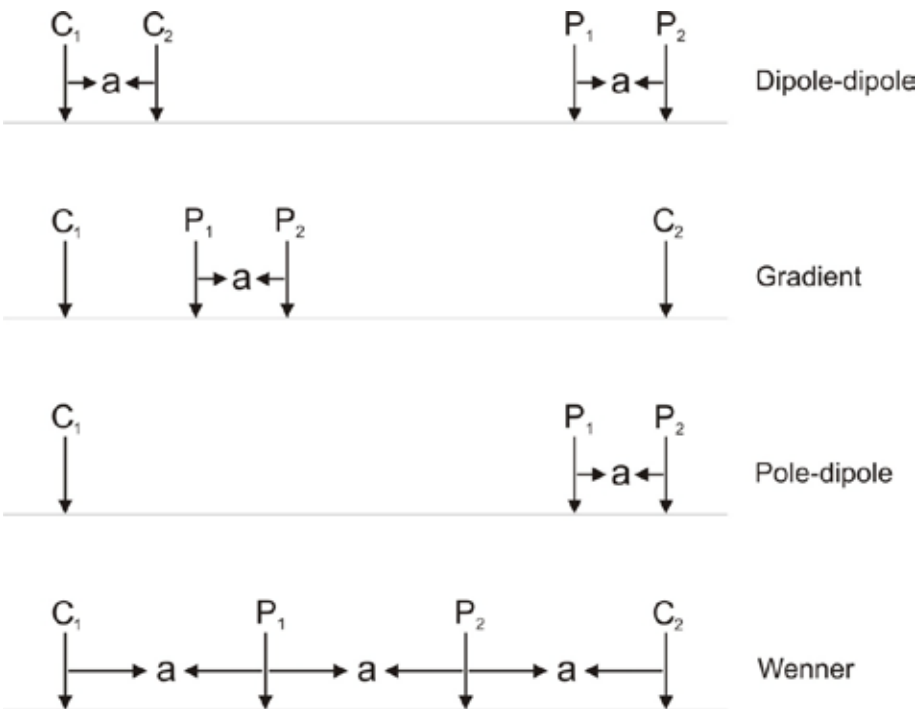

Figure 2.1: The electrode configurations used in the modeling . C is current electrode and P is potential electrode (Loke, 2002).

.

Dipole-dipole performs depth sounding in the way that the distance “a” normally is kept constant whereas the distance between the pairs of potential electrodes and current electrodes is increased. As the distance enlarges, the current is forced to flow deeper and hence reveals more information about lower regions. To increase data quality, also the distance "a" has to be increased.

For the Gradient configuration, the potential electrodes are moved along the line between the current electrodes with a constant separation. To get information about the deeper subsurface, the distance between the current electrodes is increased.

The Pole-dipole configuration has a fixed distance between the potential electrodes. One current electrode is kept a long distance from the measured line. The depth sounding is carried out by gradually increasing the distance between the current electrode in line and the potential electrodes.

Wenner shows a constant distance between all the electrodes. For a higher penetration depth the distance "a" has to be increased progressively. As a result, the current and the potential electrodes have to be changed for each measurement.

Lateral information in two dimensions is achieved letting the soundings described above roll along the cable spread (Figures 2.2 and 2.3). Data about each electrode configuration are shown in table 1.

Electrode configuration	No. of data points	No. of data lines in pseudosection	Name of protocol files for the modeling
Dipol/Dipol	1525	15	DipolDipol4LS_10m
Gradient	1416	15	Grad4XLS8plus_10m
Pol/Dipol	3173	21	PolDip4LSplus_10m
Wenner	445	15	WennerXLS_10m

Table 1: Technical data and names of protocol files for the forward modeling (provided by Thorleif Dahlin)

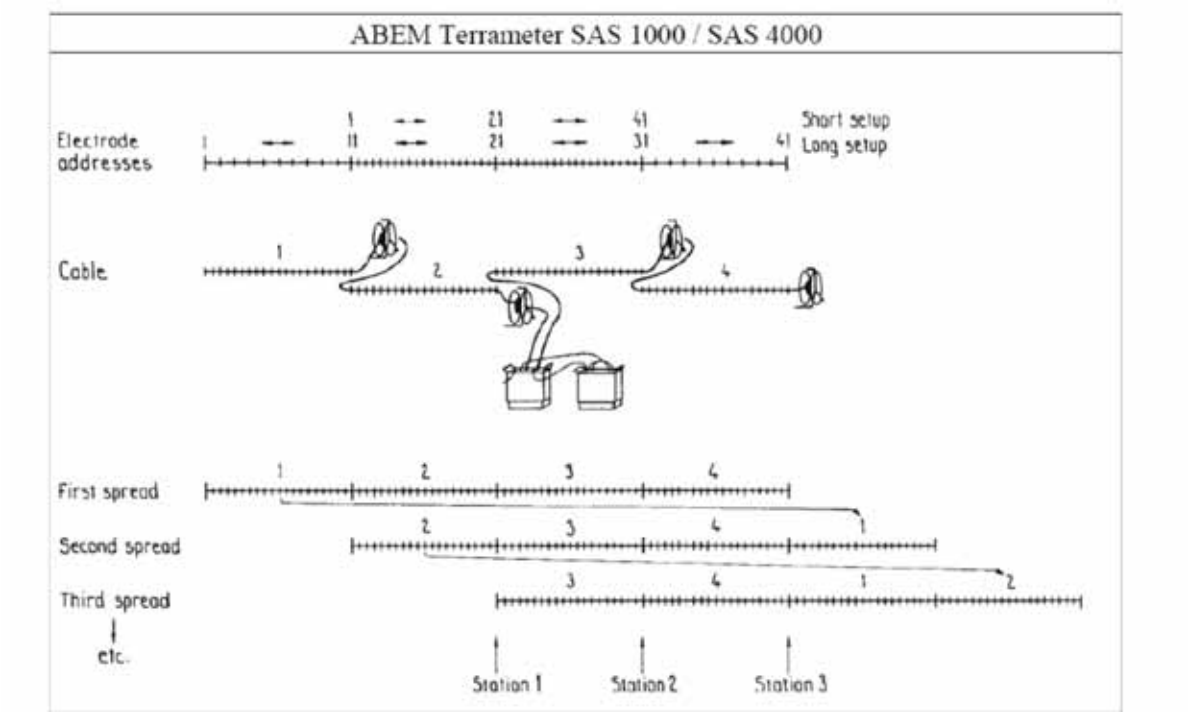

Figure 2.2: Measuring procedure in the field using 4 cables in a spread (From Dahlin 1993).

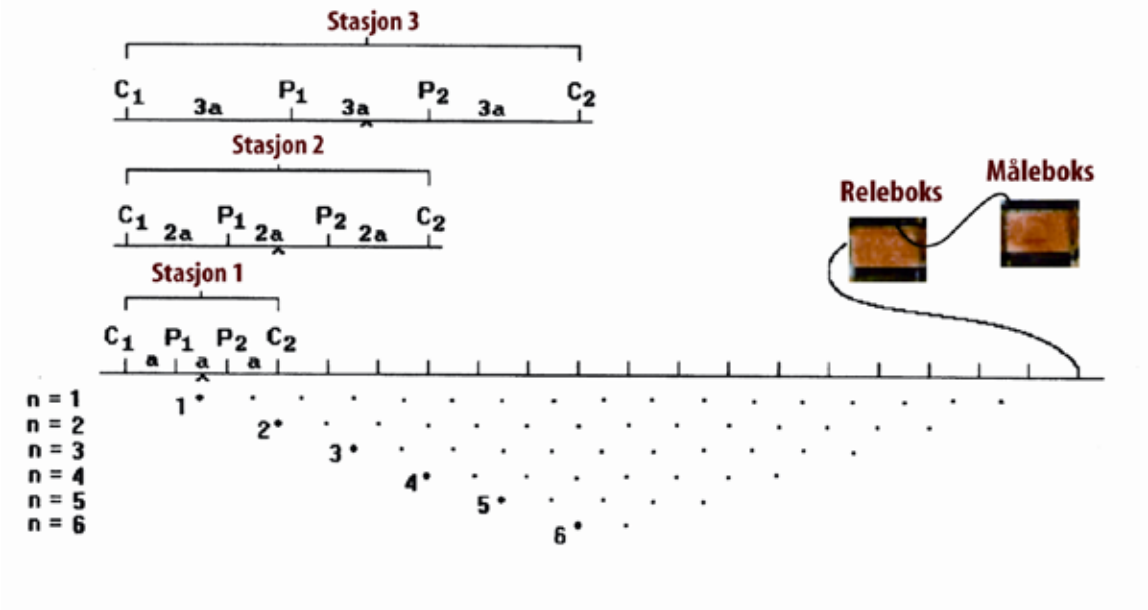

Figure 2.3: Roll along principle with the Wenner electrode configuration (After Barker 1992).

3. RESULTS

3.1 Vertical Fracture Zone – Different Depth

Model description

In order to examine the image capability of a vertical zone with different depth, a 10 m thick zone of 500 ohmm embedded in a bedrock of 5000 ohmm was modeled. 500 ohmm may correspond to a clay bearing fracture zone (Rønning et al. 2009). Five different values for the depth were chosen such as 10 m, 20 m, 40 m, 80 m and 150 m and the resolution was analyzed. Geologically this could depict a fracture zone varying in depth surrounded by crystalline bedrock.

Modeling results

For a depth of up to 20 m, the fracture zone can be imaged very accurately. The true depth can be recovered and in addition it is possible to determine the resistivity in a confident way (figures 3.1.1-3.1.4).

Even for 40 m and 80 m can the depth be seen quite precisely (figures 3.1.5-3.1.8). However, it is a bit more troublesome to determine the true resistivity value, since the resistivity in the lower part shows slightly too high and in the top part rather too small values. The low resistivity distribution covers a larger area and therefore it is more difficult to see the width. As a result the width can only be determined near the surface, since the boundaries get less sharp with increasing depth. The fracture zone displays a wider response in deeper regions and hence shows an artificial effect. Nevertheless it can be said that Dipole-dipole, Pole-dipole and Gradient illustrate fairly accurate results. Wenner has some limitations in resolving the depth penetration. Changing the vertical/horizontal filter from 1 to 2 depicts in some cases large differences between the images. The depth occasionally reaches infinite extensions when the filter value is 2 and therefore it is difficult to detect the termination of the fracture zone (figure 3.1.7, figure 3.1.8).

For a depth of 150 m, the low resistivity zone can be followed in larger depth. However, a fracture zone down to 150 m describes a model zone which is deeper than the penetration depth. Therefore the reliability of the image in the undermost part is clearly small and is not reasonable to make conclusions about the real structure. Dipole-dipole and Gradient achieved good results for mapping a deep fracture zone. The depth extension of the fracture zone is not limited but shows a response down to 150 m (figure 3.1.9, figure 3.1.10). However, the increased depth has an effect on the resolution. The width expands although the fracture zone in the synthetic model is continuously 10 m thick. Moreover the resistivity shows clearly too high values in the lower part. Therefore only the near surface allows drawing concrete conclusions about the true resistivity and width.

Summary
All in all Dipole-dipole and Gradient show the best results in mapping a fracture zone with various depths. Good assumptions about the true resistivity, width and depth can be made. As the depth increases, the width takes larger values and this has to be taken into account for the interpretation. Consequently it is of highly importance to reveal the true resistivity and width in the shallow subsurface.

3.2 Vertical Fracture Zone – Different Width

Model description
A more than 150 m deep vertical zone of 500 ohmm was mapped within bedrock of 5000 ohmm. Different values for the width were tested in order to see the effect on the resolution. The fracture zone was imaged with 5 m, 10 m, 20 m and 40 m thickness.

Modeling results
For a width of 5 m it can be noted that the low resistivity zone is clearly visible, but it is difficult to assess the depth extent. The true resistivity can only be determined from the upper 10 meters since the shape of the zone blurs out towards the depth (figure 3.2.1). If the vertical/horizontal filter is set to 2, much better results can be achieved. The low resistivity in the deeper part of the model approaches more the real value and shows a response down to 150 m (figure 3.2.2).

If the zone is 10 m wide the true thickness can be revealed near the surface. As the depth increases, the width of the fracture zone yields a bulge (figure 3.2.3). Therefore it is particularly hard to make conclusions about the thickness in deeper regions. The best response was achieved with Gradient, especially regarding the depth. Pole-dipole shows the biggest bulge and makes it problematic to determine the width whereas Wenner is occasionally not able to map the fracture zone deep enough (figure 3.2.3).

A width of 20 and 40 m gives significantly better results. The thickness can also be estimated from the lower part of the model and the resistivity yields more accurate values (figure 3.2.6). For 40 m it is worth mentioning that a low resistivity feature in the middle of the fracture zone is present for all the arrays apart from Dipole-dipole. This region underestimates the resistivity and hence could be misleading for determining the true resistivity (figure 3.2.8).

Summary
To sum up, it has to be stressed that Gradient and Dipole-dipole give the best results for identifying the width of a fracture zone. The wider the low resistivity zone, the more accurate statements can be made. It is outstanding that if the vertical/horizontal filter is set to 2 much better results can be achieved. Therefore it is strongly recommended to choose the value 2 if vertical structures are expected to be present in the subsurface.

3.3 Vertical Fracture Zone – Different Contrast

Model description
Embedded in bedrock of 5000 ohmm a 10 m thick and more than 150 m deep vertical zone was imaged. The resistivity of the vertical zone was varied in order to study the limitations of mapping contrasts. The different resistivities were chosen to be 250 ohmm, 500 ohmm, 1000 ohmm and 2000 ohmm, which correspond to contrasts of 1:20, 1:10, 1:5 and 1:2.5.

Modeling results
Generally it can be noted that the resolution of the image is better with higher contrasts. Consequently, a vertical zone with a contrast of 1:20 shows fairly accurate results. The resistivity can be estimated quite well, especially in the shallow subsurface. The width on the other hand is moderately accurate. The low resistivity region spreads out in the lower parts and the width can therefore only be determined near the surface (figure 3.3.1). This effect can also be seen for a contrast of 1:10. The resistivity is however more precise and can also be recognized in greater depth. All configurations show satisfactory results, though Gradient is slightly superior regarding the true depth extent and width of the vertical zone (figure 3.3.3).

The quality of the image decreases for a resistivity of 1000 ohmm which represents a contrast of 1:5. The true resistivity can only be seen at the top, since the vertical zone cannot be followed down to 150 m (figure 3.3.5). The resolution can be improved by setting the vertical/horizontal filter to 2. The boundaries of the vertical zone get slightly sharper, the depth penetration increases, but still the exact resistivity values cannot be illustrated (figure 3.3.6).

For a contrast of 1:2.5 the resolution decreases dramatically and the image has clear deviations from the true model. The vertical zone can only be revealed in the upper 20 m and no response is coming from deeper regions. However, it is possible to determine the resistivity from the shallow subsurface. In comparison Wenner generates the worst response for a contrast of 1:2.5 since the resistivity reflects a too high value and the zone can hardly be detected (figure 3.3.7).

Summary
In conclusion, it can be said that for a contrast up to 1:10 the vertical zone can be imaged relatively accurate with all configurations. For a contrast of 1:5 the limitations lie in depth imaging. For very small contrasts, such as 1:2.5 the resolution decreases enormously and Wenner turned out to have the worst response. In general, the best results were achieved with Gradient and a vertical/horizontal filter value of 2.

3.4 Fracture Zone – Different Dip

Model description
A 10 m thick and more than 150 m deep zone of 500 ohmm was imaged surrounded by bedrock of 5000 ohmm. Different dips were mapped in order to study how well the four arrays can describe the sloping structure. Dips ranging from 15 to 80 degrees were examined and the resolution was analyzed. For steeply dipping structures the vertical/horizontal filter values 1 and 2 were tested, whereas for shallow dipping structures a comparison of the values 1 and 0.5 was done.

Model results
For steeply dipping structures it is quite challenging to recognize the dip. Basically only the Gradient configuration is able to map the tilt in a reasonable way. The other arrays depict a vertical structure and show therefore deviations from the true model (figures 3.4.1-3.4.4). Gradient can map the sloping structure down to about 80 m. In larger depth the true dip can't be resolved and the model illustrates a slightly too flat response.

For a dip of 60 degrees the imaging capability strongly increases. All configurations are able to map the dip relatively accurate (figure 3.4.5). Wenner shows some limitations in depth penetration. The dip can be identified, but the low resistivity zone vanishes already in shallow depth. The effect of changing the vertical/horizontal filter value can also be observed. If the filter is set to 2, the low resistivity zone gets more elongated along the vertical axis and hence maps the dipping too steep. As a result, the filter rather distorts the picture and misplaces the zone (figure 3.4.5, figure 3.4.6.).

If the dip is less than 45 degrees the tilt can be mapped very accurate. Although it is not possible to make statements about the exact value, good assumptions can be made. As the dip gets more flat, the low resistivity zone approaches the surface and can therefore be detected much easier. Also Wenner shows highly accurate results for the flat dipping structures (figures 3.4.8-3.4.11). The width of the zone can be determined from the shallow subsurface. In deeper regions, the low resistivity zone shows a bulge and hence a too wide response. The less steep the structure the easier it is to identify the width and also the resistivity.

Summary
All in all, it can be recommended to choose the Gradient configuration if almost vertical structures are expected to be present in the subsurface. Gradient is able to map steeply dipping structures whereas the other arrays show some limitations in that they yield a vertical zone. As the tilt angle decreases the quality of the image is clearly improving and all arrays can map the structure precisely.

For very steeply/shallow dipping structures it is recommended to use the vertical/horizontal filter value 2 respectively 0.5. However, between 15 and 75 degrees, more accurate results can be achieved with the filter value 1.

3.5 Vertical Fracture Zone – Different Top Layer Thickness and Resistivity

Model description

A more than 150 m deep vertical fracture zone of 500 ohmm embedded in a bedrock of 5000 ohmm was modeled with varying low resistive top layers. The superficial layers differed in thickness and resistivity in order to study the decrease in resolution with a conductive layer at the top. The problem encountered is due to the current which prefers to travel in the low resistive layer and avoids less conductive regions. Consequently there is not much current penetrating in the depth. It is therefore hard to get any information about the lower part, and especially troublesome in great depth. Five different top layer resistivities were mapped, whereas they range from 10 ohmm to 1000 ohmm. Geologically 10 ohmm represents marine clay (Solberg et al. 2008), 50 ohmm stands for possible quick clay (Solberg et al. 2008), 100 ohmm for silty material or moraine and 500 ohmm and 1000 ohmm for dry sand and gravel. Since the thickness has a great effect on the final resolution, imaging of 5 m, 10 m, 20 m and 40 m of top layer thickness was done. The goal was to gain more understanding how the resolution changes with different top layer thickness and resistivity.

Modeling results

Generally it can be noted that the higher the resistivity and the smaller the thickness of the superficial layer, the easier it is to see the fracture zone. If the top layer has a resistivity of 1000 ohmm, the resolution is particularly good (figures 3.5.1-3.5.8). For a top layer thickness up to 20m the fracture zone can be mapped quite accurately regarding to resistivity, thickness and depth. However, only Dipole-dipole, Pole-dipole and Gradient seem to give accurate results. Wenner shows surprisingly bad images and has problems in mapping the fracture zone, even for thin top layers. The bad results can be explained by the amount of data points. Wenner has a particularly bad coverage compared to the other arrays and is therefore not able to map as detailed as the other configurations.

As the resistivity of the top layer decreases, the resolution gets worse. With a thin top layer with resistivity of 100 ohmm, it is possible to see the low fracture zone with all arrays. Some good assumptions can be made for the true resistivity, the width and the depth of the fracture zone. Especially with Dipole-dipole, Pole-dipole and Gradient, the width and the resistivity can be identified in the top part (figure 2.16). Even with a thickness of 20m it is possible to detect a fracture zone with these three arrays.

It is particularly challenging to see structures in the subsurface if there is a layer of 10 ohmm at the top. This layer could represent undisturbed marine clay, which has especially low resistivity and prevents the current from flowing deeper. If the layer is less than 10 m thick, it is possible to detect a low resistivity zone with Dipole-dipole and Pole-dipole, but the resistivity values are far too high and the geometry of the fracture zone is not in agreement with the true model (figures 2.1.-2.4.). Gradient and Wenner show hardly a response, so they are clearly affected by this low resistive layer.

Summary

In conclusion it can be said that a low resistivity layer at the top decreases the resolution and makes it hard to assess the subsurface in a confident way. The lower the resistivity and the larger the thickness of the top layer, the more difficult it is to detect any structures beneath. As

the top layer thickness increases, the fracture zone shows too high resistivity values and the depth and width get more inaccurate.

With the vertical/horizontal filter set to 2, the response is generally enhanced, especially regarding the depth. It can be seen that the fracture zone penetrates down and is not limited to a certain depth.

The best results were achieved with Dipole-dipole and Pole-dipole. Therefore it is recommended to choose one of those arrays, if a low resistivity layer exists at the top. The Gradient configuration seems to give satisfied results as well and can be a good solution if the background noise is relatively high.

3.6 Horizontal Layers

Model description
A variety of horizontally layered models were imaged in order to compare the vertical resolution of the four different arrays.

The first models illustrate a subsurface consisting of 2 layers and describing an increase of resistivity with depth. To investigate the effect of a low resistivity layer on the top, different resistivity values were tested for a superficial layer in a 3 layer model. Geologically this could represent gneiss as host rock, overlaid by a sediment layer and a top layer of clay.

To examine the change in resolution with depth, modeling of a 10 m zone (500 ohmm) in different depth was done. This could depict a horizontal fracture zone at various locations embedded in crystalline bedrock. Since it is of high interest to see the limitations of imaging in deeper regions, mapping of a 1m zone (10 ohmm, 100 ohmm) in a depth of 100 m was done and the capability of resolving horizontal structures was analysed.

Modeling results
Generally speaking it is possible to distinguish the different horizontal structures in the 2 and 3-layer models very clearly, even with a low resistivity top layer of 25 m. The presence of a superficial layer can lead to rather undulating contour lines between the 1000 ohmm and 5000 ohmm layer (e.g. figure 3.6.3). Wenner is only slightly interfered by this effect and is hence a good choice for imaging horizontal structures. However, if the dominating structure is present in great depth, this aspect has to be taken into account. The resolution decreases with depth and the response for the different arrays starts to vary (figure 3.6.12). Up to a depth of 20 m the 10 m zone of 500 ohmm can be mapped particularly accurate with all configurations (figure 3.6.10). But as the depth increases, the resolution gets worse and it is only possible to see a low resistivity zone, without being able to make an exact statement about the absolute values of the resistivity and the thickness of the layer.

It can also be seen that there are differences in the imaging capability of the four arrays. It emerges that Dipole-dipole and Pole-dipole show the best resolution for mapping a zone deeper than 40m (figure 3.6.12, figure 3.6.17).

The limitation of mapping a low resistivity zone in 100 m depth can be seen in figures 3.6.17-3.6.22. A 1 m layer of 100 ohmm which corresponds to a contrast of 1:50 cannot be detected, whereas a contrast of 1:500 can be seen very clearly. However, the thickness of the layer

cannot be determined. It appears that the low resistivity layer is continuing towards the depth (figure 3.6.19), although it corresponds to 1 m thickness. Since the current is not able to penetrate any deeper, the ongoing low resistivity zone describes an artifact.

Summary
Generally, for horizontal layers, a better result is achieved by setting the vertical/horizontal filter to 0.5. The structures get consequently slightly more elongated along the horizontal axis and the contour lines appear to be less curved and more compact.
Overall, it can be noted that Wenner is particularly good at mapping horizontal structures. However, if the prominent feature is in great depth, Dipole-dipole and Pole-dipole have to be considered as a better option.

4. CONCLUSION

2D resistivity modeling is of great importance since it clearly improves the ability of choosing the right array in a given geological setting.

The results reveal that the Gradient configuration is especially good at mapping fracture zones. Gradient is the only array that can map a steeply dipping structure. Fracture zones with a dip of 60 degrees and less can also be detected by the other arrays.

Gradient and Dipole-dipole depict particularly good results for mapping different depth, width and contrast. Up to 80 m the depth can be illustrated fairly accurate and widths larger than 10 m show quite exact responses. Mapping contrasts of up to 1:10 lead to precise images whereas limitations start for contrasts smaller than 1:5.

Dipole-dipole and Pole-dipole are generally good at revealing a fracture zone if a low resistivity top layer is present. However, if the superficial layer is less than 50 ohmm it is difficult to make precise conclusions about the subsurface.

In most cases a vertical/horizontal filter value of 2 clearly improves the image of vertical structures and depicts more accurate values for the fracture zone.

Wenner shows the best response for mapping horizontal layers unless the depth of the prominent feature is at great depth. For horizontal layers the vertical/horizontal filter value of 0.5 increases the quality of the picture and the image approaches more the true model.

5. REFERENCES

Dahlin, T. 1993: On the Automation of 2D Resistivity Surveying for Engineering and Environmental Applications. Dr. Thesis, Department of Engineering Geology, Lund Institutute of Technology, Lund Univesity. ISBN 91-628-1032-4.

Barker, R. 1992: A simple algorithm for electrical imaging of the subsurface. First Break Vol. 10, No.2, pp. 53 – 62.

Ganerød, G. V., Rønning, J.S., Dalsegg, E., Elvebakk, H., Holmøy, K., Nilsen, B. & Braathen, A. 2006: Comparison of geophysical methods for sub-surface mapping of faults and fracture zones in a section of the Viggja road tunnel, Norway. Bull. Eng. Geol. Env. (2006) 65: 231 – 243). ISSN: 1435-9529 (Paper) 1435-9537 (Online)

Loke, M.H. 2002: RES2DMOD Geoelectrical Imaging 2D & 3D. Instruction manual. www.geoelectrical.com.

Loke, M.H. 2008: RES2INV ver. 3.56. Geoelectrical Imaging 2D & 3D. Instruction manual. www.geoelectrical.com.

Reynolds 1997: An Introduction to Engineering and Environmental Geophysics. Wiley & Sons, UK.

Rønning, J.S. 2003: Miljø- og samfunnstjenlige tunneler. Sluttrapport delprosjekt A, Forundersøkelser. Statens vegvesen, Publikasjon 102.

Rønning, J.S., Dalsegg, E., Elvebakk, H. & Storrø, G. 2003: Characterization of fracture zones in bedrock using 2D resistivity. 9th EEGS European Meeting, Prague, August 31 – September 4 2003. Extended Abstract: Proceedings P005.

Rønning, J.S., Dalsegg, E., Elvebakk, H., Ganerød, G.V. & Heincke, B.H. 2009:
Characterization of fracture zones in bedrock using 2D resistivity. Proceedings from 5th Seminar on Strait Crossings, Trondheim, June 21 – 24 2009, p. 439 - 444 (SINTEF/NTNU)

Solberg, I.L., Rønning, J.S., Dalsegg, E., Hansen, L., Rokoengen, K. & Sandven, R. 2008:
Resistivity measurements as a tool for outlining quick-clay extent and valley-fill stratigraphy: a feasibility study from Buvika, central Norway. Canadian Geotechnical Journal, 45: 210-225, doi:10.1139/T07-089.

Modelling results: Vertical Fracture Zone – Different Depth

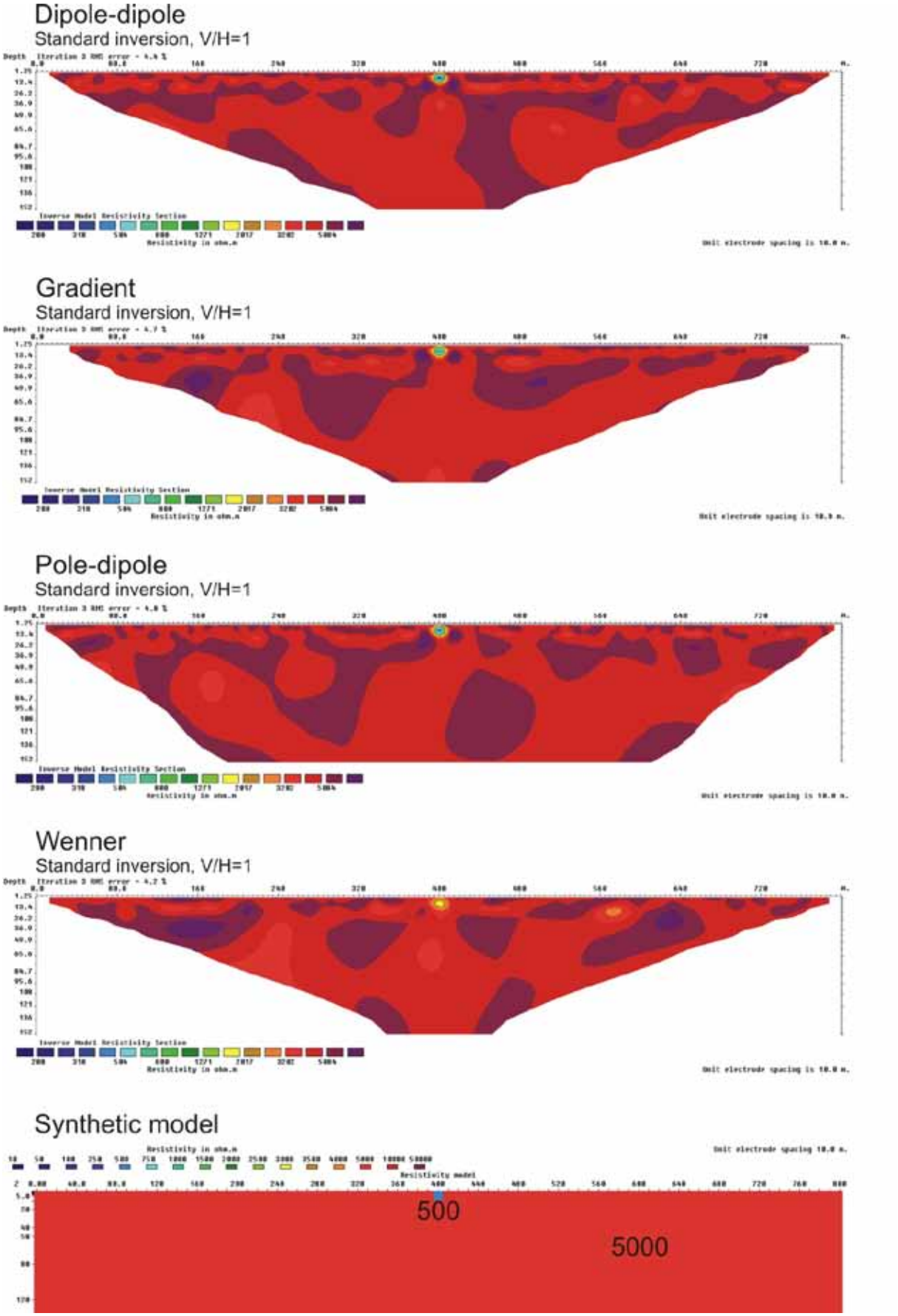

Figure 3.1.1: 10 m zone (500 ohmm) with a depth of 10 m, V/H=1

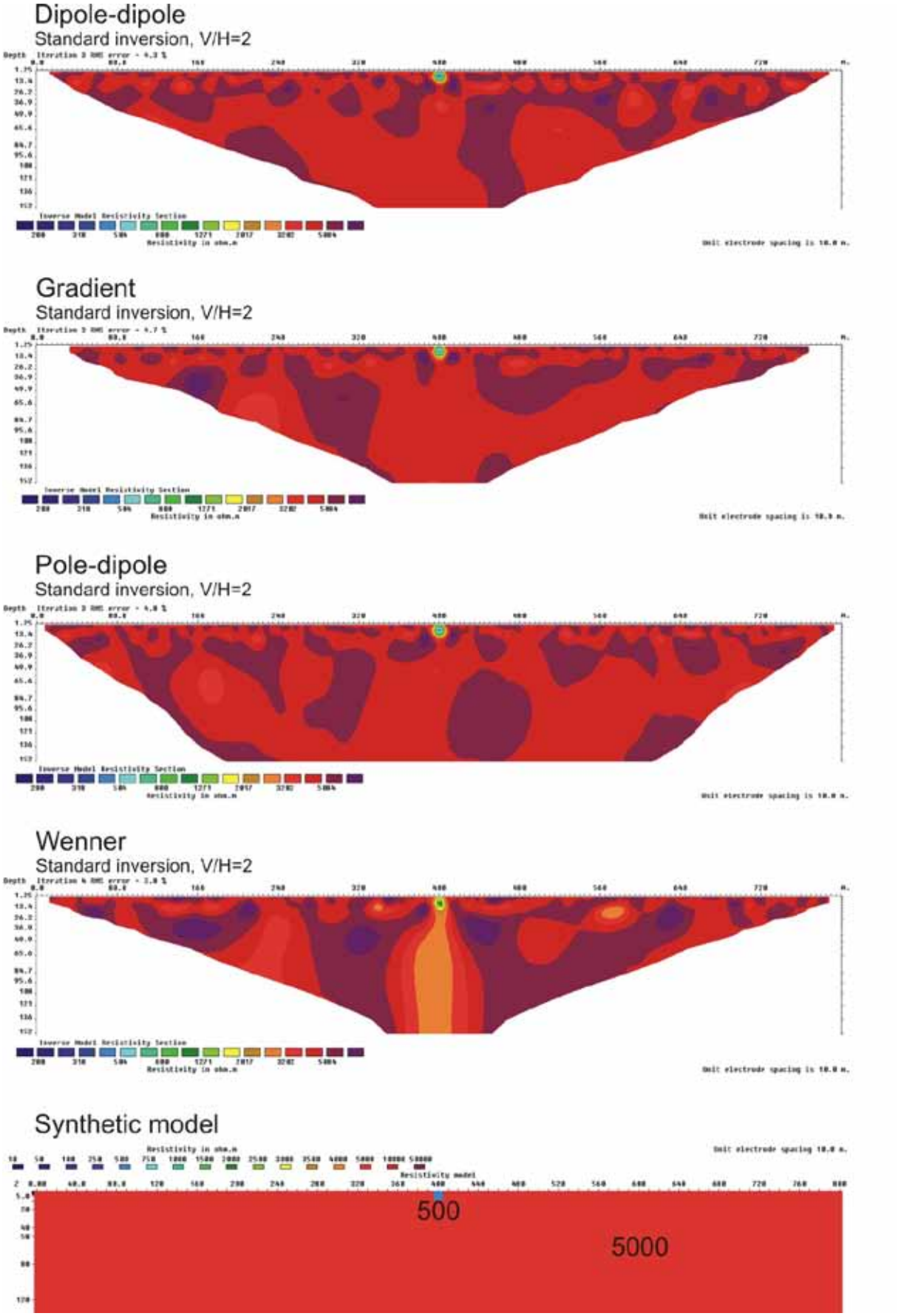

Figure 3.1.2: 10 m zone (500 ohmm) with a depth of 10 m, V/H=2

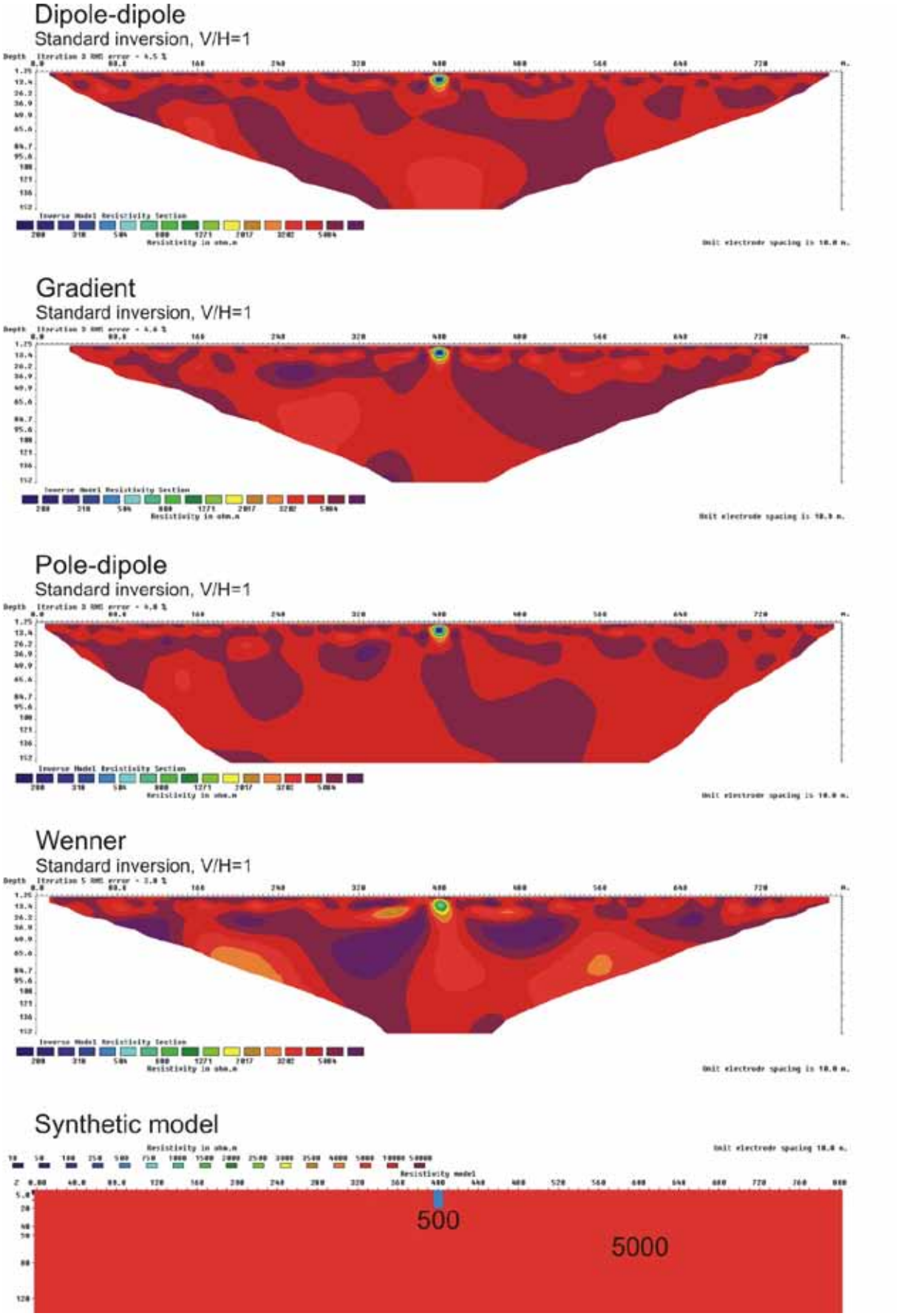

Figure 3.1.3: 10 m zone (500 ohmm) with a depth of 20 m, V/H=1

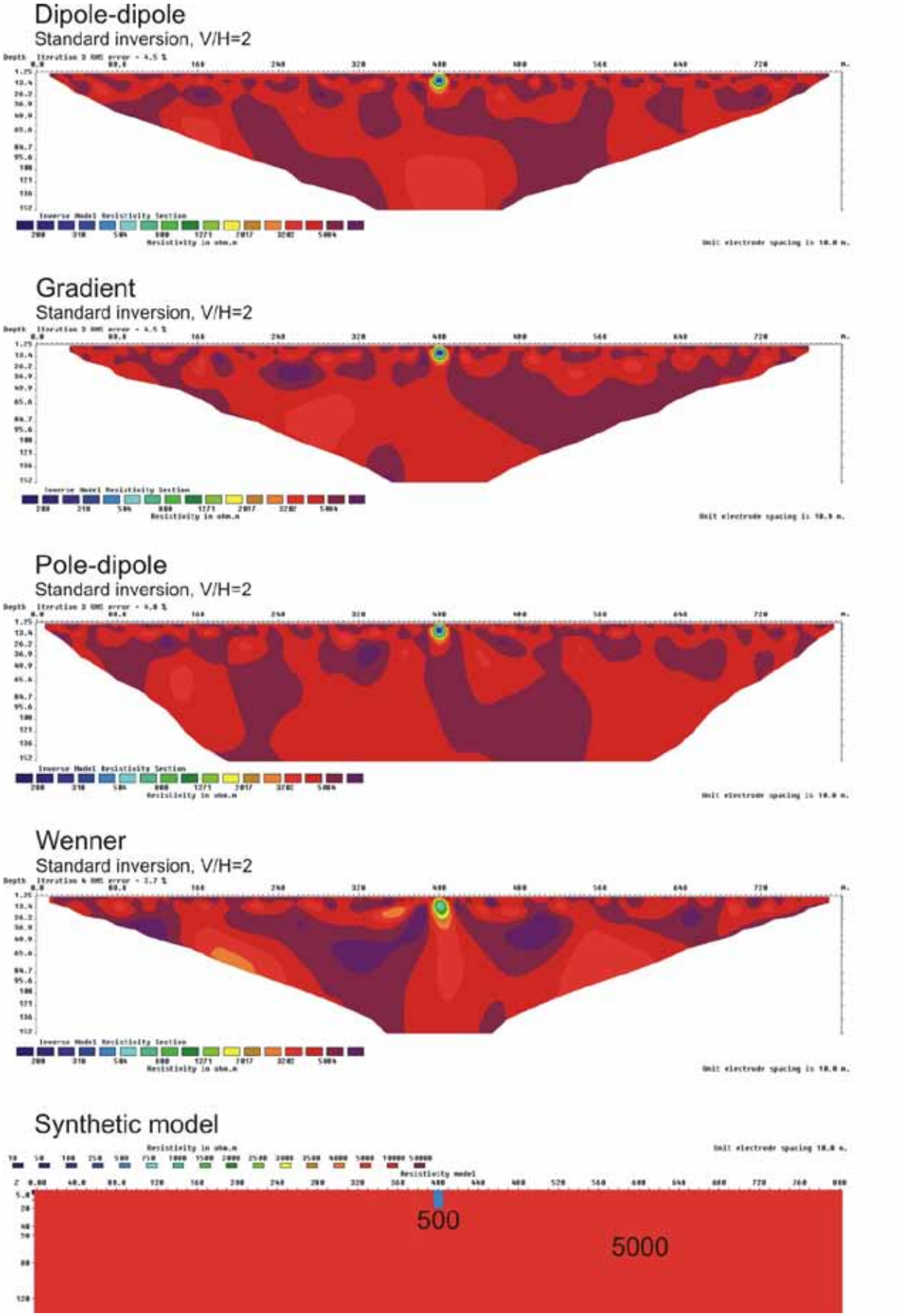

Figure 3.1.4: 10 m zone (500 ohmm) with a depth of 20 m, V/H=2

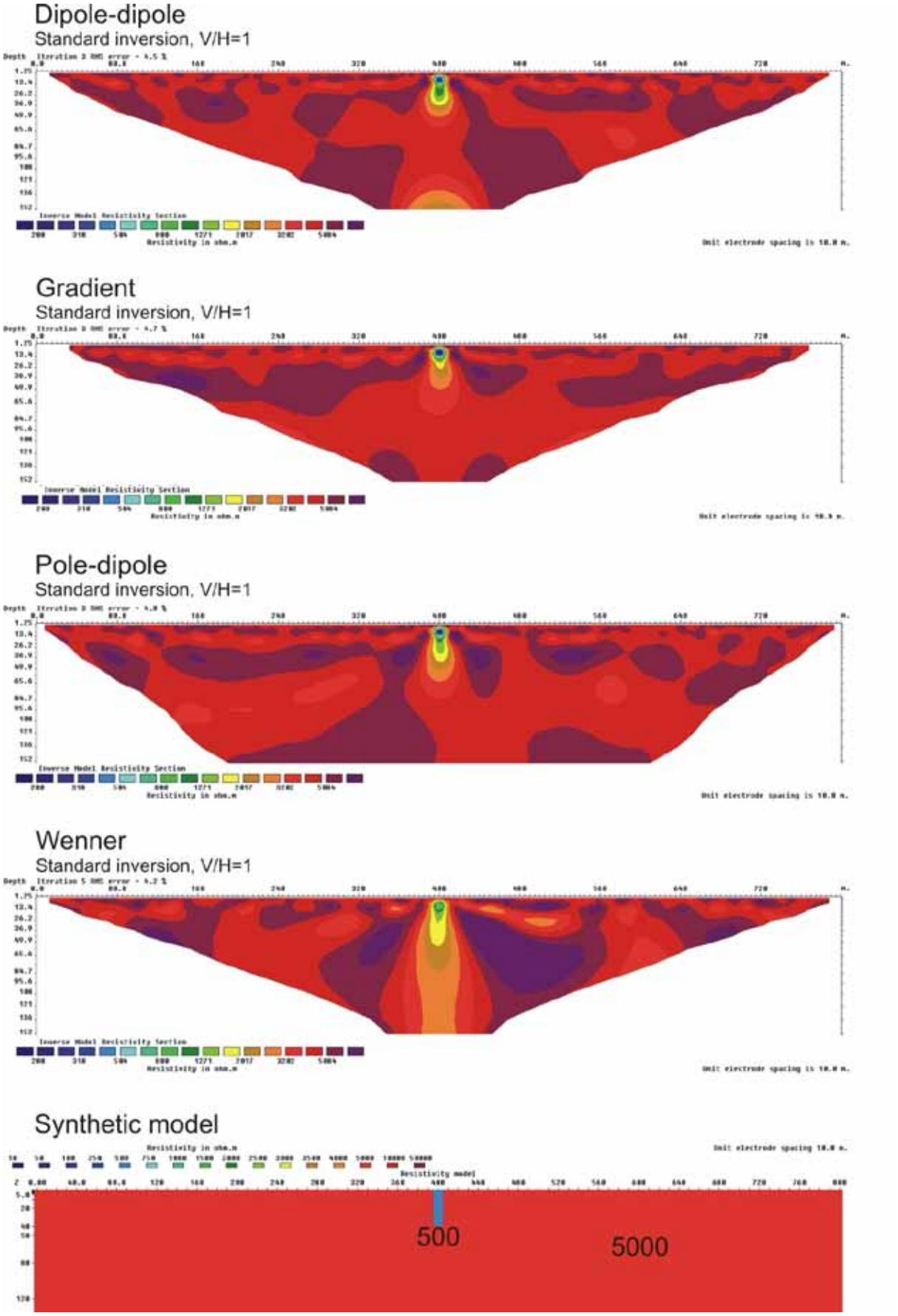

Figure 3.1.5: 10 m zone (500 ohmm) with a depth of 40 m, V/H=1

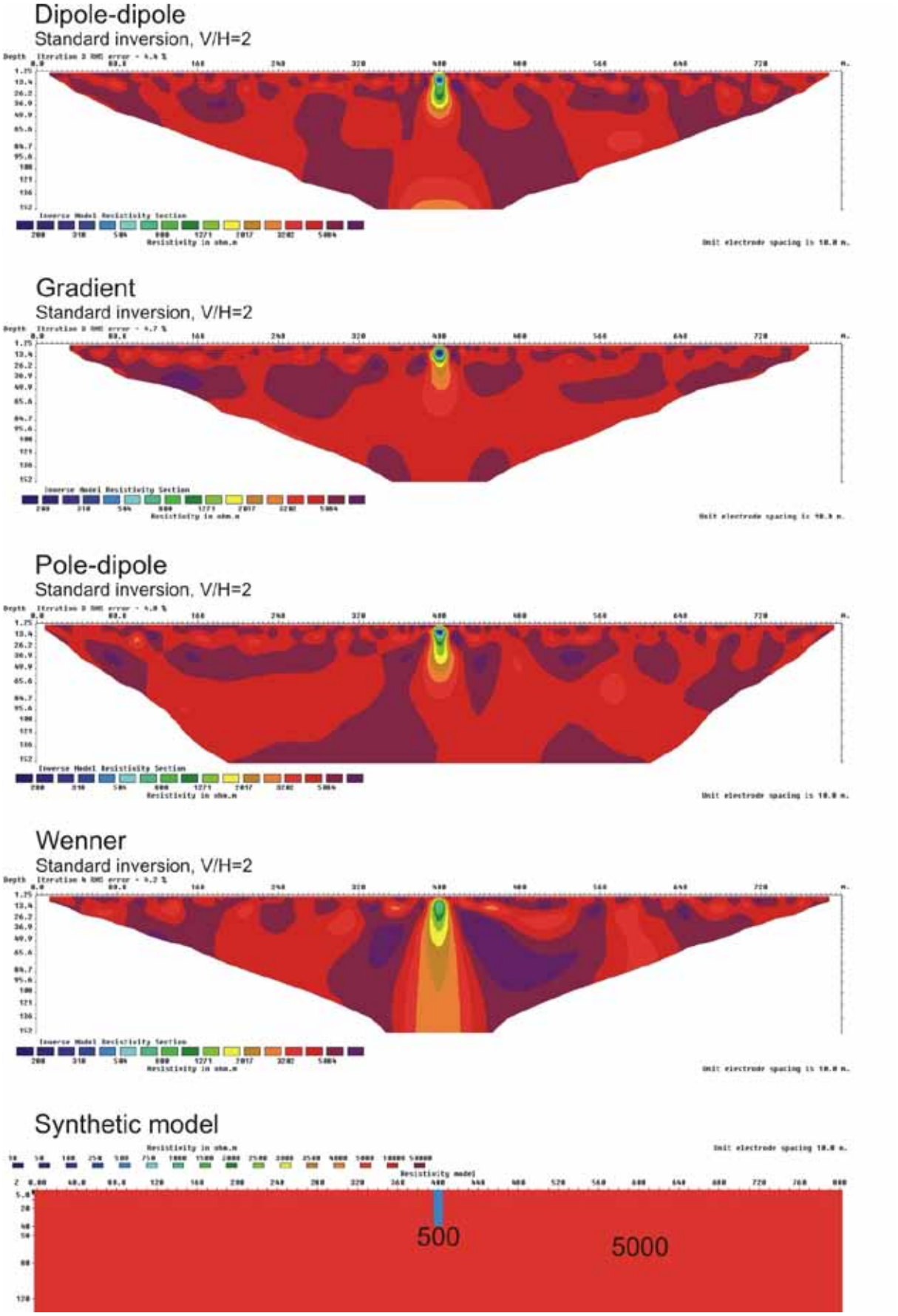

Figure 3.1.6: 10 m zone (500 ohmm) with a depth of 40 m, V/H=2

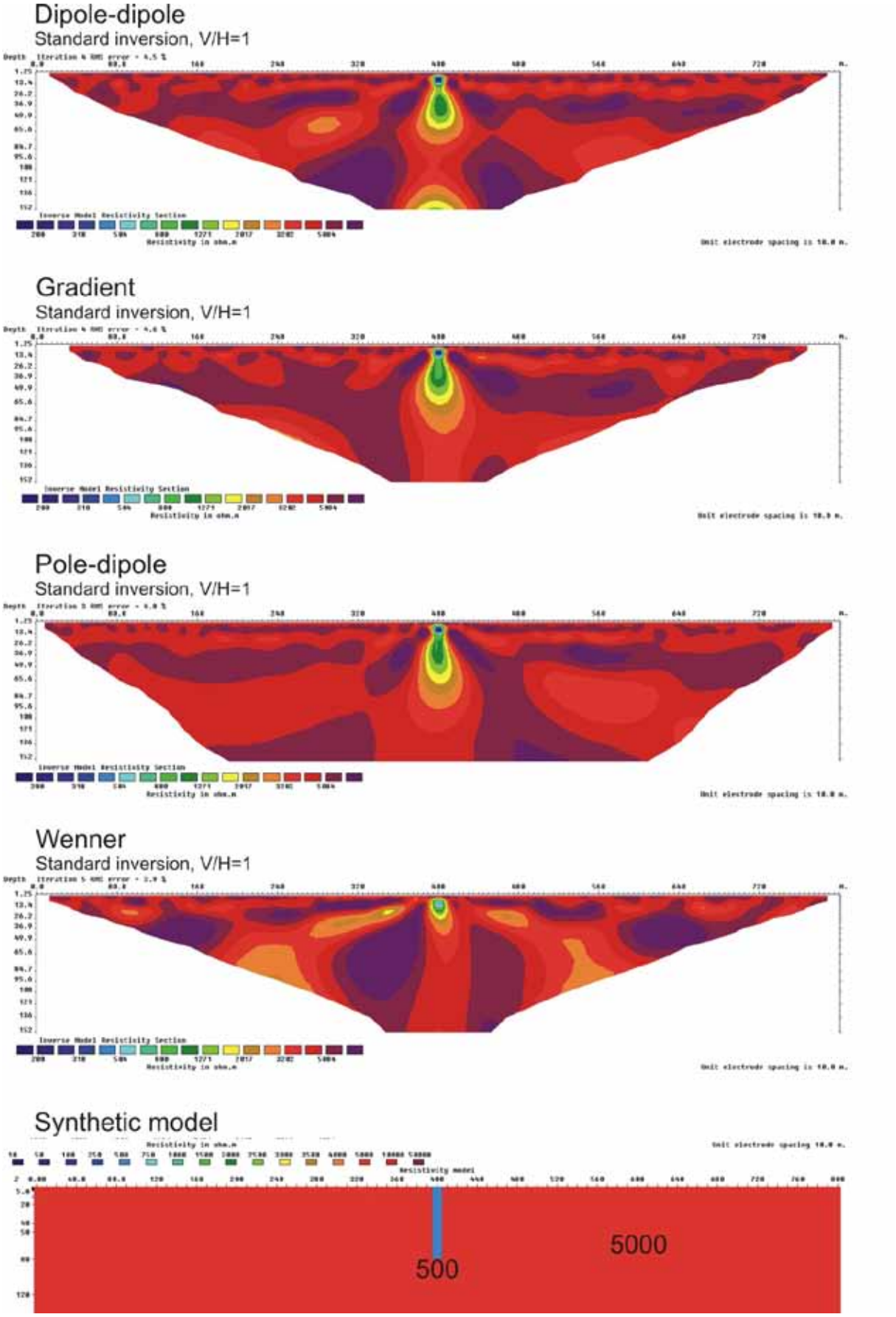

Figure 3.1.7: 10 m zone (500 ohmm) with a depth of 80 m, V/H=1

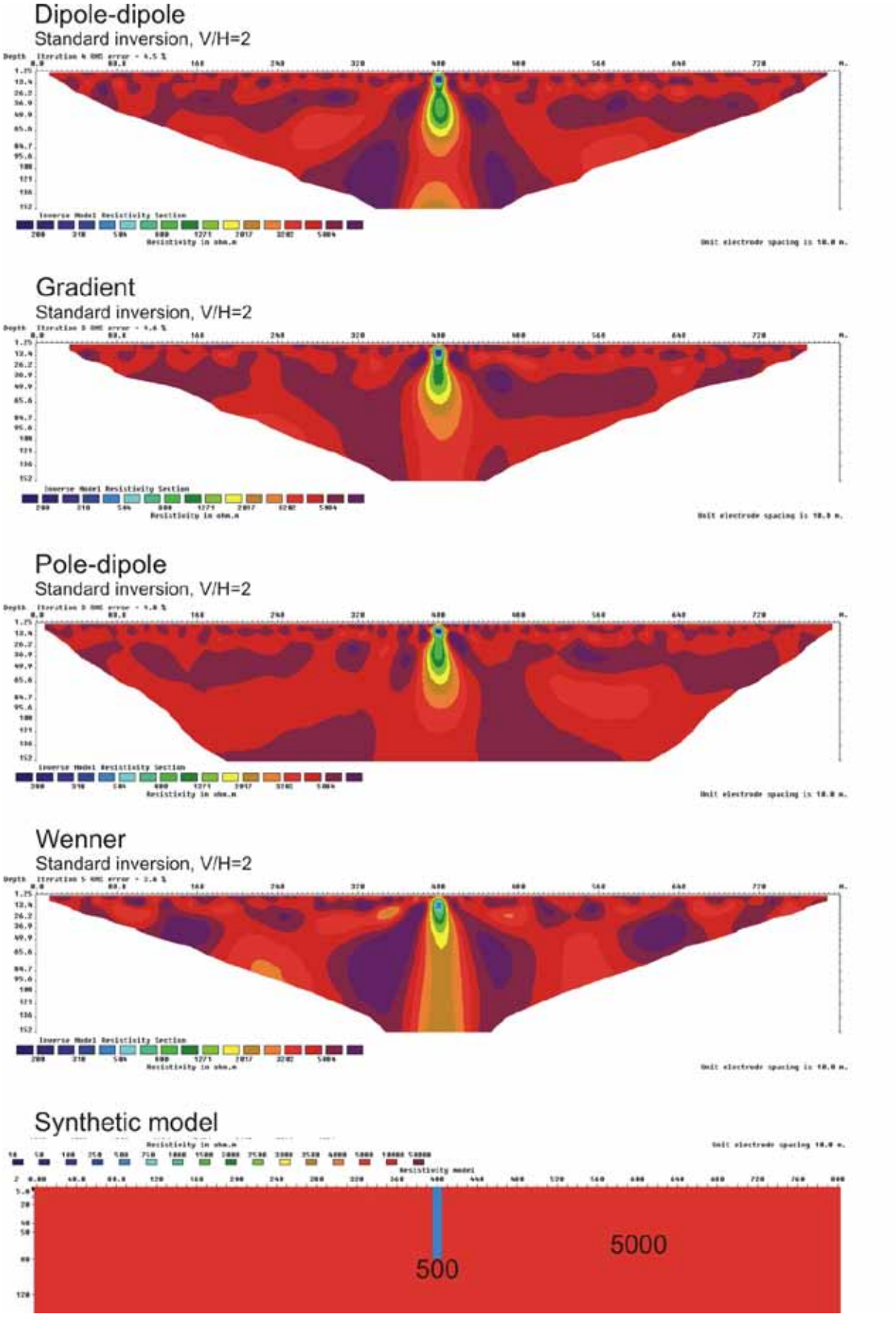

Figure 3.1.8: 10 m zone (500 ohmm) with a depth of 80 m, V/H=2

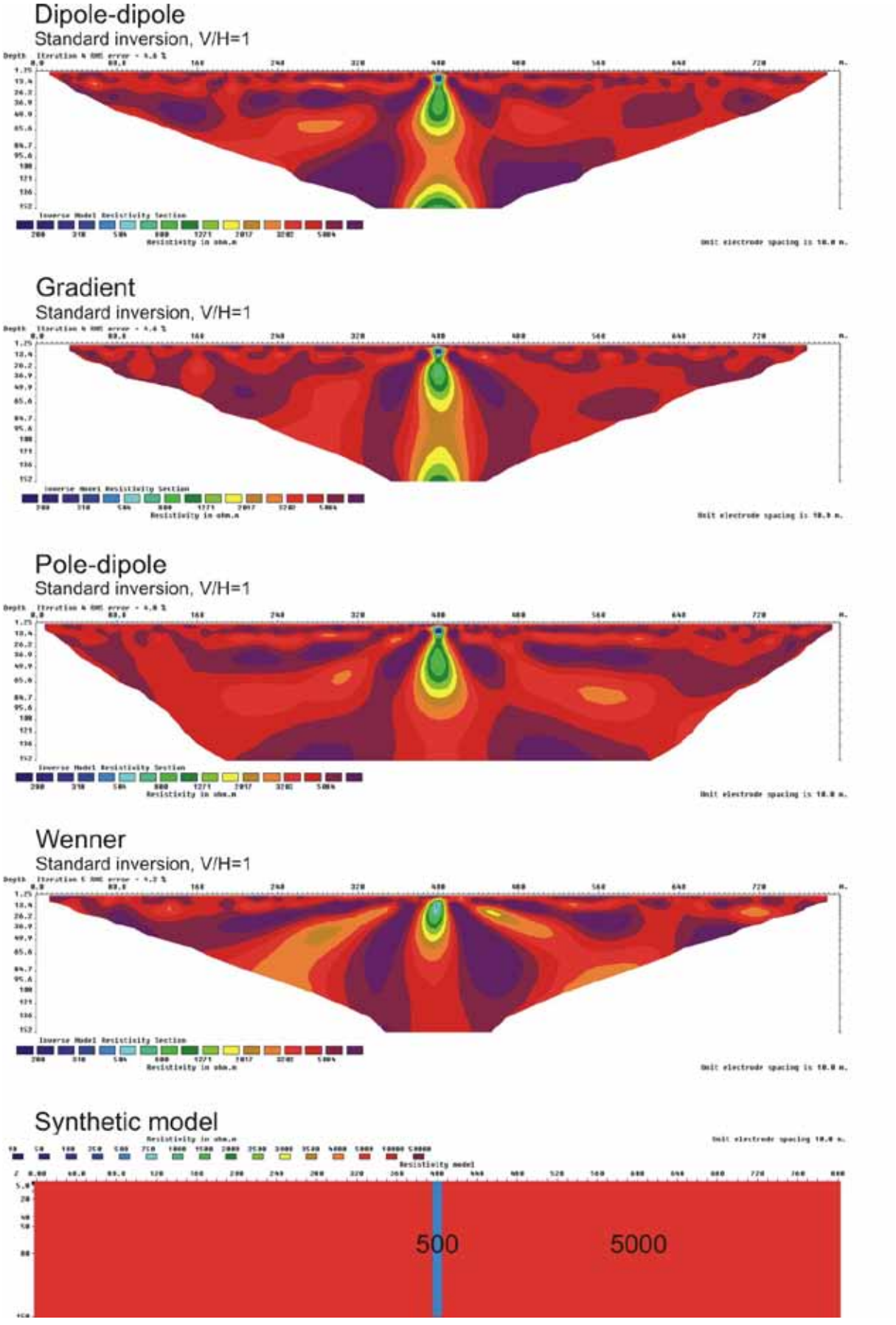

Figure 3.1.9: 10 m zone (500 ohmm) with a depth of 150 m, V/H=1

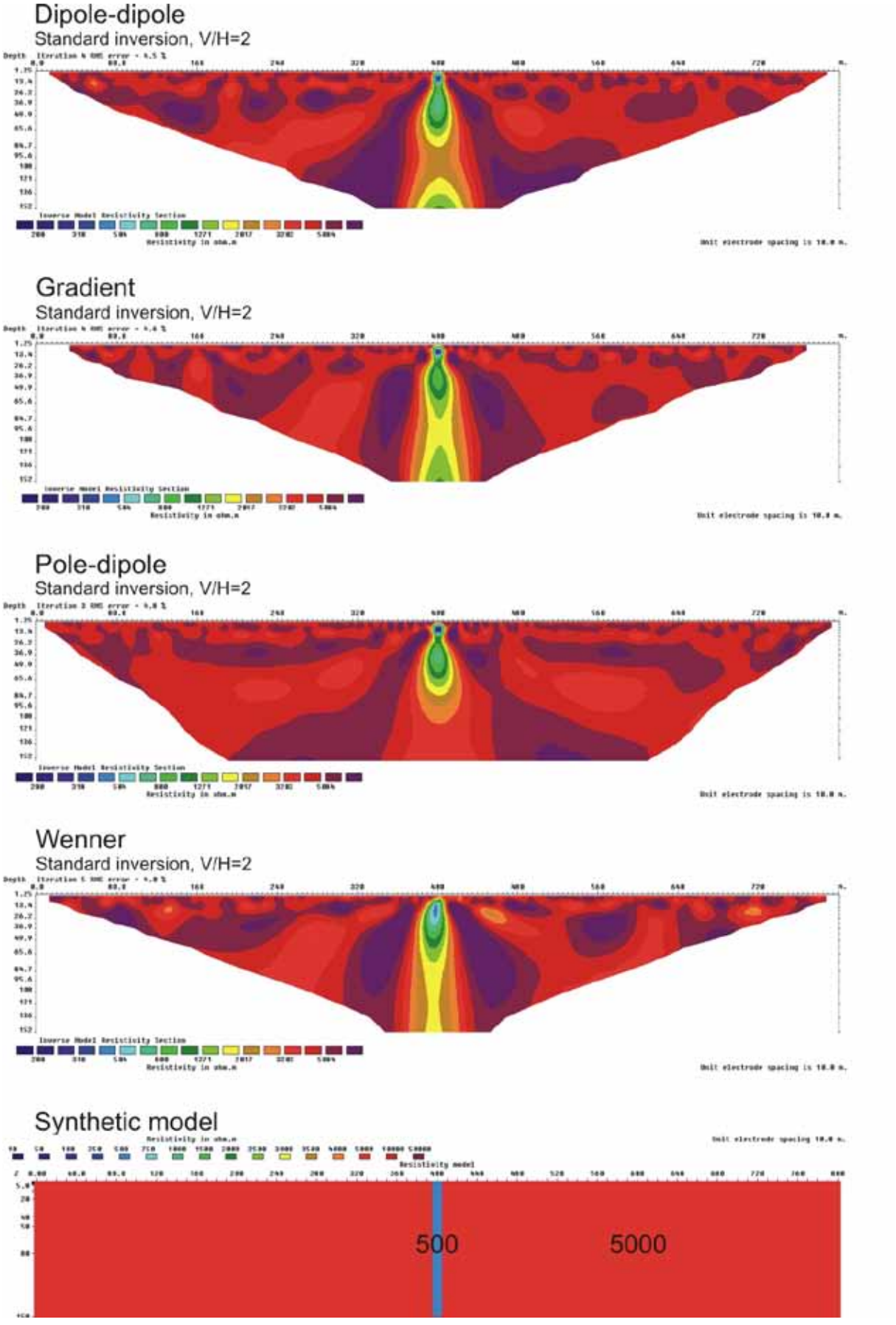

Figure 3.1.10: 10 m zone (500 ohmm) with a depth of 150 m, V/H=2

Modelling results: Vertical Fracture Zone – Different Width

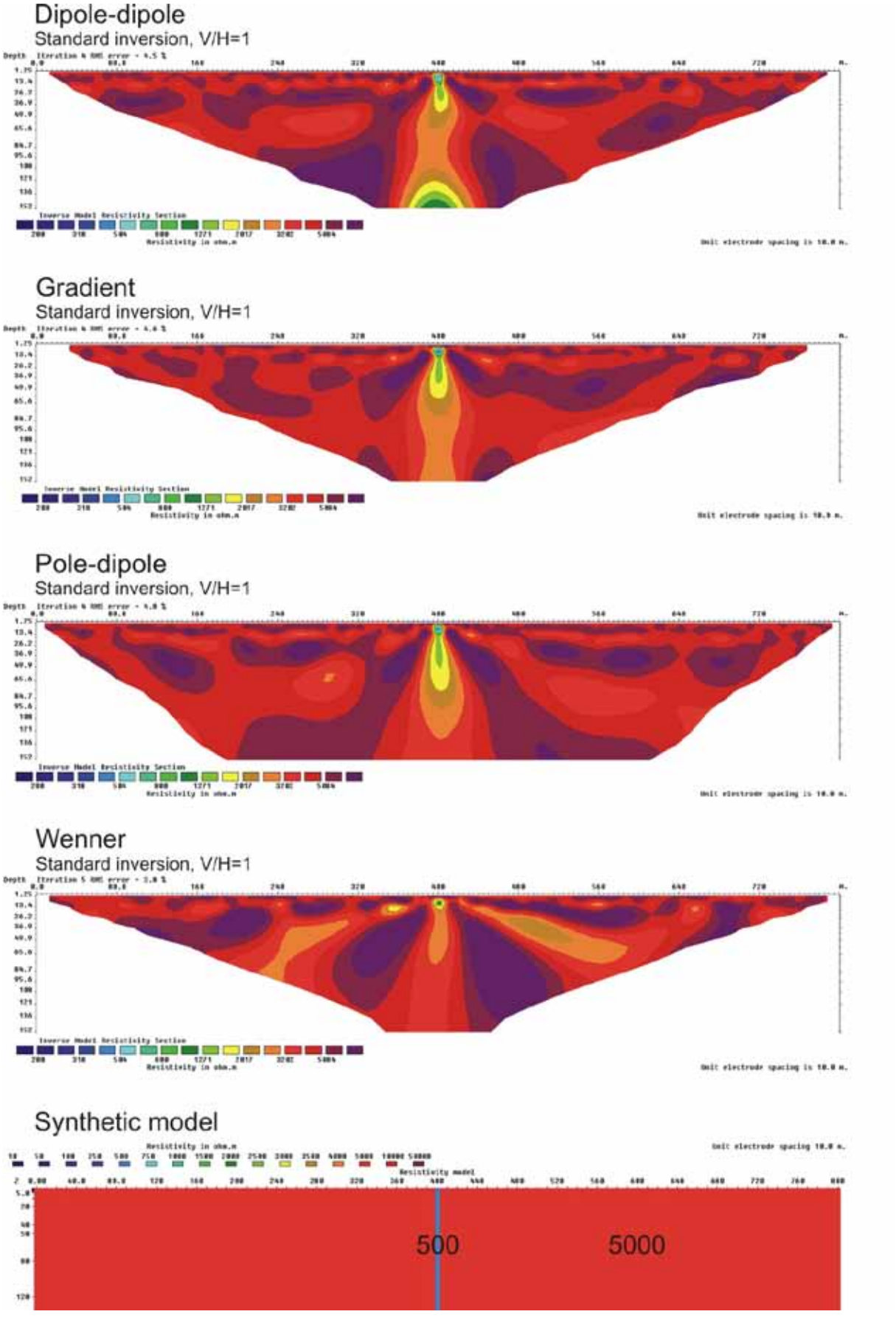

Figure 3.2.11: 5 m zone (500 ohmm), V/H=1

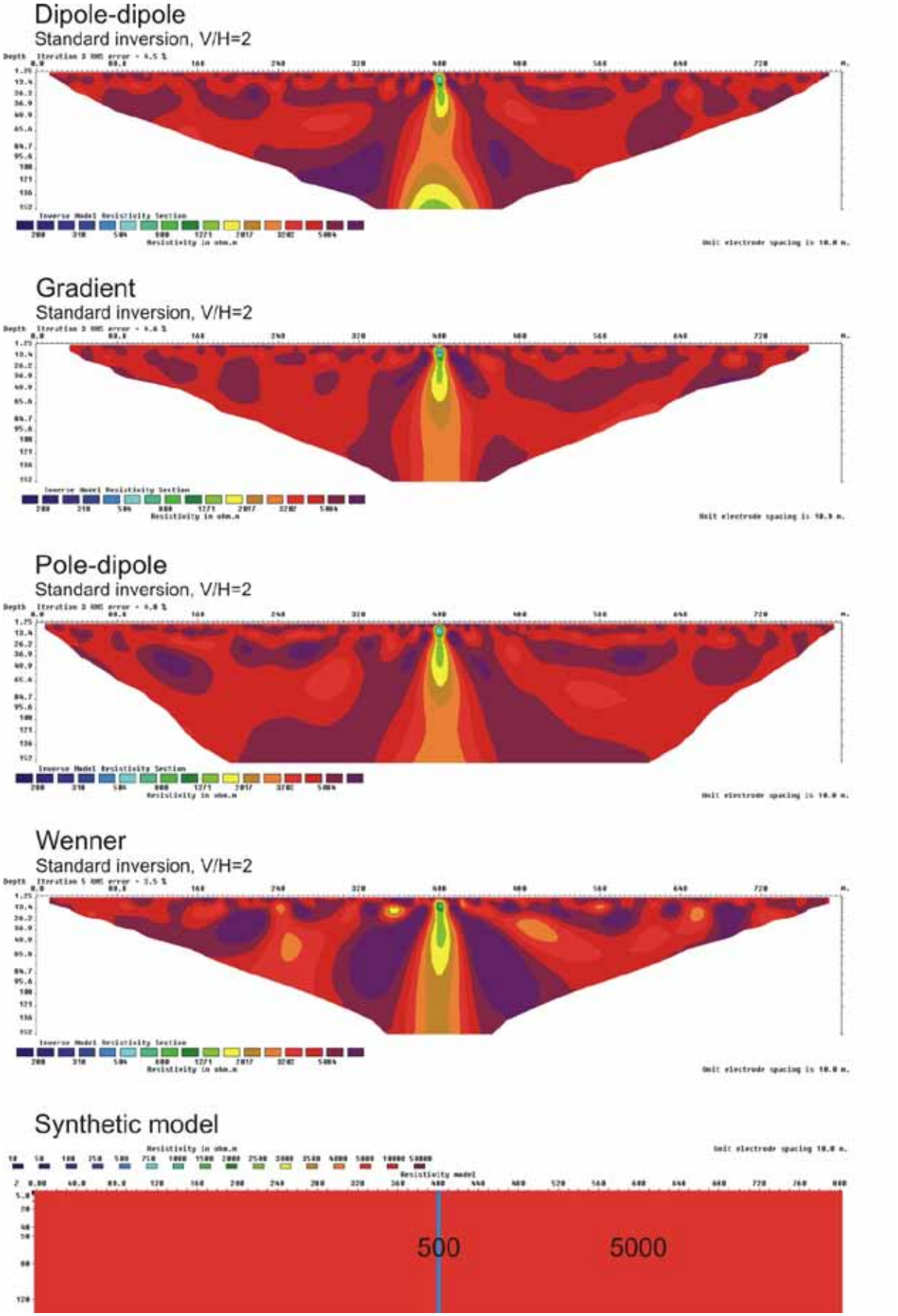

Figure 3.2.12: 5 m zone (500 ohmm), V/H=2

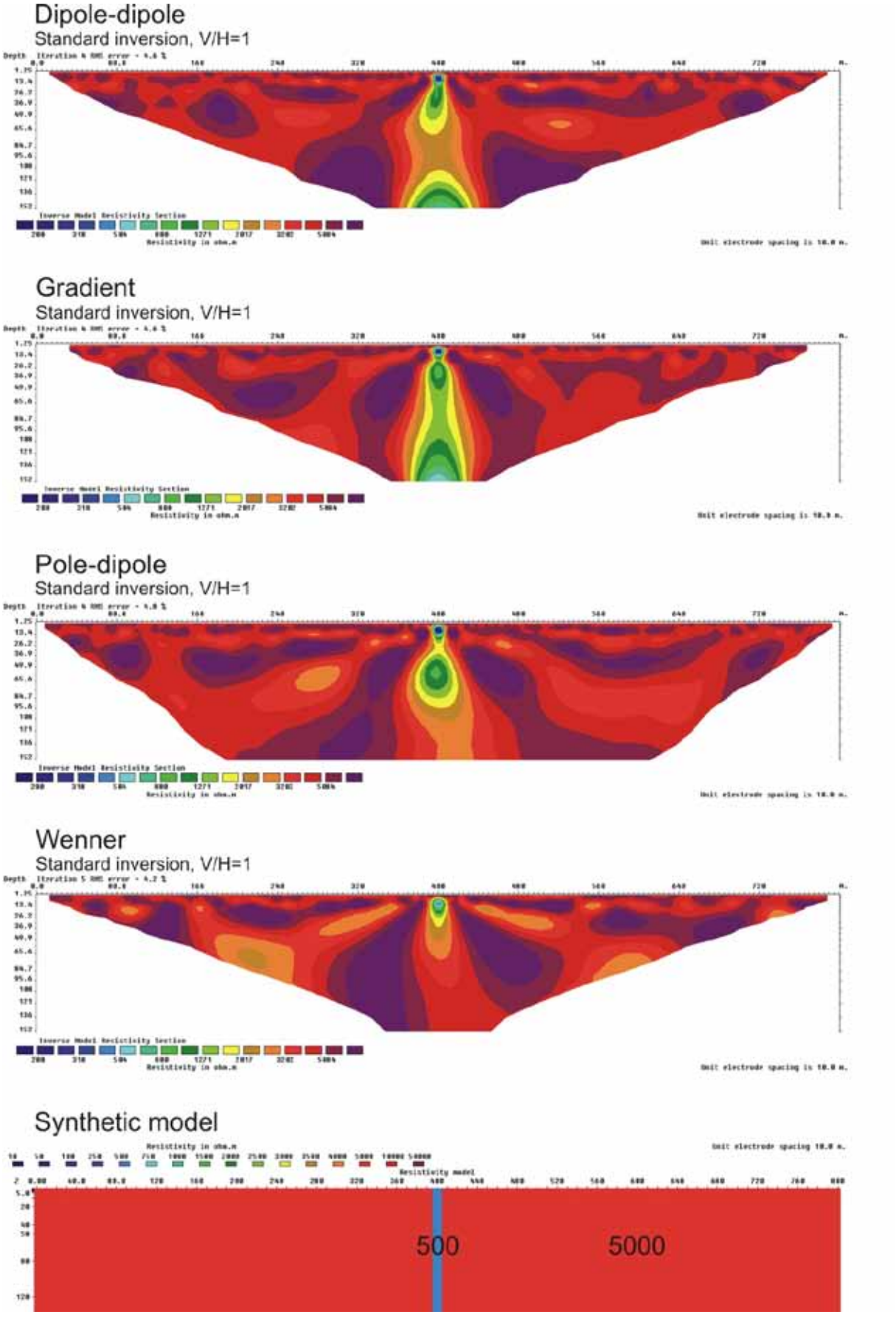

Figure 3.2.13: 10 m zone (500 ohmm), V/H=1

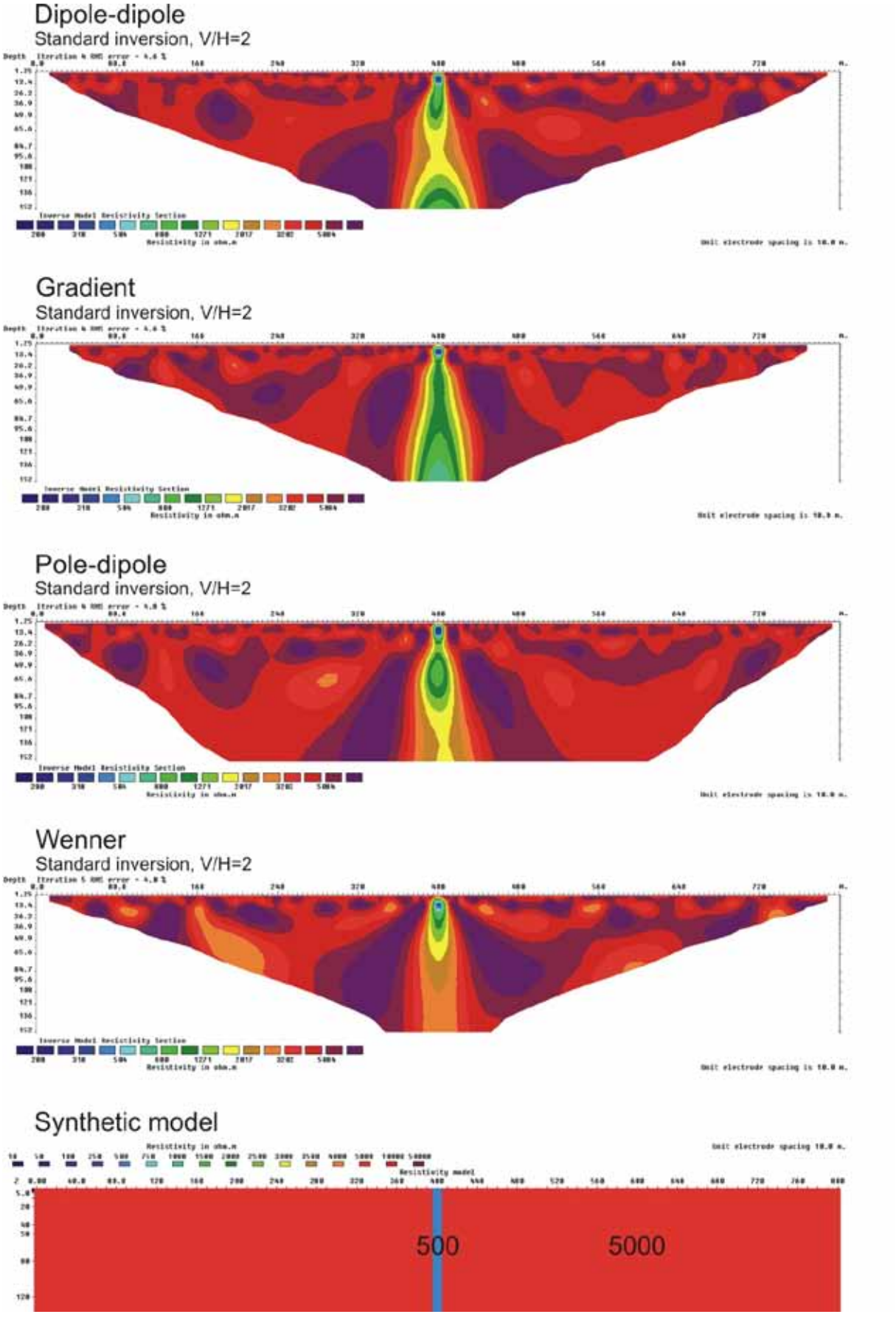

Figure 3.2.14: 10 m zone (500 ohmm), V/H=2

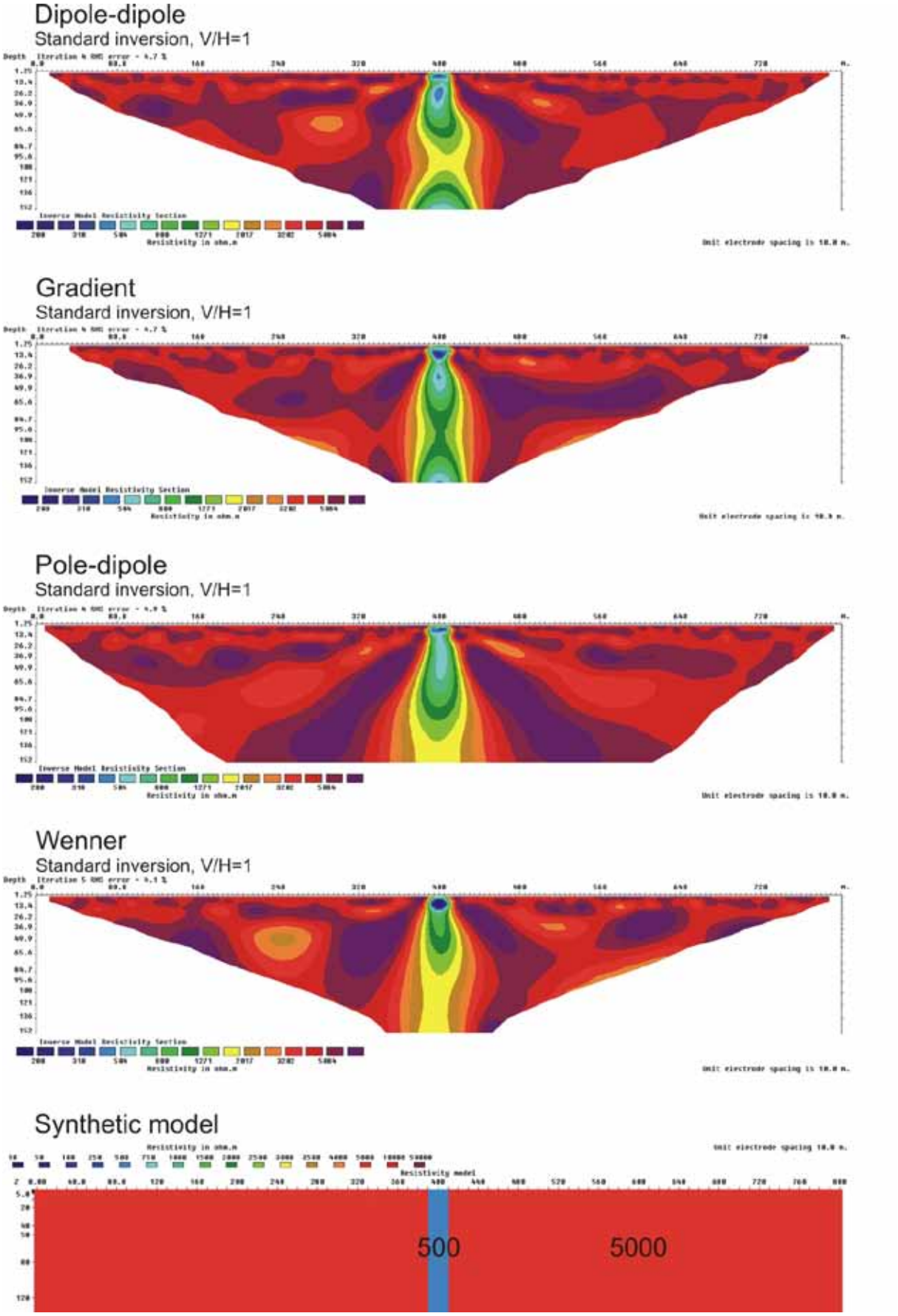

Figure 3.2.15: 20 m zone (500 ohmm), V/H=1

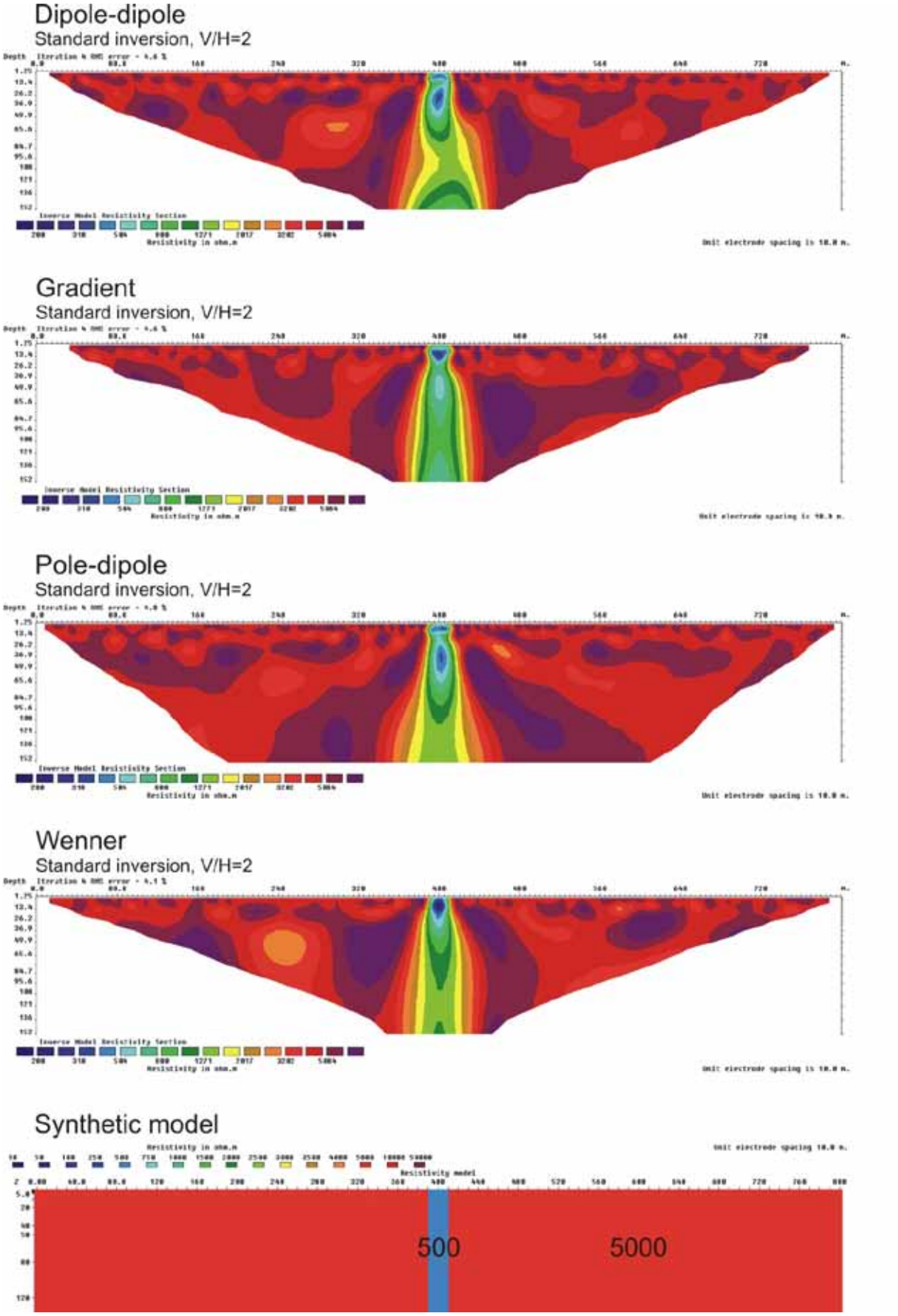

Figure 3.2.16: 20 m zone (500 ohmm), V/H=2

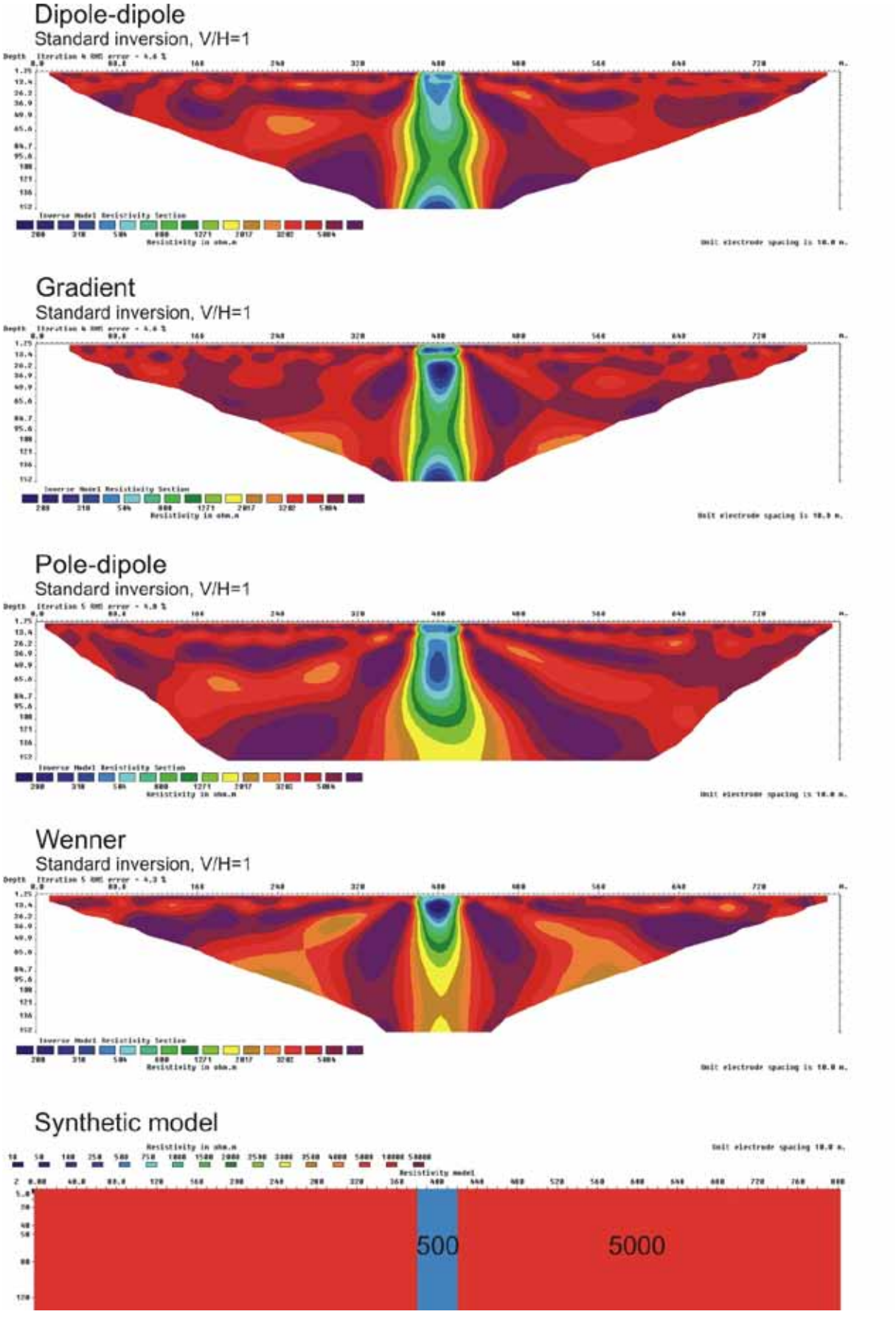

Figure 3.2.17: 40 m zone (500 ohmm), V/H=1

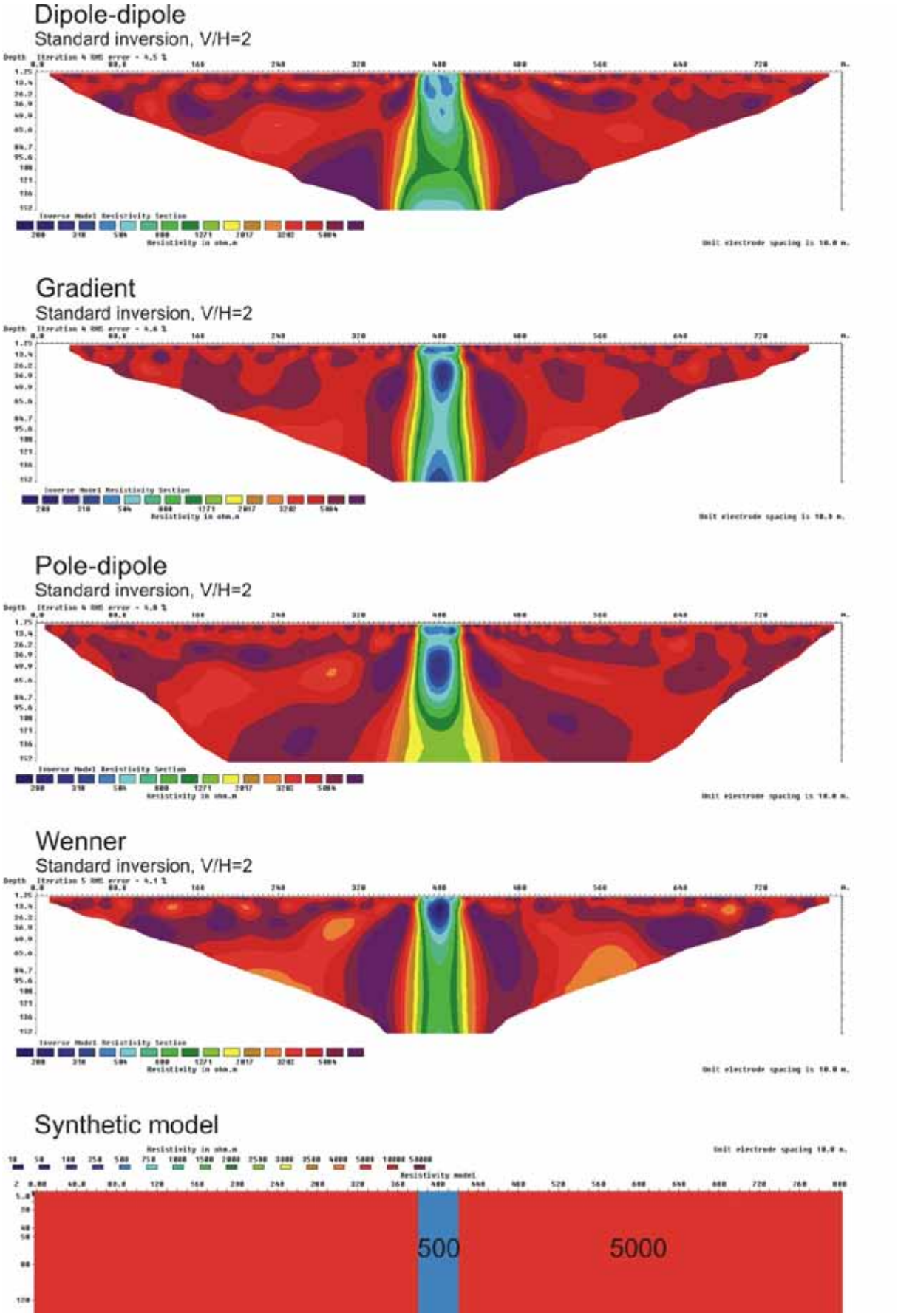

Figure 3.2.18: 40 m zone (500 ohmm), V/H=2

Modelling results: Vertical Fracture Zone – Different Contrast

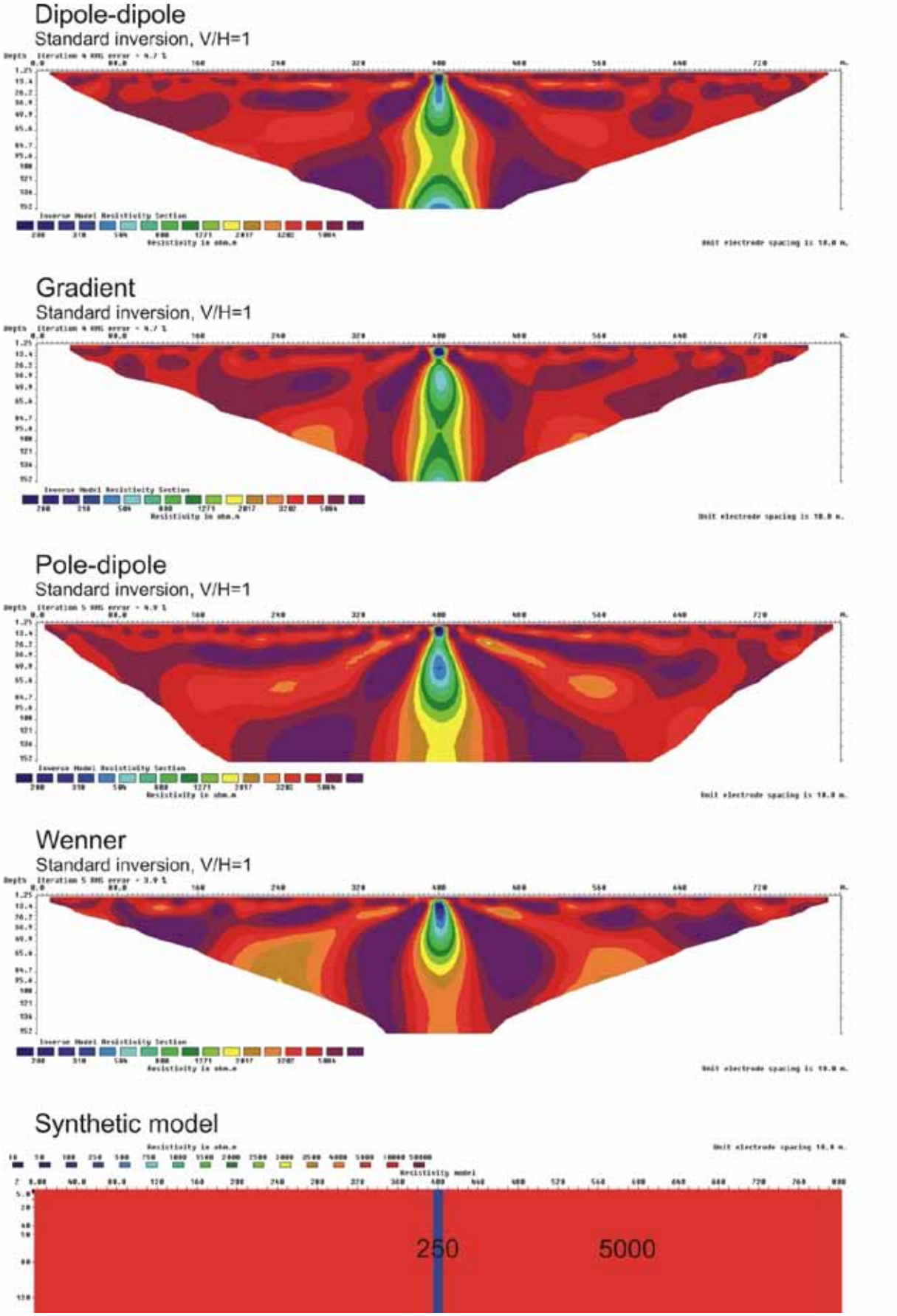

Figure 3.3.19: 10 m zone (250 ohmm) in bedrock (5000 ohmm), V/H=1

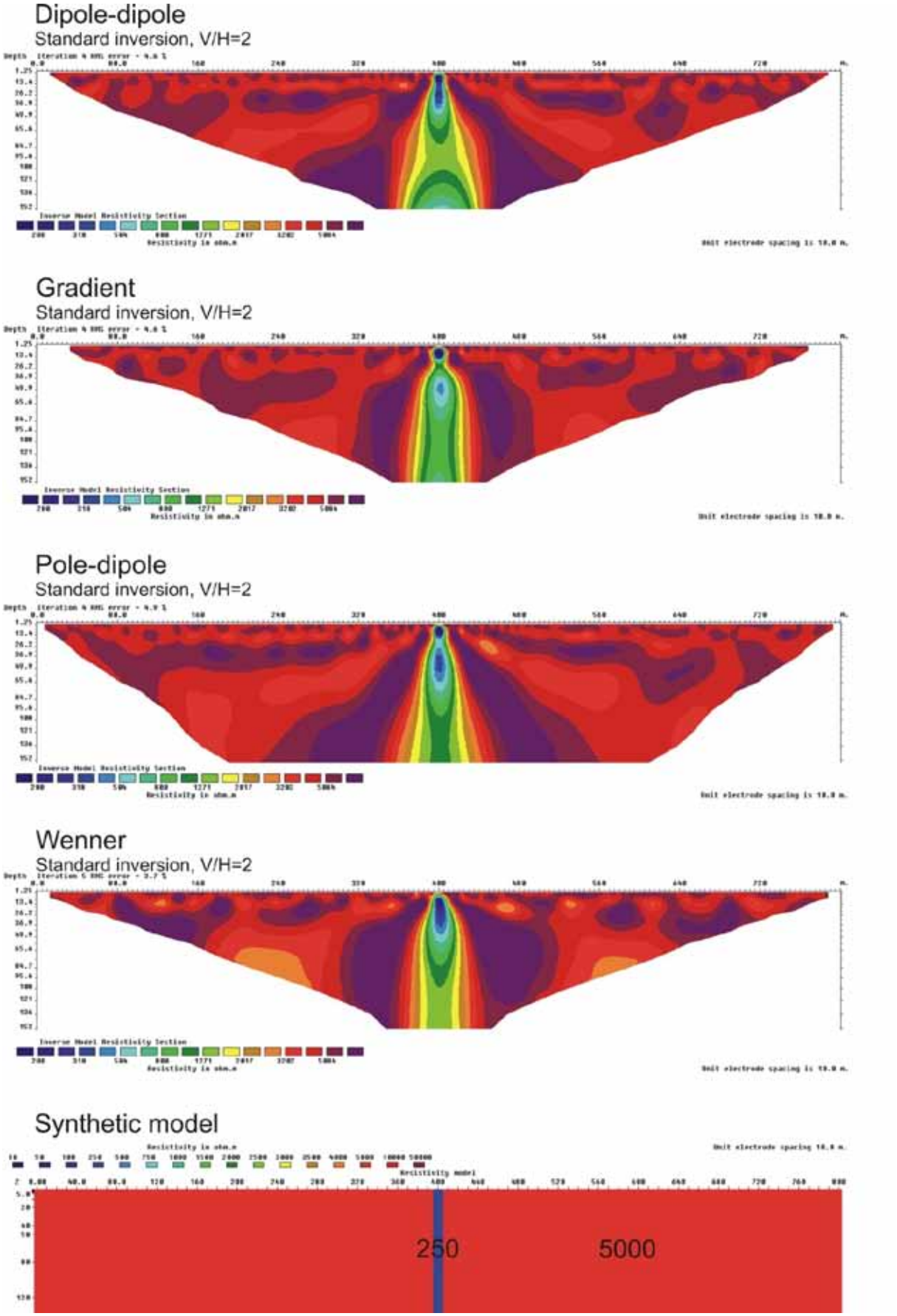

Figure 3.3.20: 10 m zone (250 ohmm) in bedrock (5000 ohmm), V/H=2

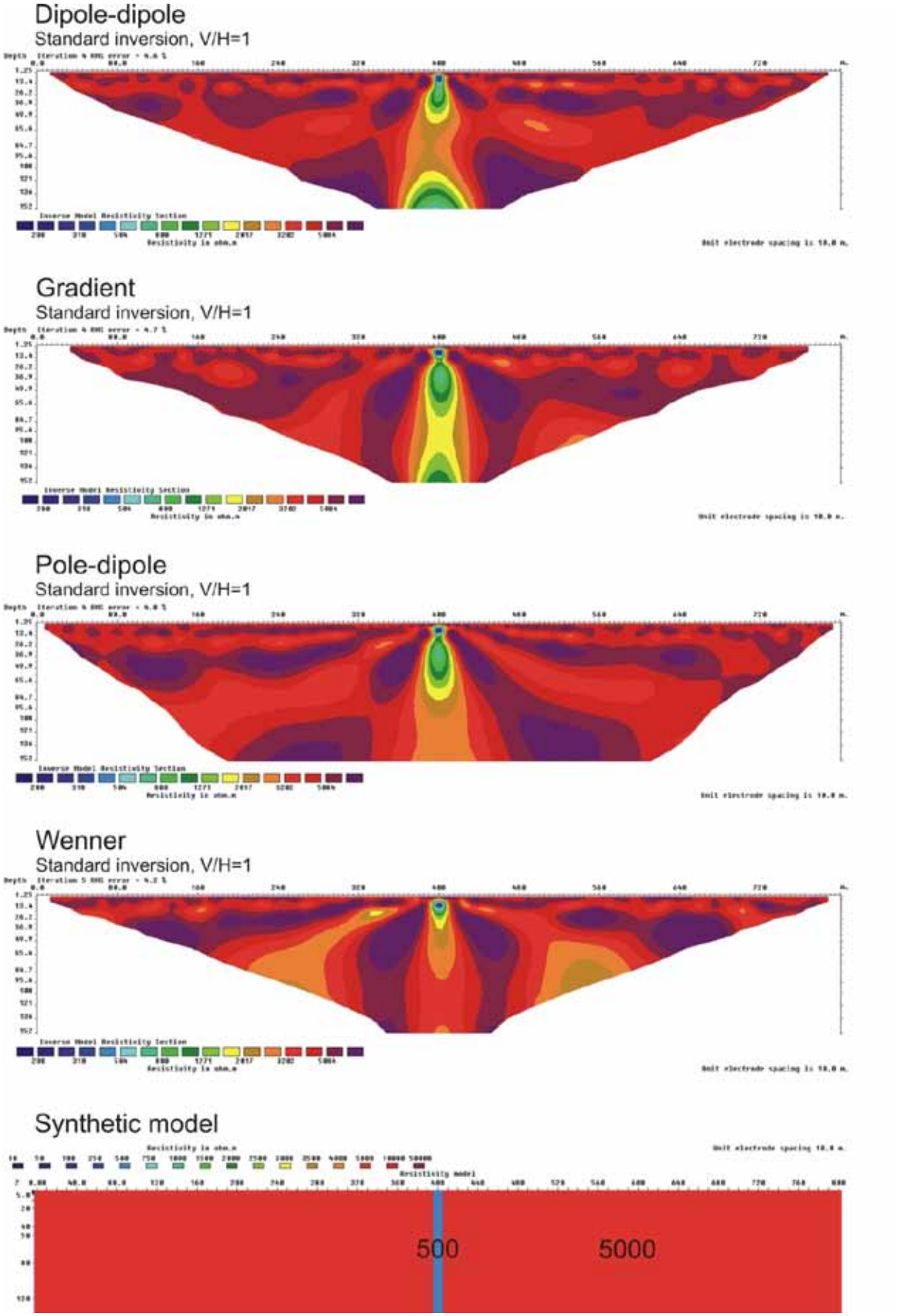

Figure 3.3.21: 10 m zone (500 ohmm) in bedrock (5000 ohmm), V/H=1

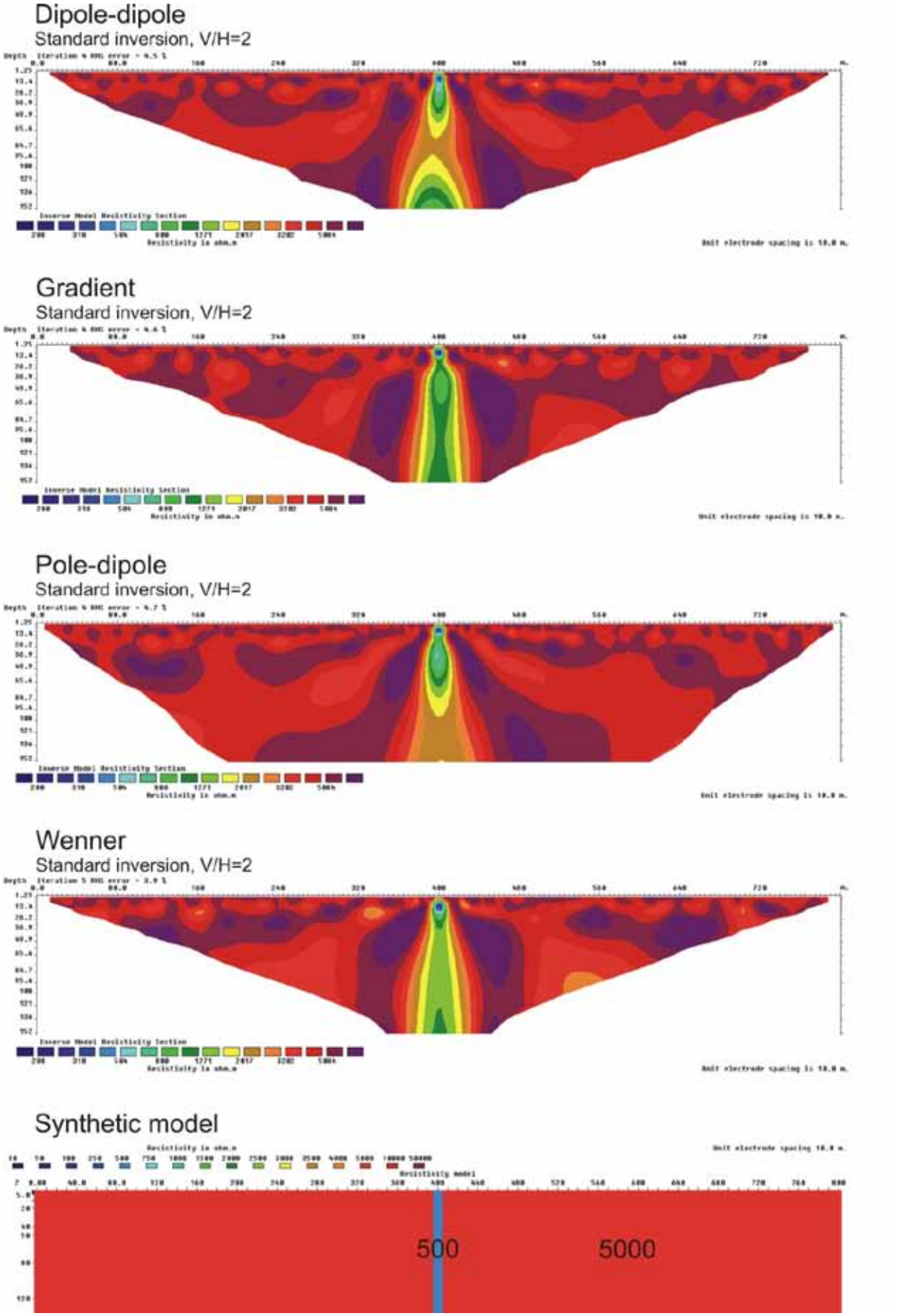

Figure 3.3.22: 10 m zone (500 ohmm) in bedrock (5000 ohmm), V/H=2

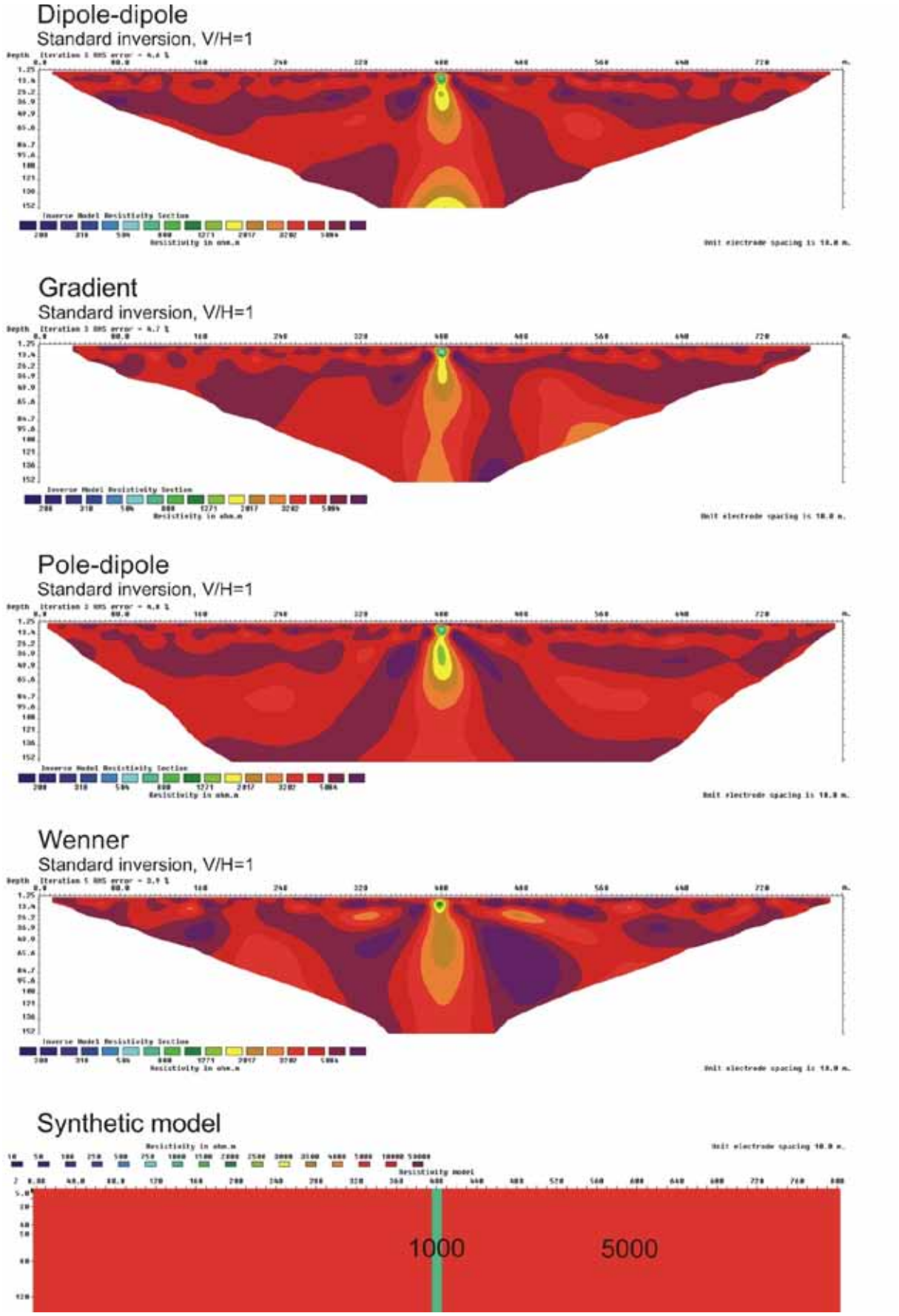

Figure 3.3.23: 10 m zone (1000 ohmm) in bedrock (5000 ohmm), V/H=1

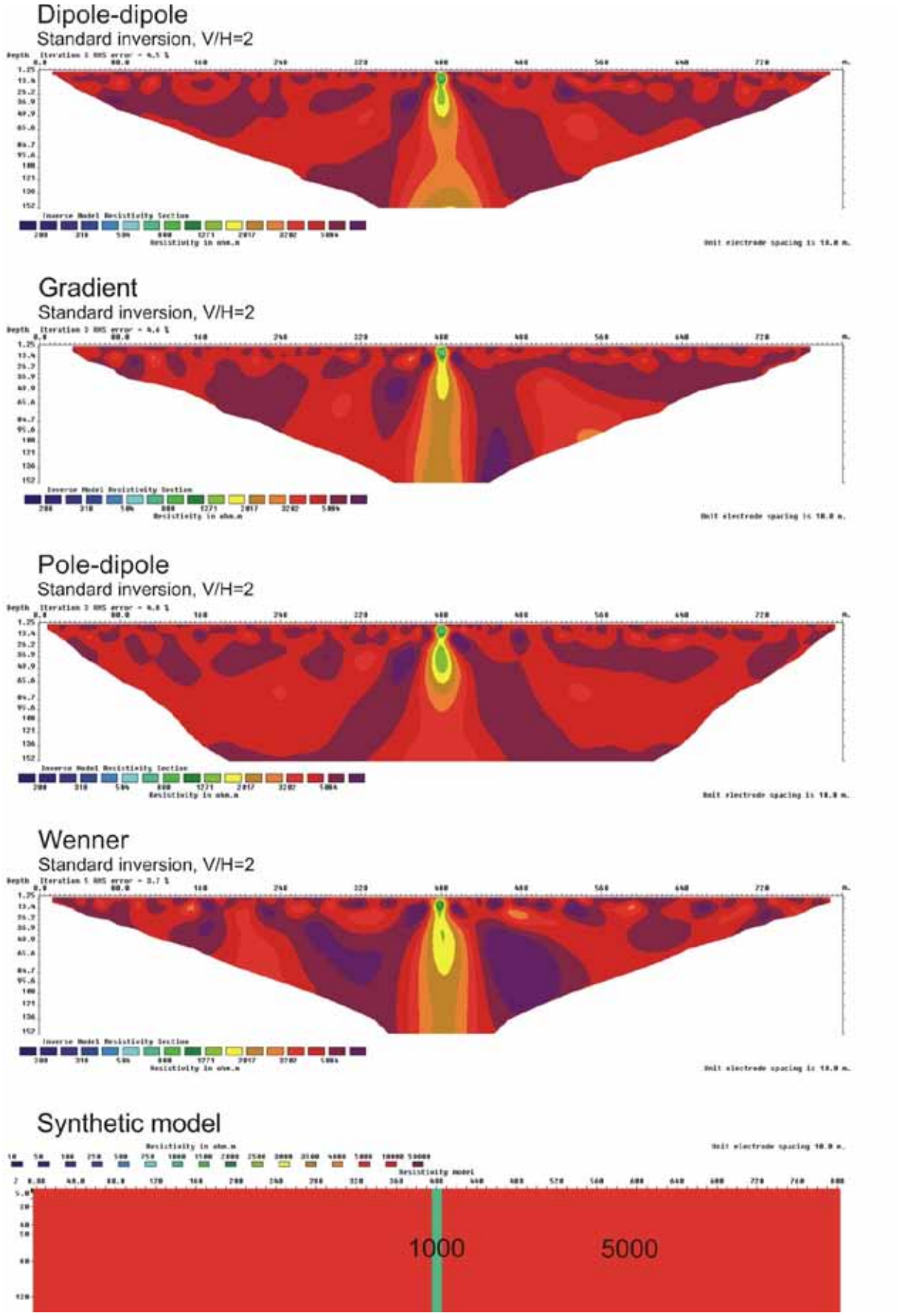

Figure 3.3.24: 10 m zone (1000 ohmm) in bedrock (5000 ohmm), V/H=2

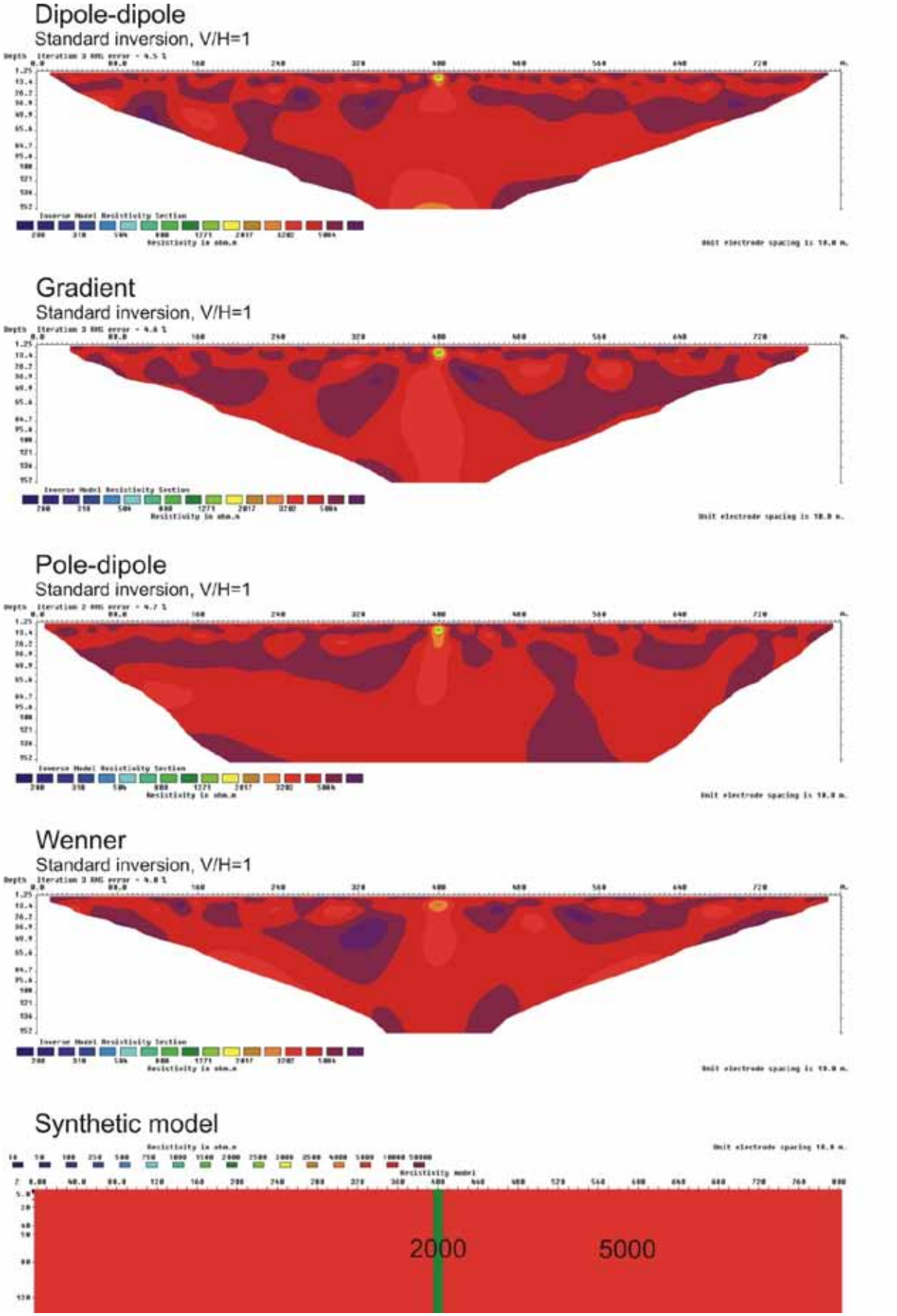

Figure 3.3.25: 10 m zone (2000 ohmm) in bedrock (5000 ohmm), V/H=1

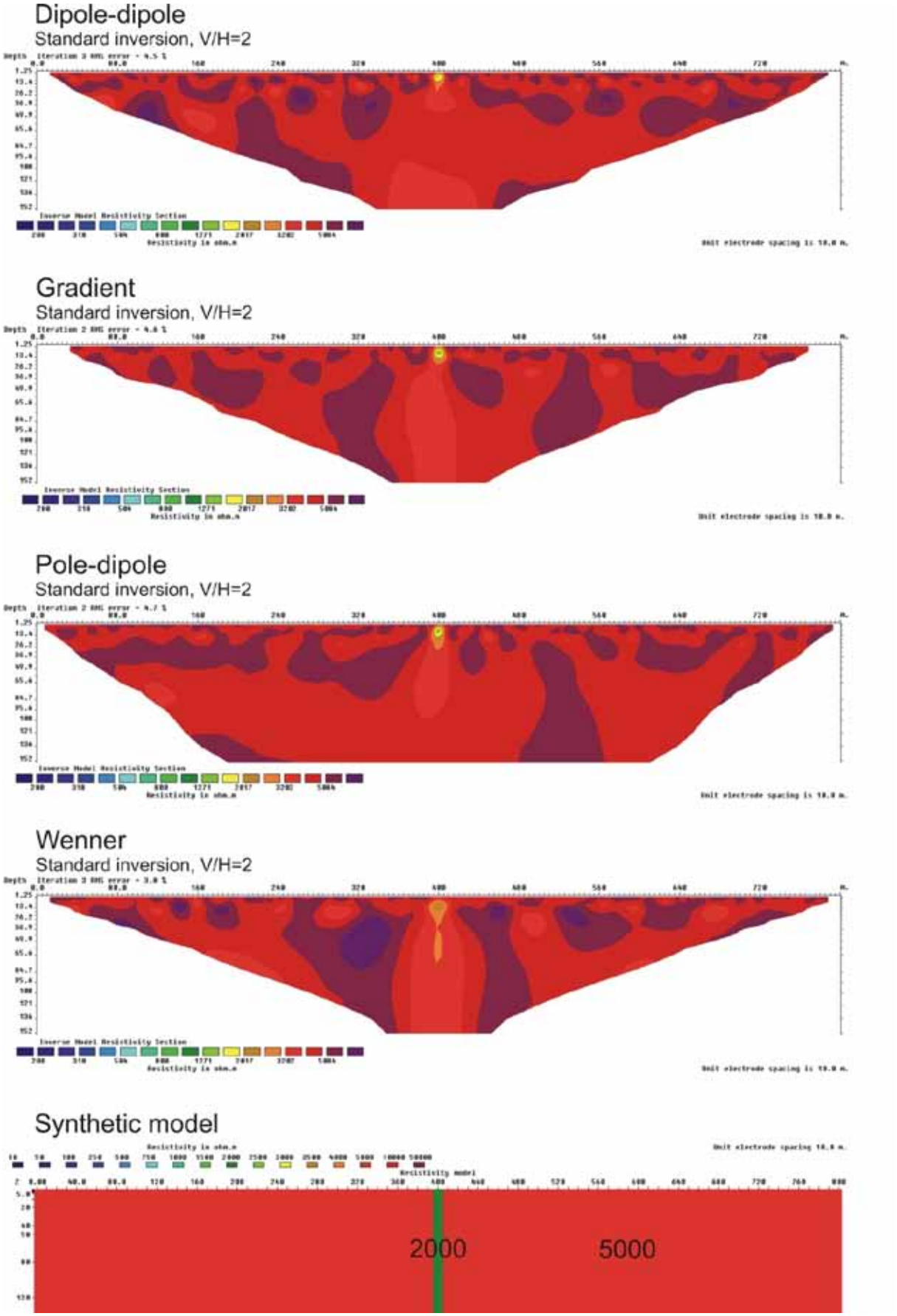

Figure 3.3.26: 10 m zone (2000 ohmm) in bedrock (5000 ohmm), V/H=2

Modelling results: Fracture Zone – Different Dip

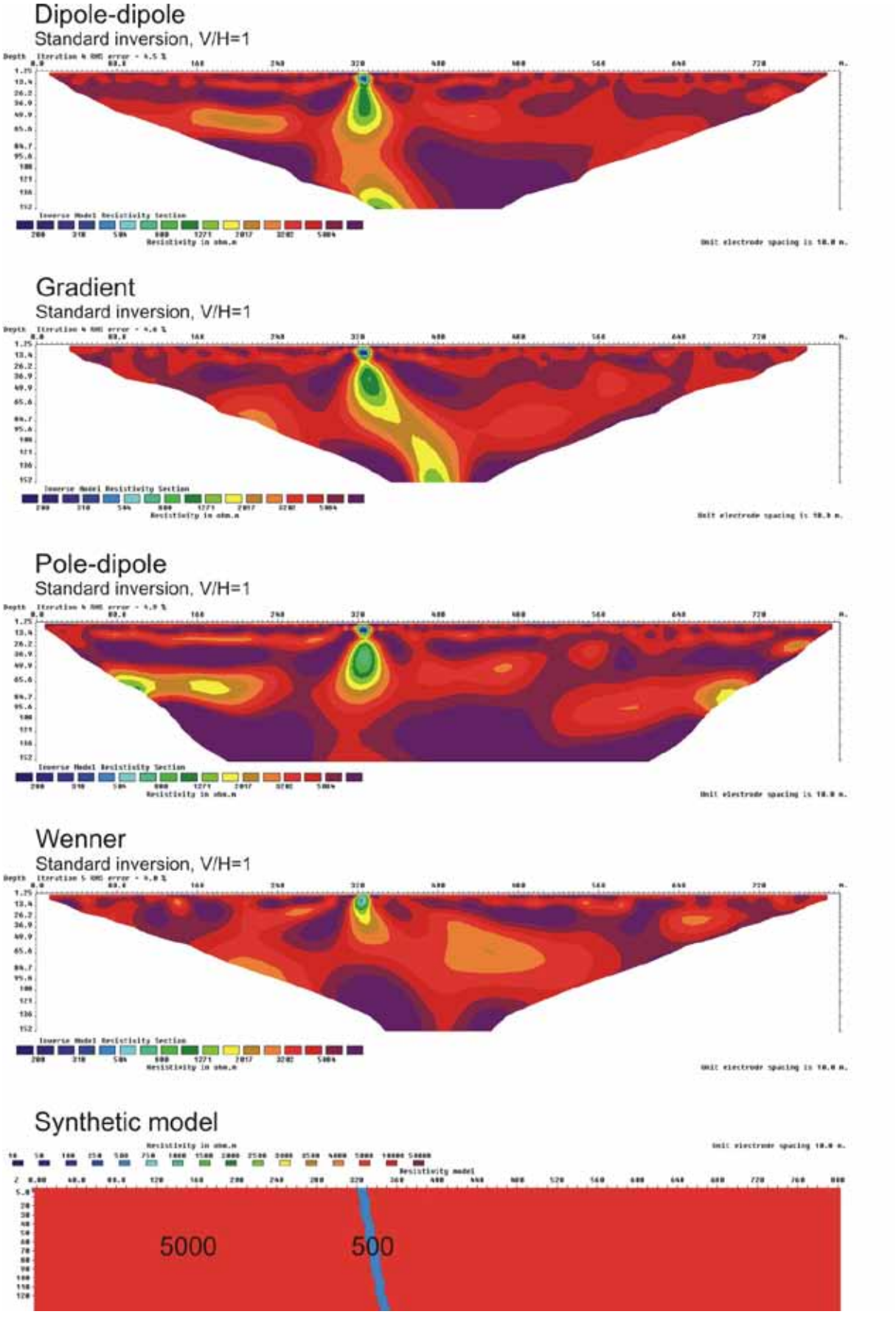

Figure 3.4.27: 10 m zone (500 ohmm) dipping with 80 degrees, V/H=1

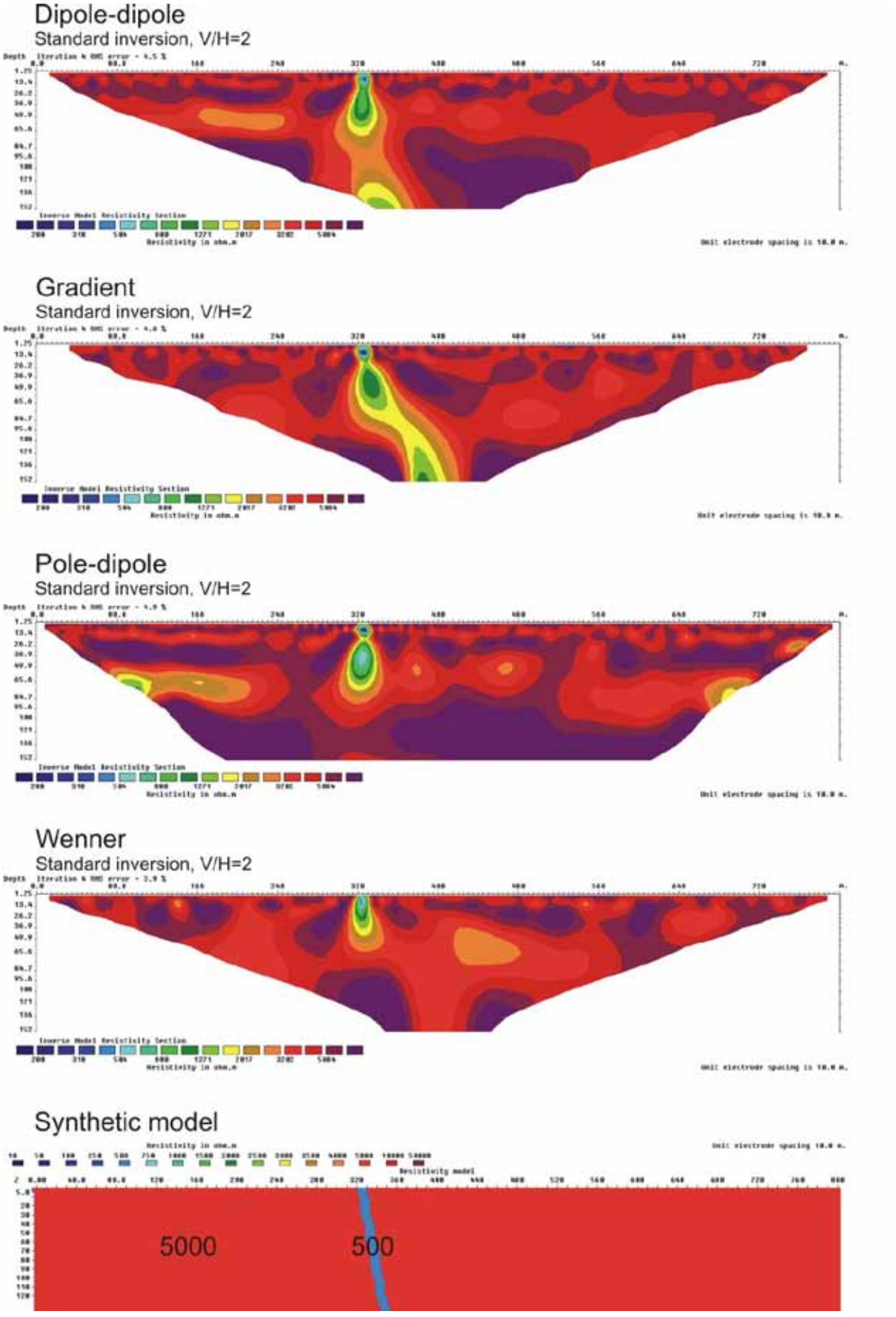

Figure 3.4.28: 10 m zone (500 ohmm) dipping with 80 degrees, V/H=2

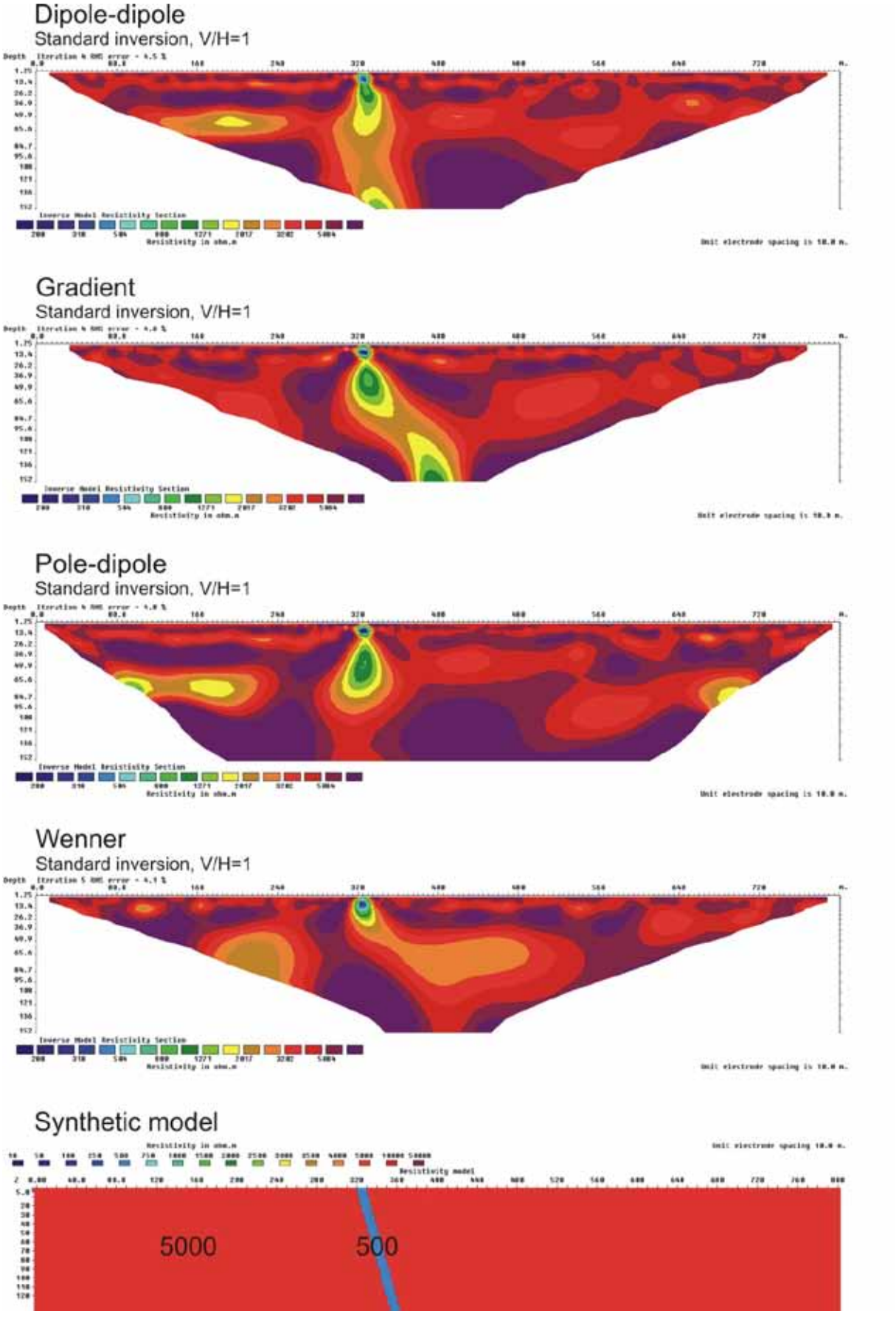

Figure 3.4.29: 10 m zone (500 ohmm) dipping with 75 degrees, V/H=1

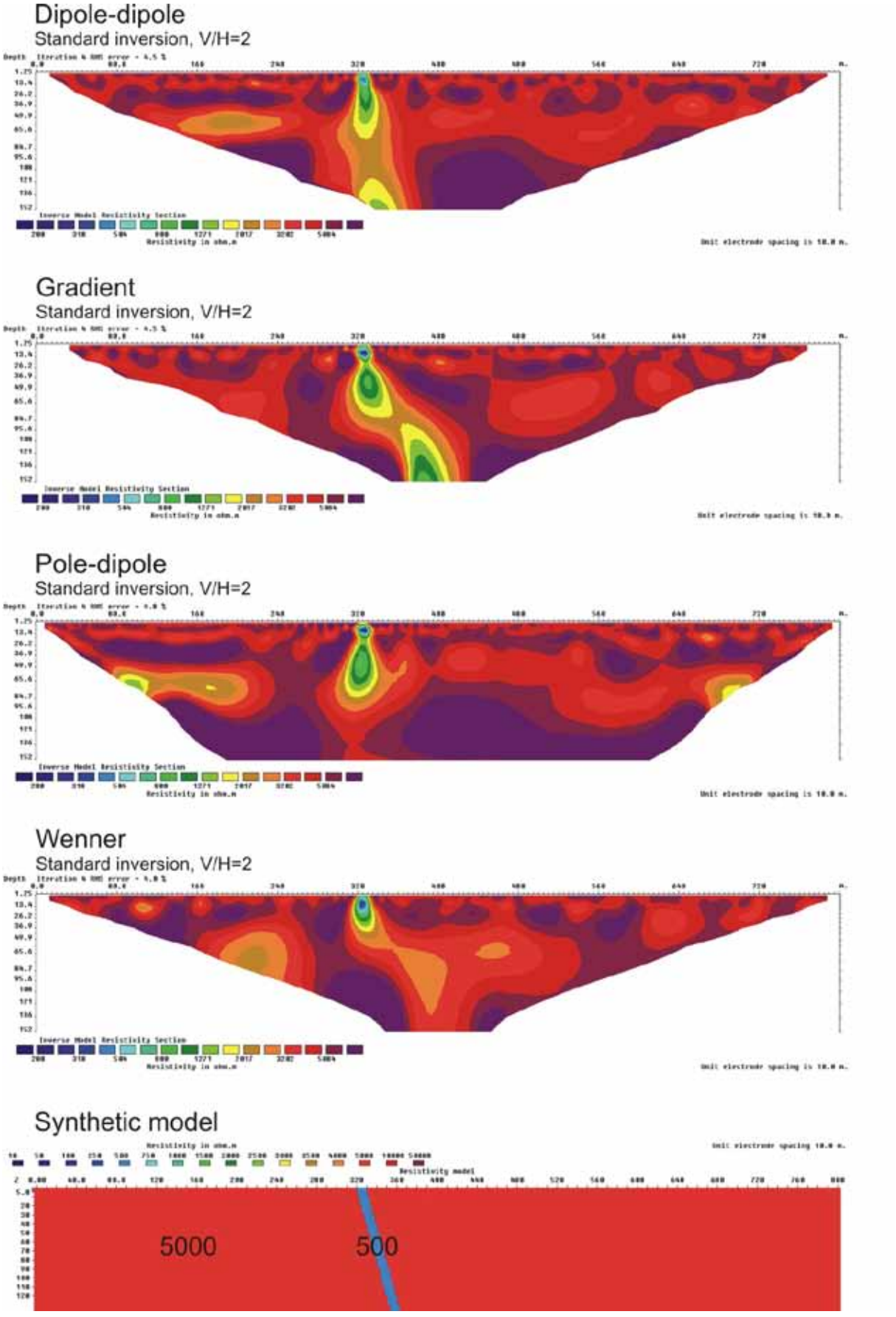

Figure 3.4.30: 10 m zone (500 ohmm) dipping with 75 degrees, V/H=2

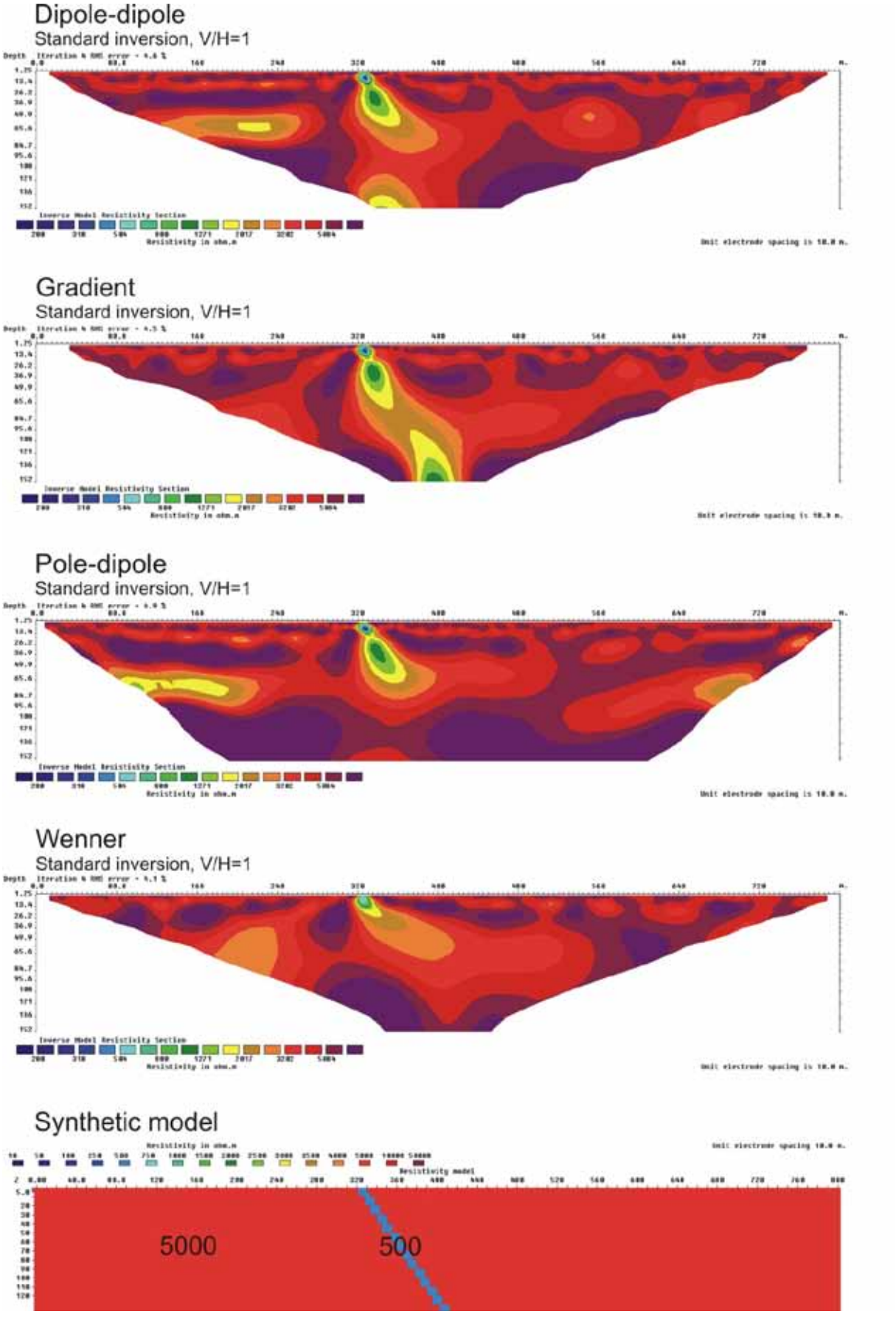

Figure 3.4.31: 10 m zone (500 ohmm) dipping with 60 degrees, V/H=1

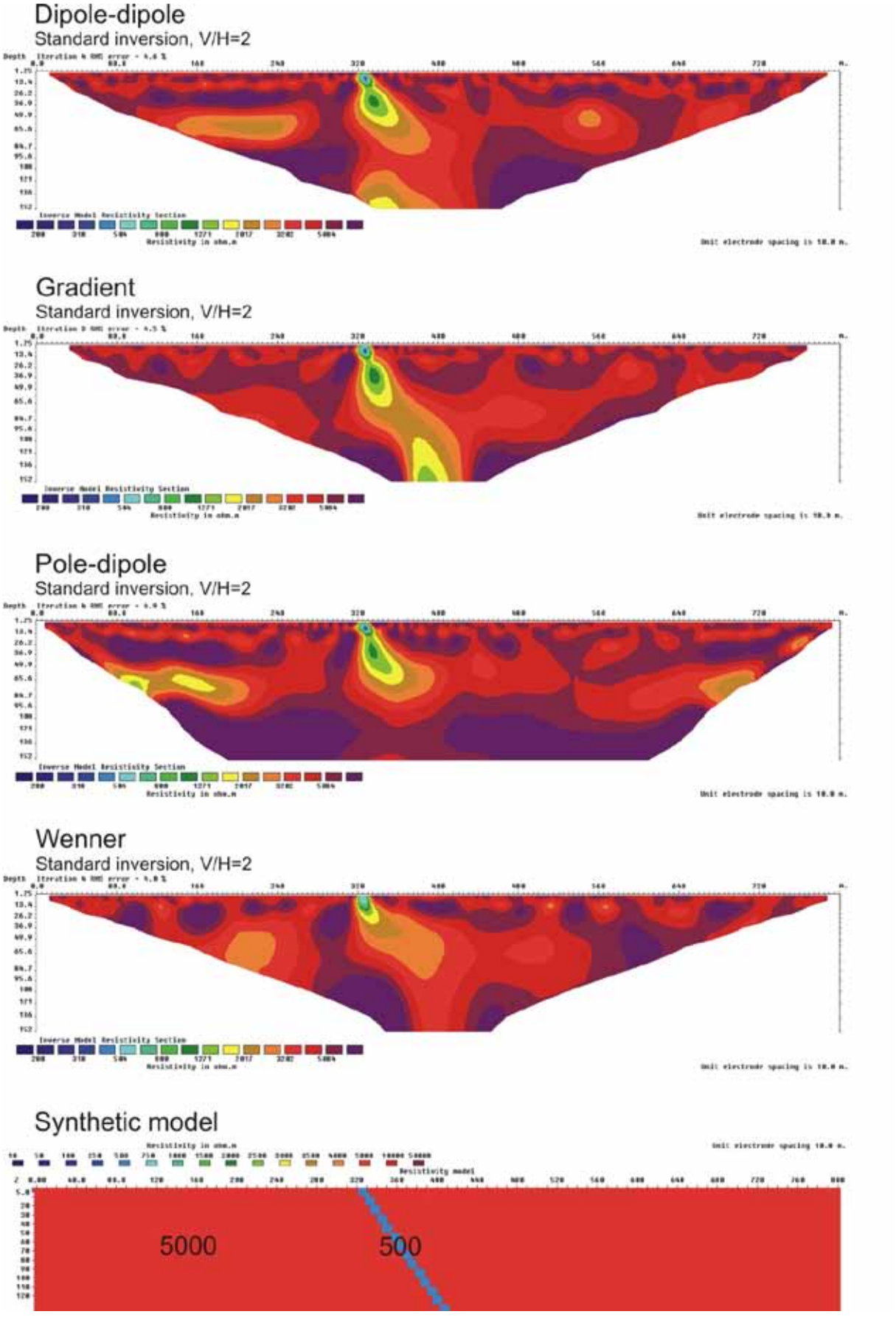

Figure 3.4.32: 10 m zone (500 ohmm) dipping with 60 degrees, V/H=2

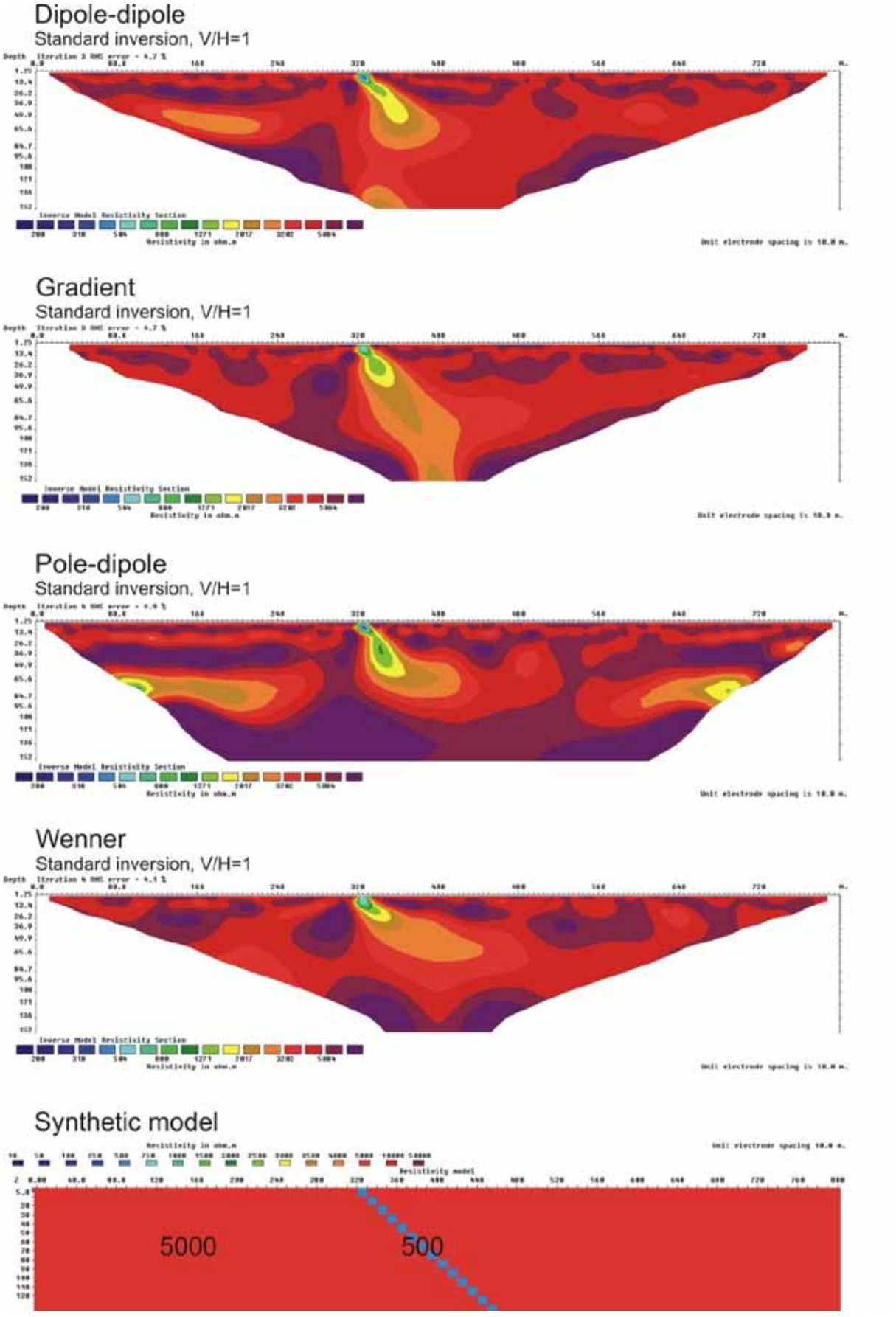

Figure 3.4.33: 10 m zone (500 ohmm) dipping with 45 degrees, V/H=1

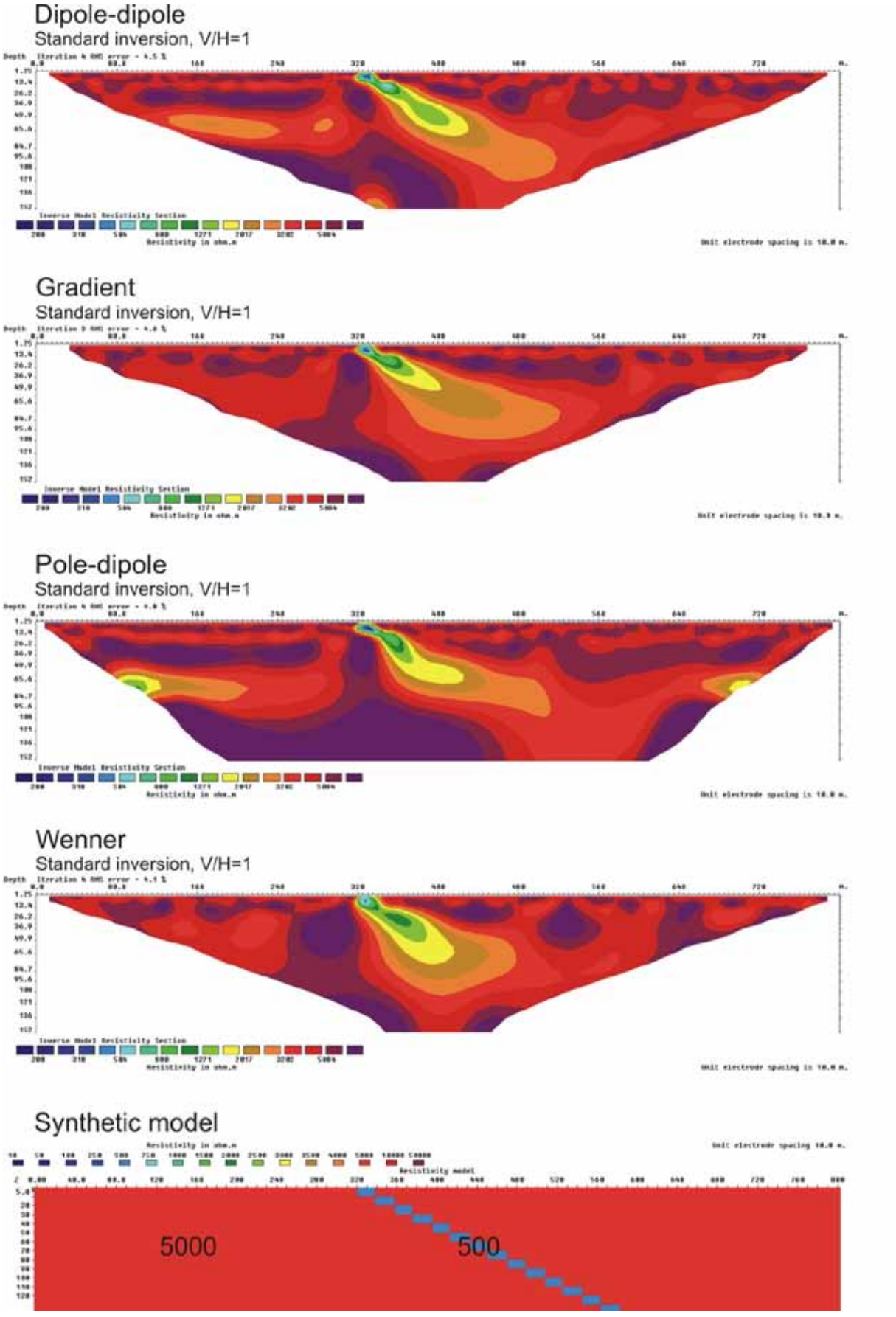

Figure 3.4.34: 10 m zone (500 ohmm) dipping with 30 degrees, V/H=1

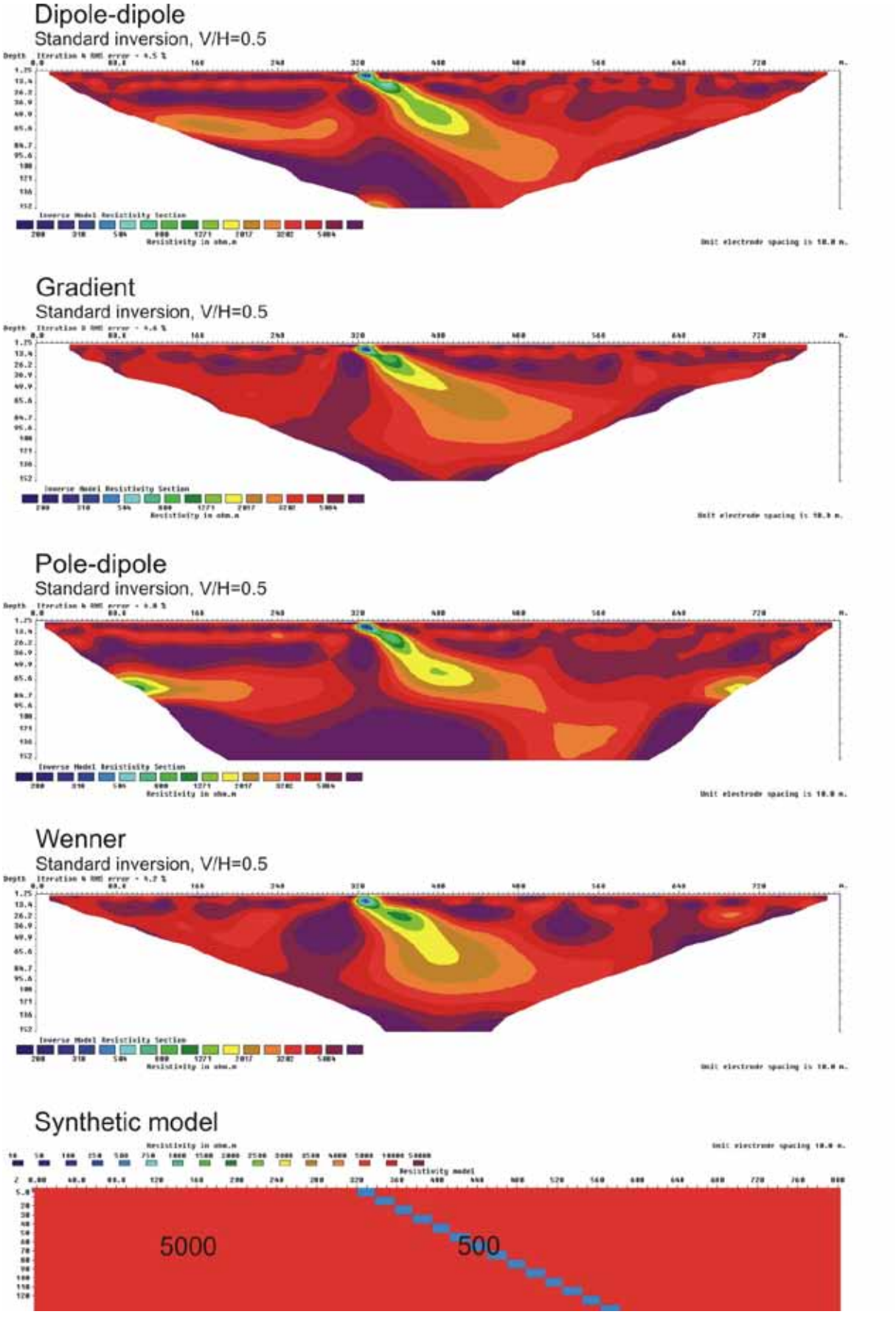

Figure 3.4.35: 10 m zone (500 ohmm) dipping with 30 degrees, V/H=0.5

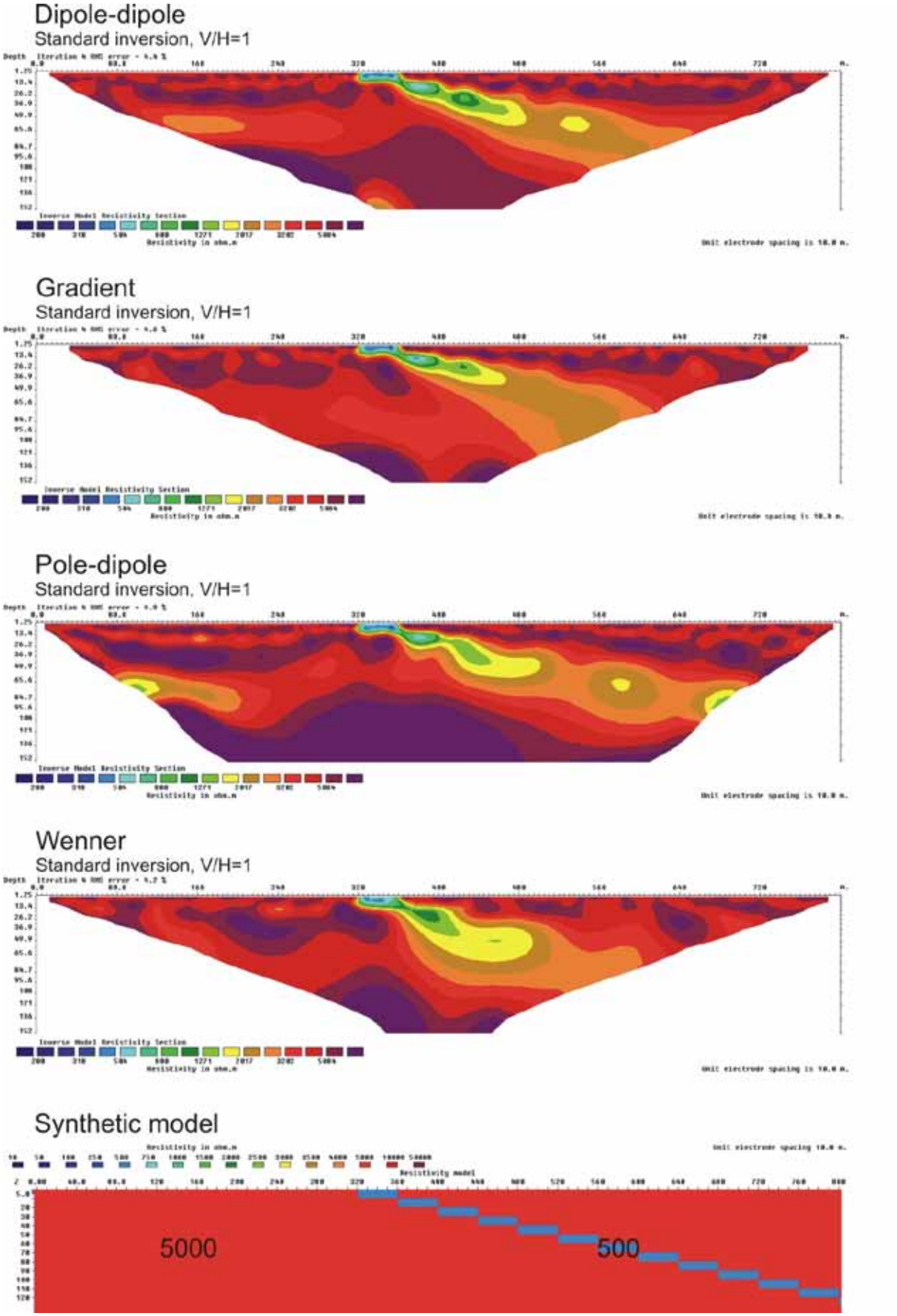

Figure 3.4.36: 10 m zone (500 ohmm) dipping with 15 degrees, V/H=1

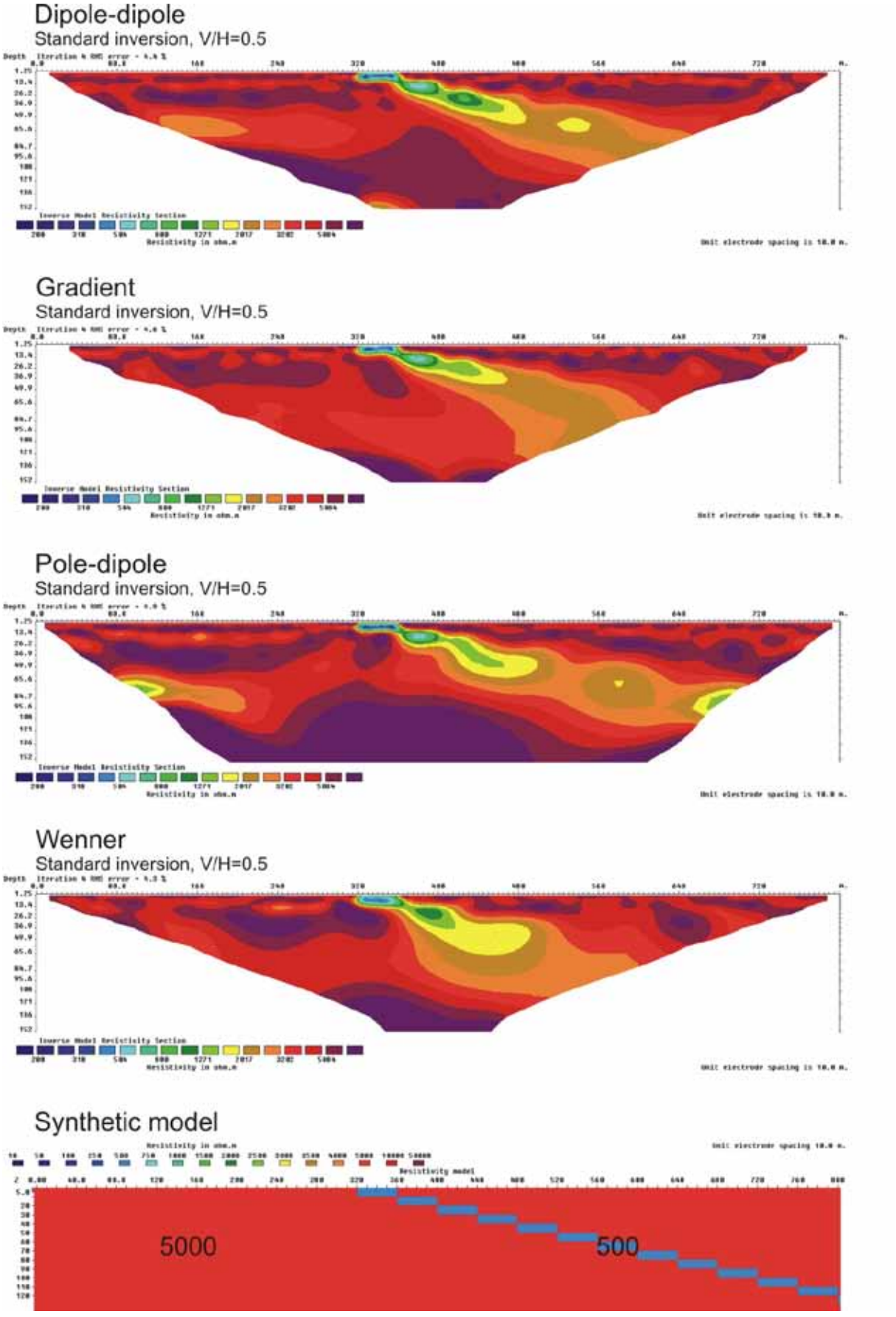

Figure 3.4.37: 10 m zone (500 ohmm) dipping with 15 degrees, V/H=0.5

Modelling results:

Vertical Fracture Zone – Different Top Layer Thickness and Resistivity

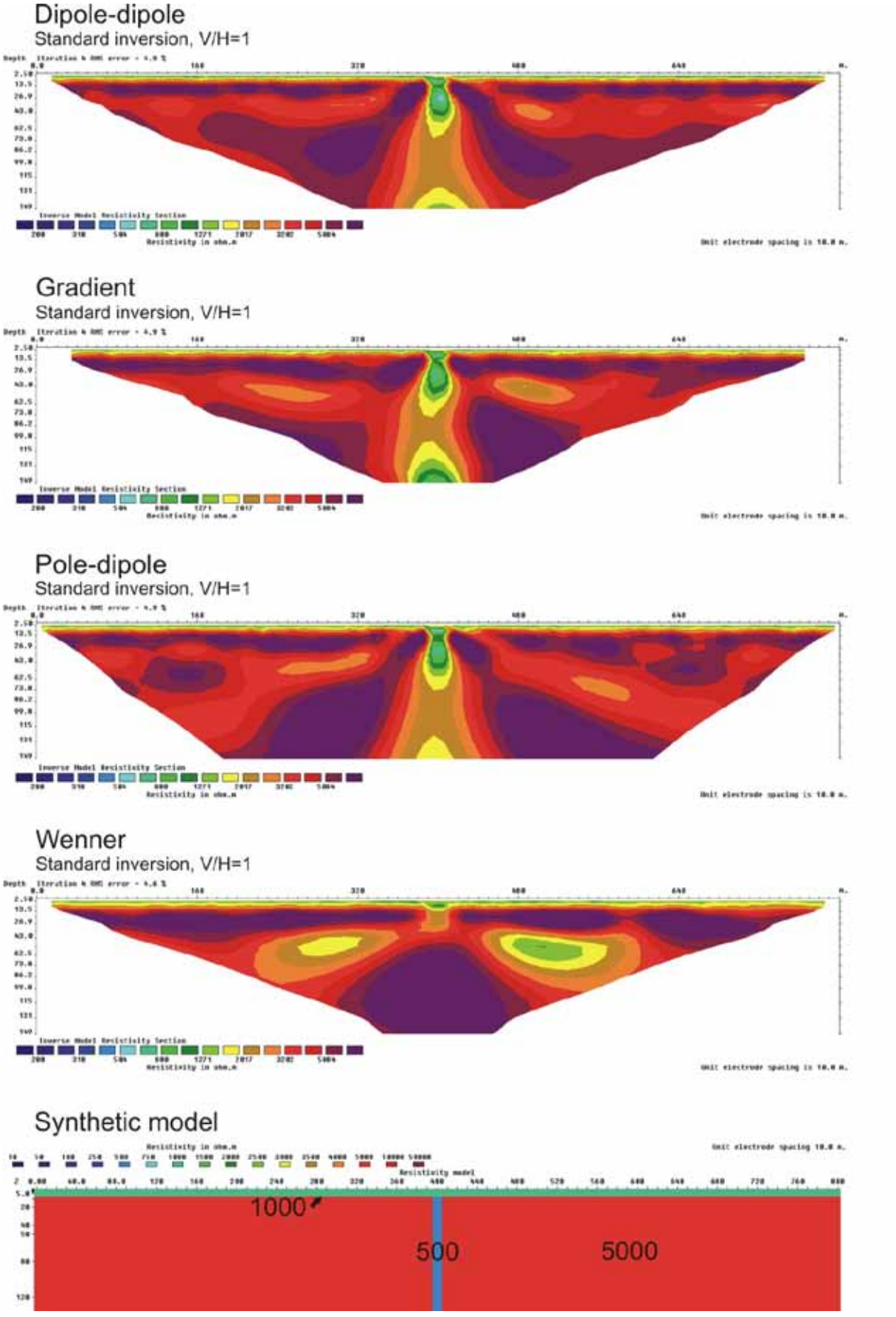

Figure 3.5.38: 10 m zone (500 ohmm) below a 5 m layer (1000 ohmm), V/H=1

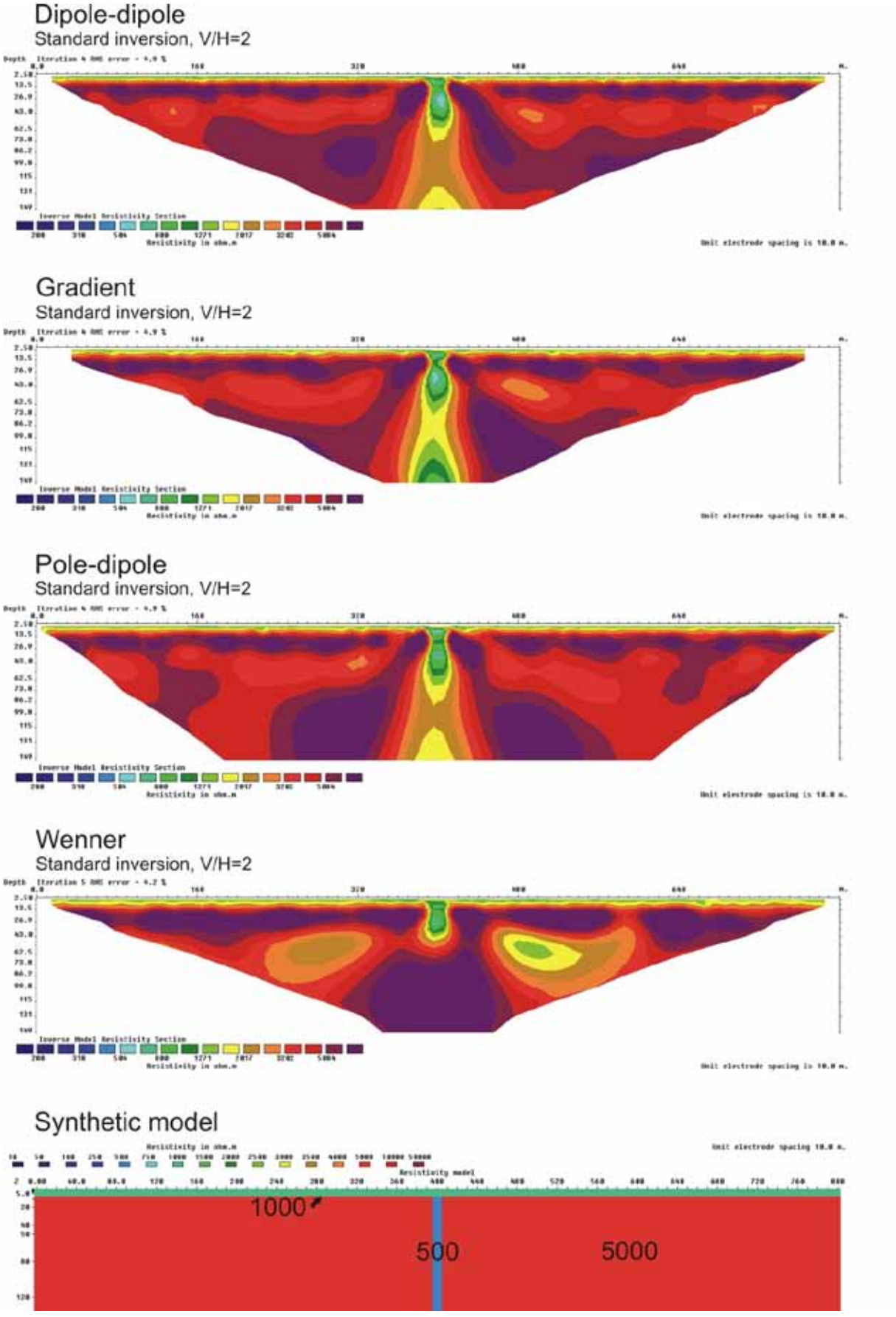

Figure 3.5.39: 10 m zone (500 ohmm) below a 5 m layer (1000 ohmm), V/H=2

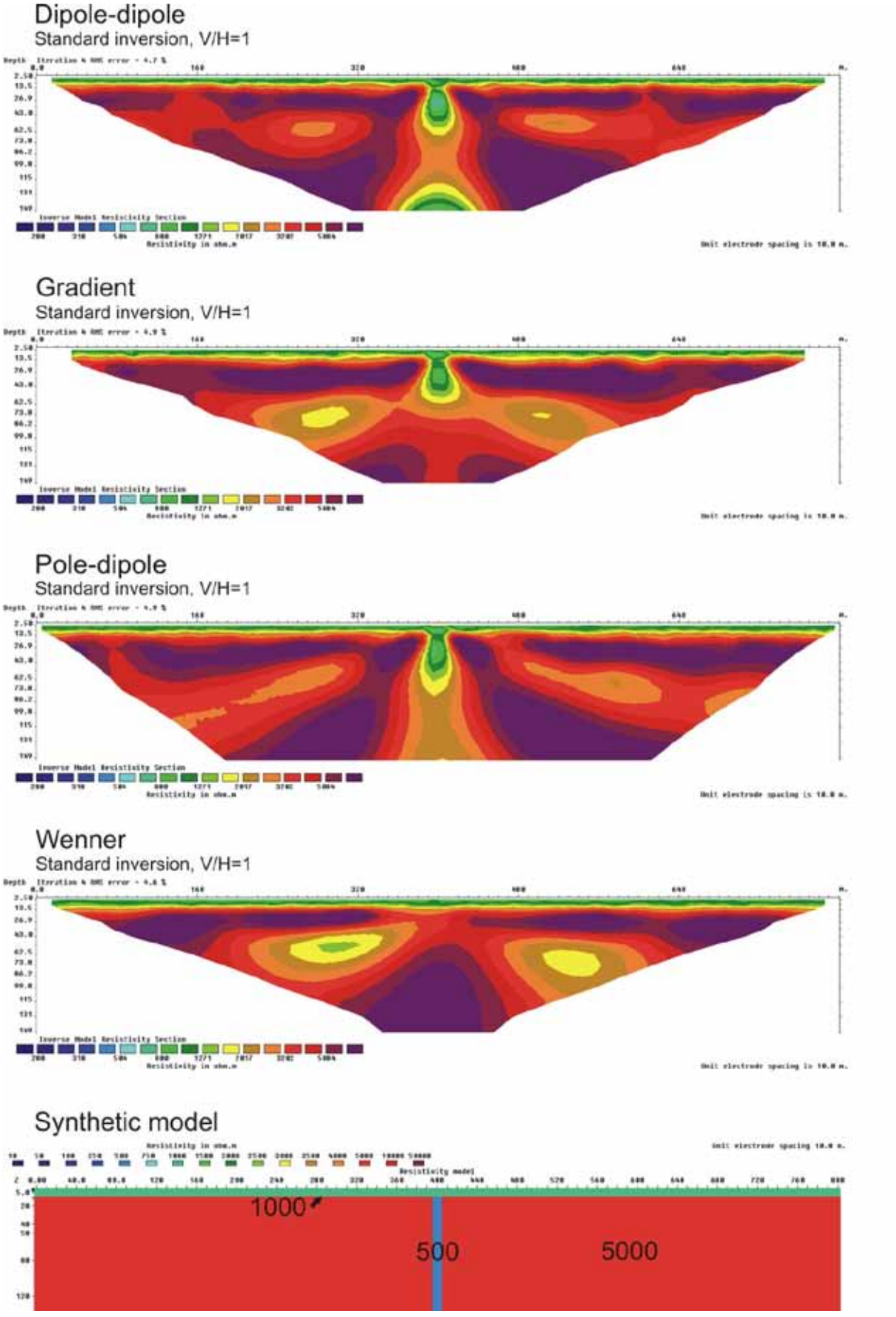

Figure 3.5.40: 10 m zone (500 ohmm) below a 10 m layer (1000 ohmm), V/H=1

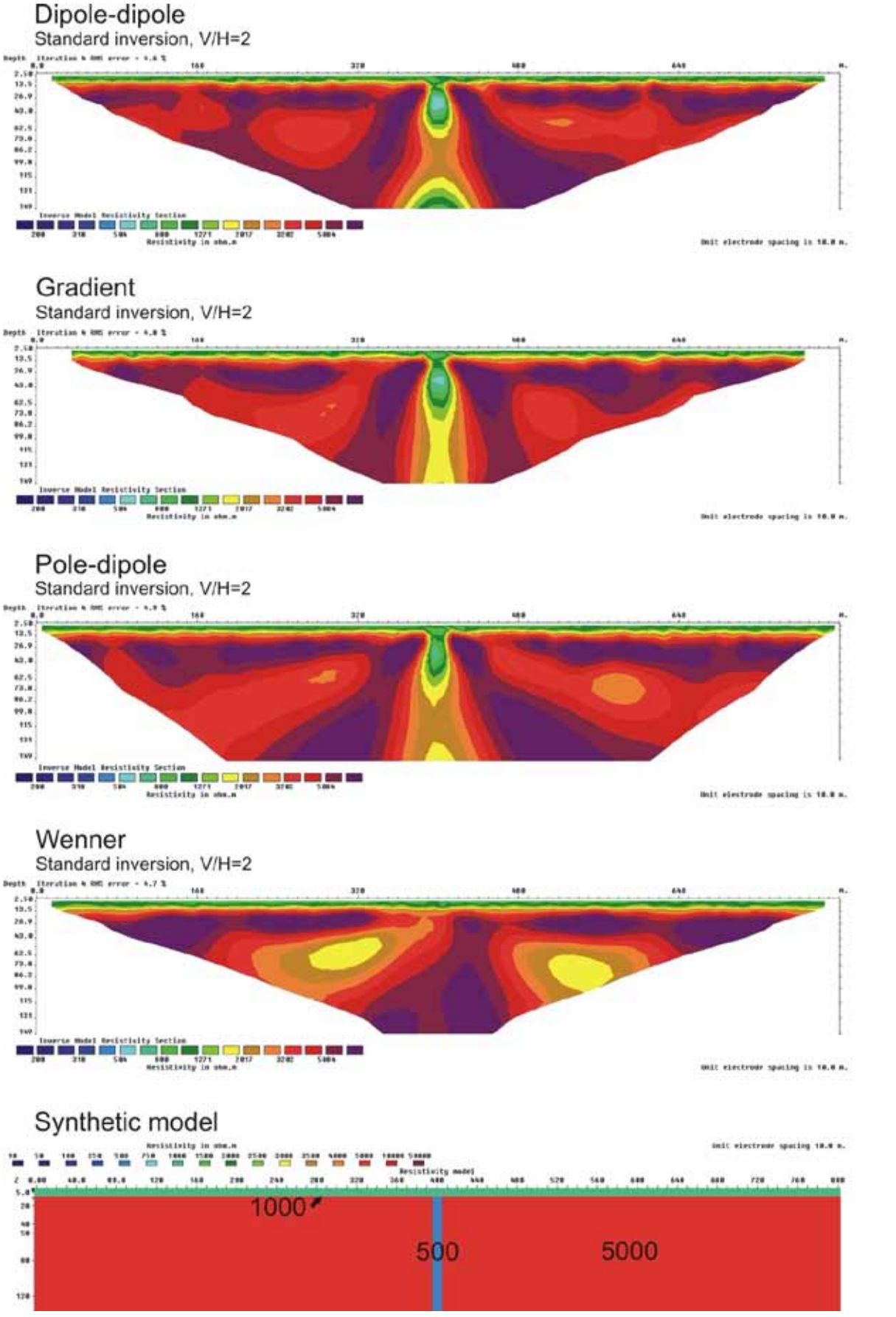

Figure 3.5.41: 10 m zone (500 ohmm) below a 10 m layer (1000 ohmm), V/H=2

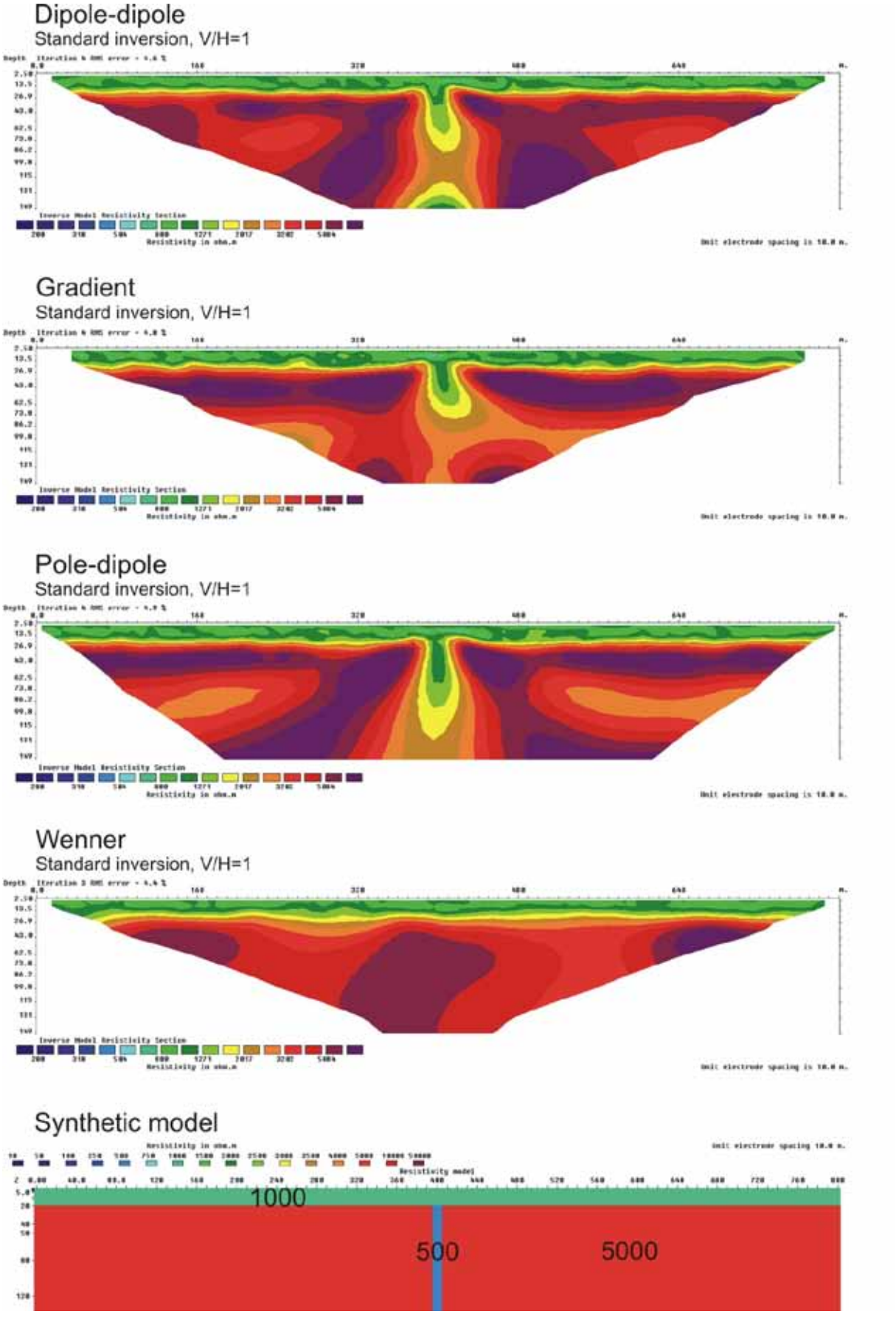

Figure 3.5.42: 10 m zone (500 ohmm) below a 20 m layer (1000 ohmm), V/H=1

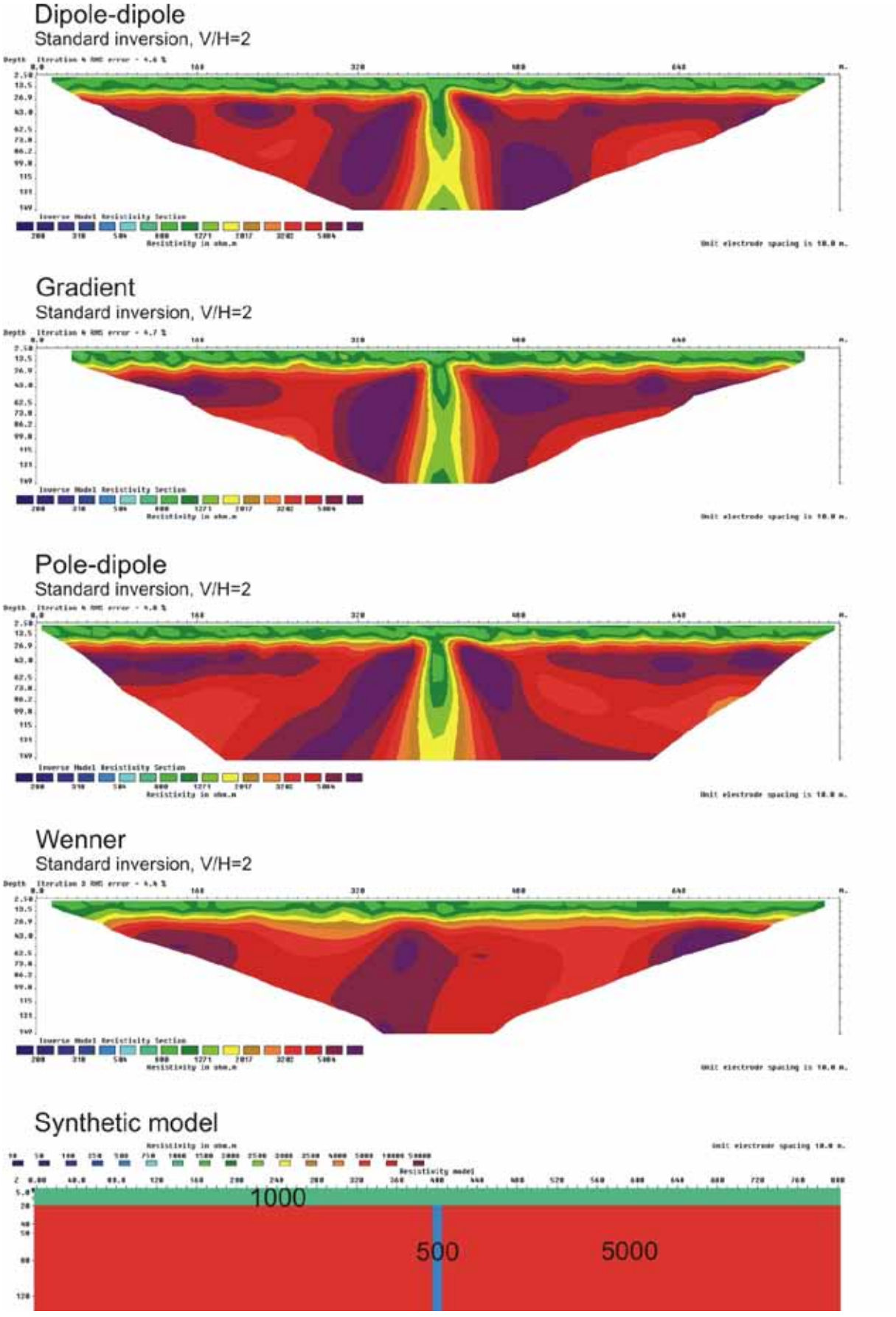

Figure 3.5.43: 10 m zone (500 ohmm) below a 20 m layer (1000 ohmm), V/H=2

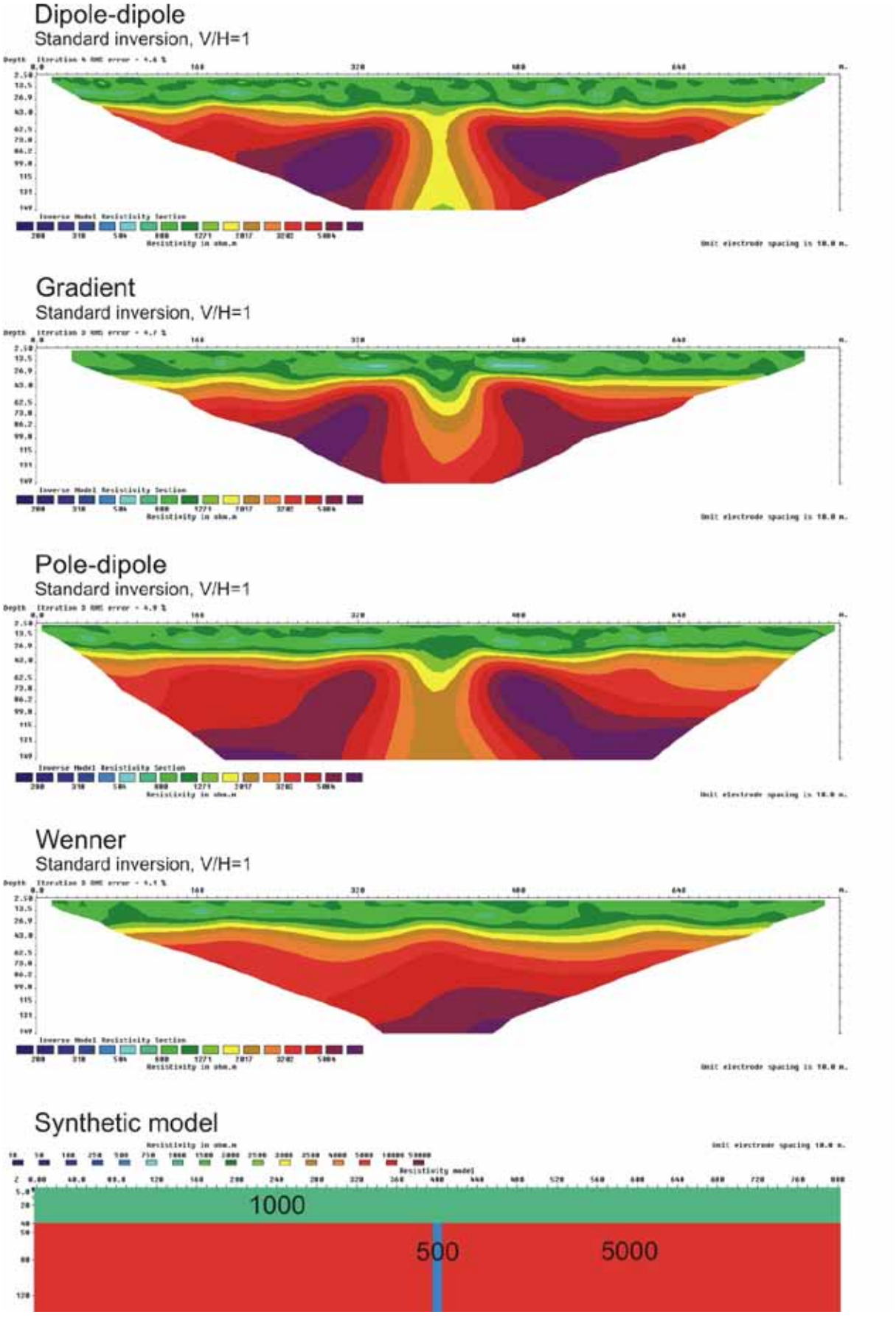

Figure 3.5.44: 10 m zone (500 ohmm) below a 40 m layer (1000 ohmm), V/H=1

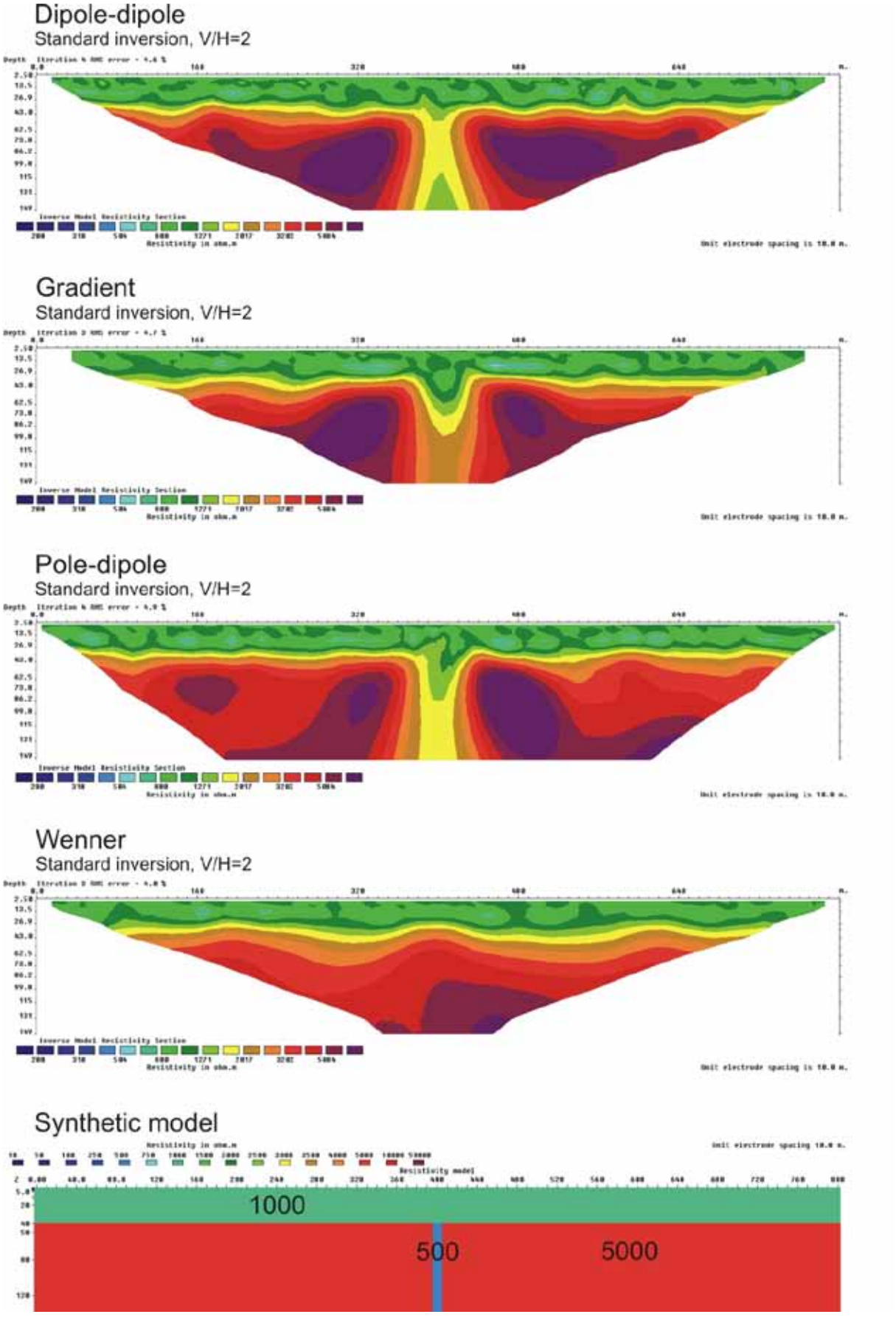

Figure 3.5.45: 10 m zone (500 ohmm) below a 40 m layer (1000 ohmm), V/H=2

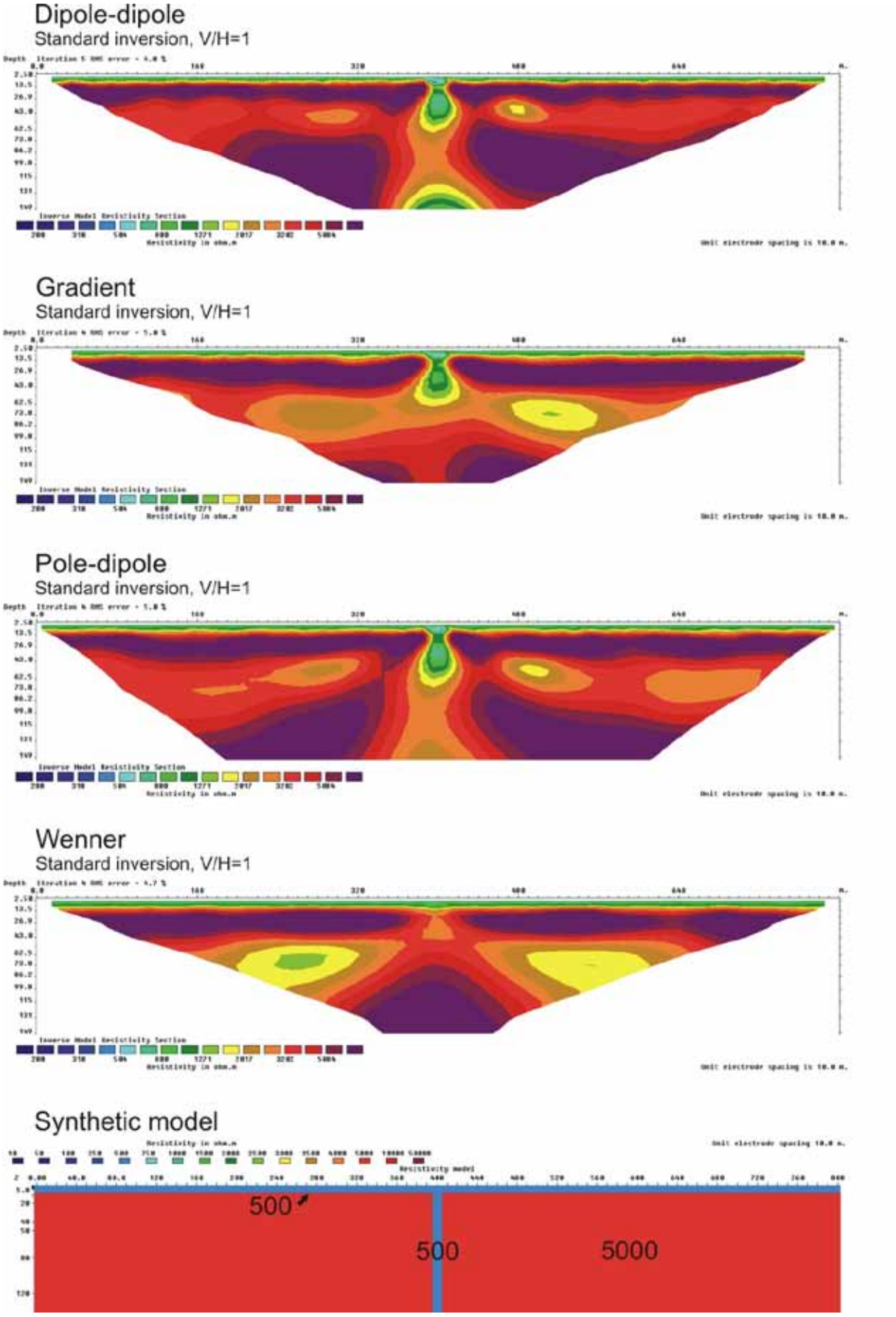

Figure 3.5.46: 10 m zone (500 ohmm) below a 5 m layer (500 ohmm), V/H=1

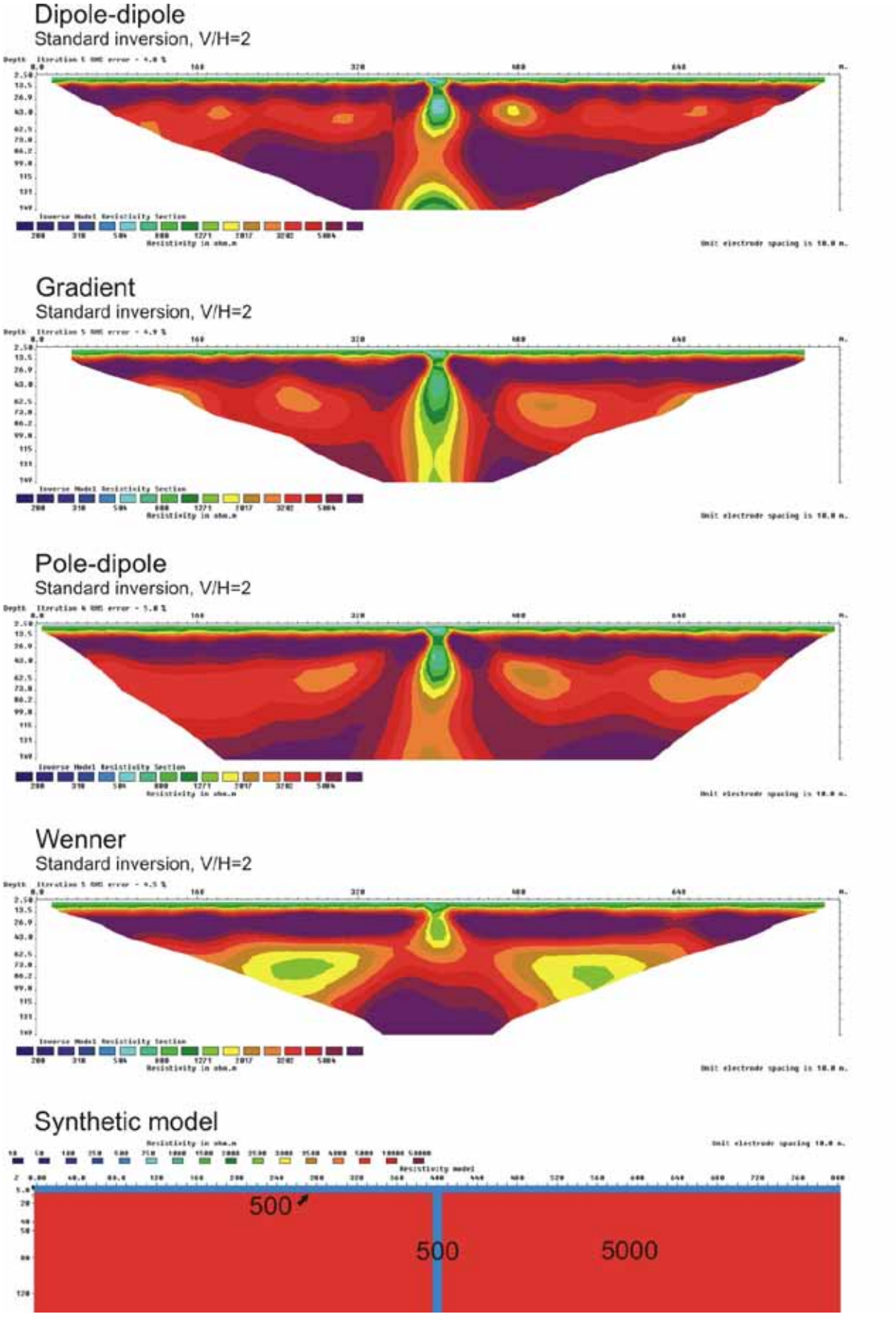

Figure 3.5.47: 10 m zone (500 ohmm) below a 5 m layer (500 ohmm), V/H=2

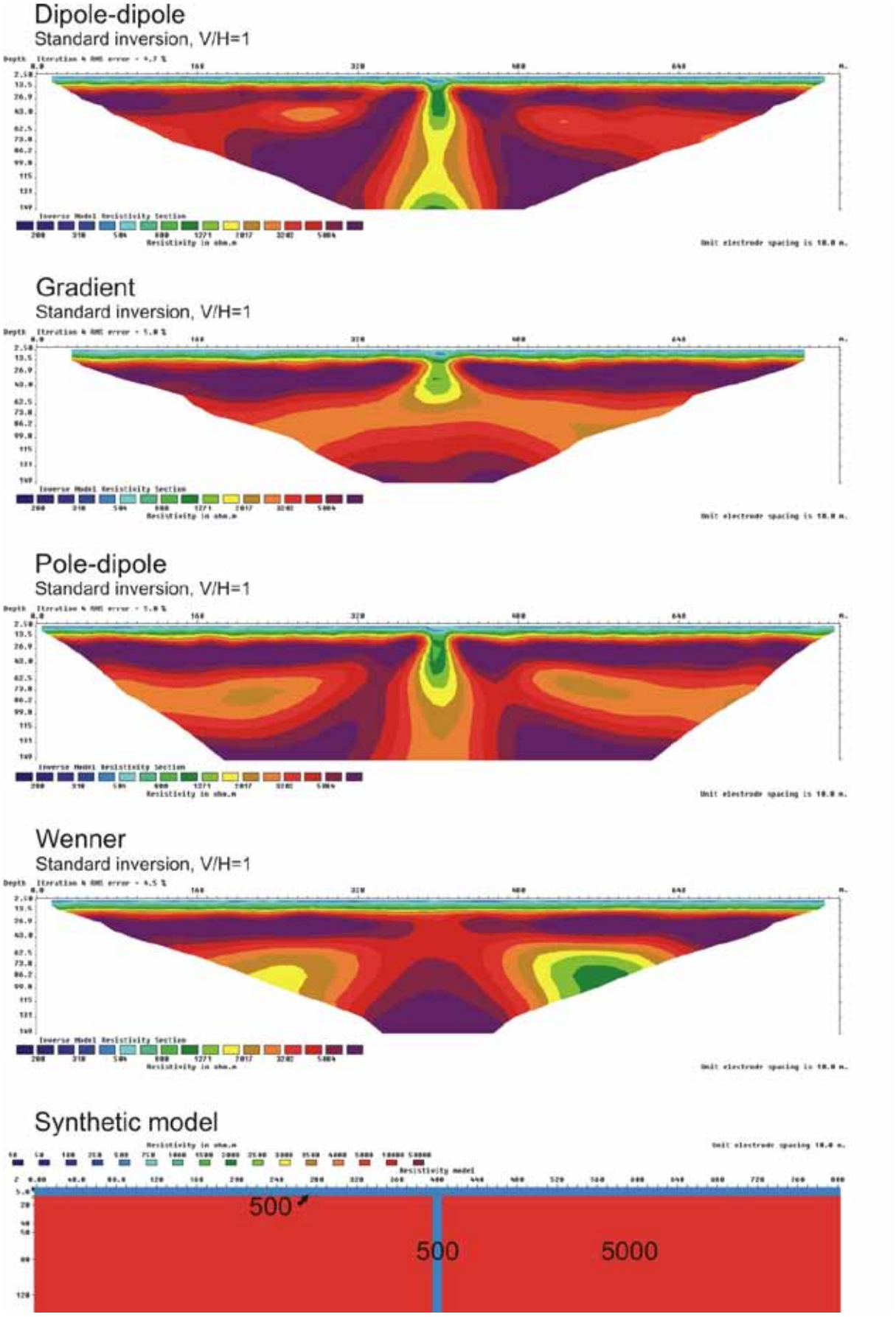

Figure 3.5.48: 10 m zone (500 ohmm) below a 10 m layer (500 ohmm), V/H=1

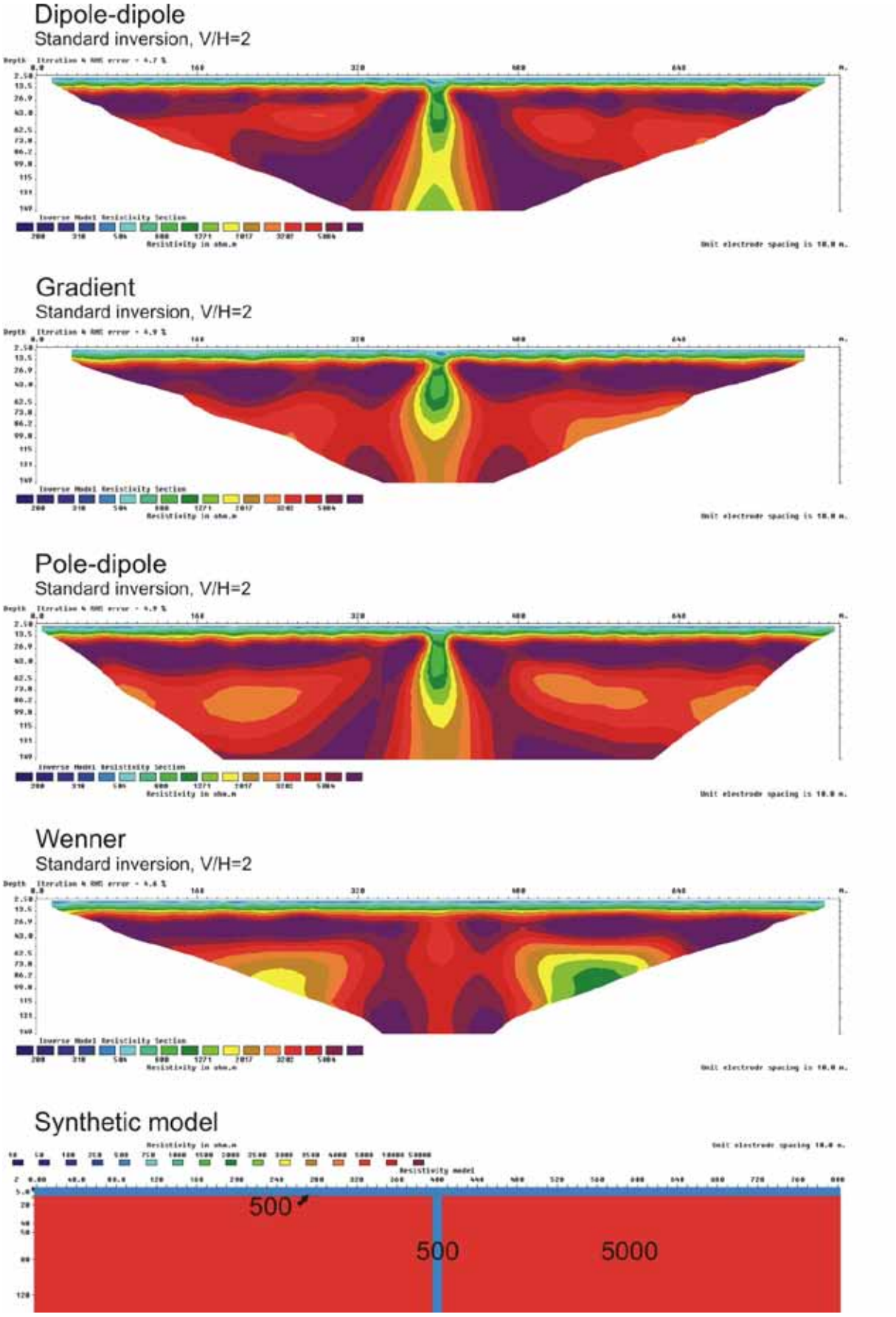

Figure 3.5.49: 10 m zone (500 ohmm) below a 10 m layer (500 ohmm), V/H=2

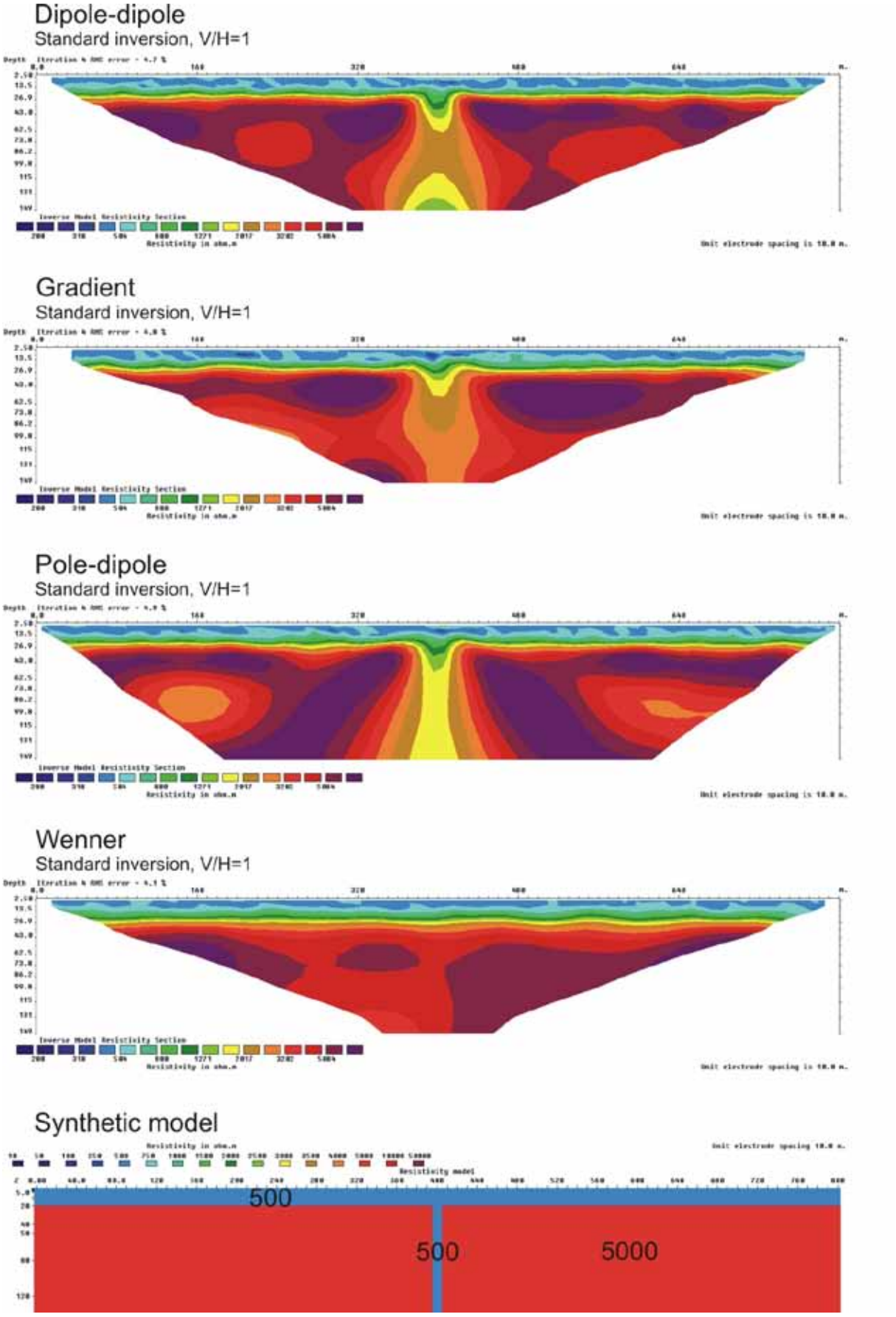

Figure 3.5.50: 10 m zone (500 ohmm) below a 20 m layer (500 ohmm), V/H=1

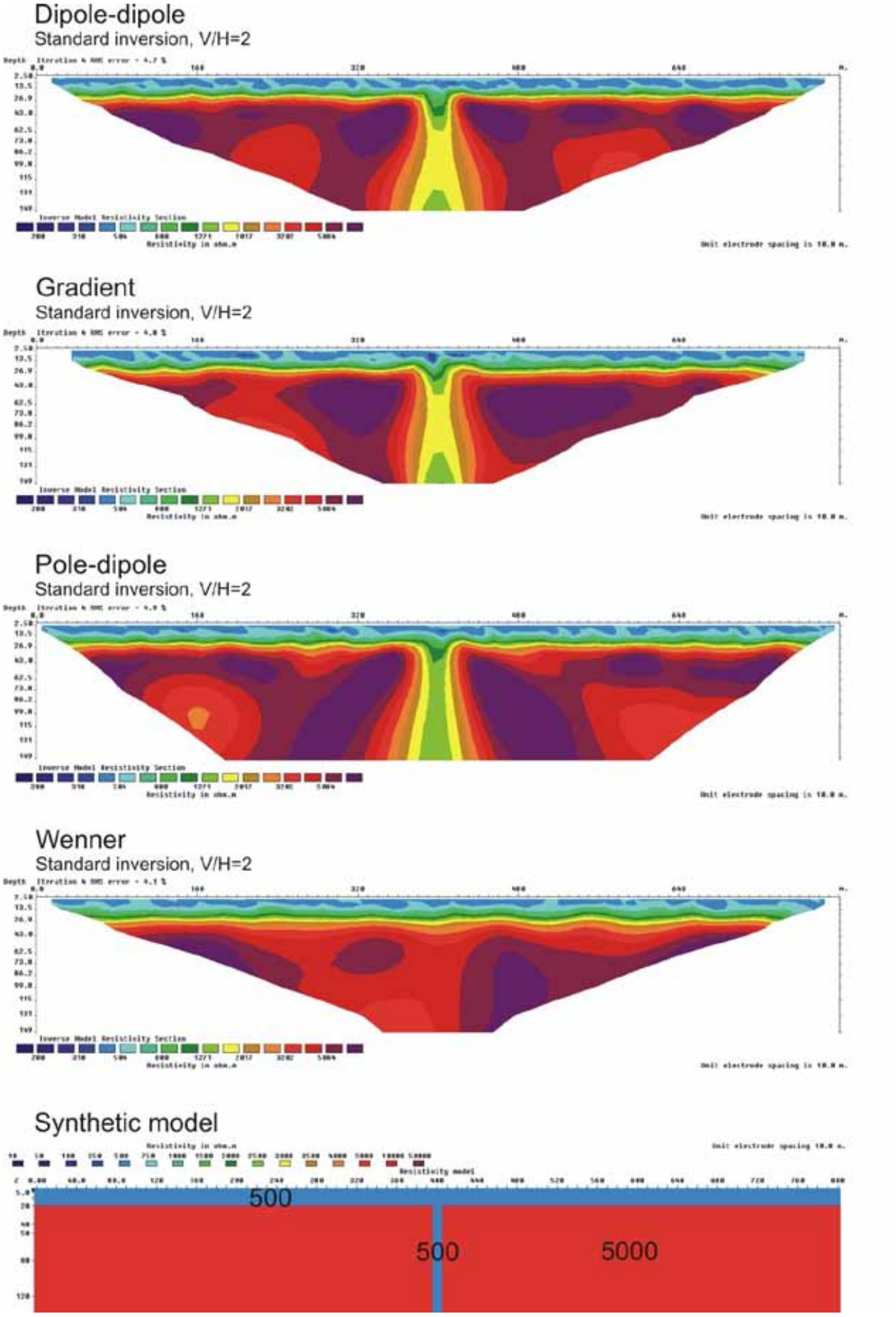

Figure 3.5.51: 10 m zone (500 ohmm) below a 20 m layer (500 ohmm), V/H=2

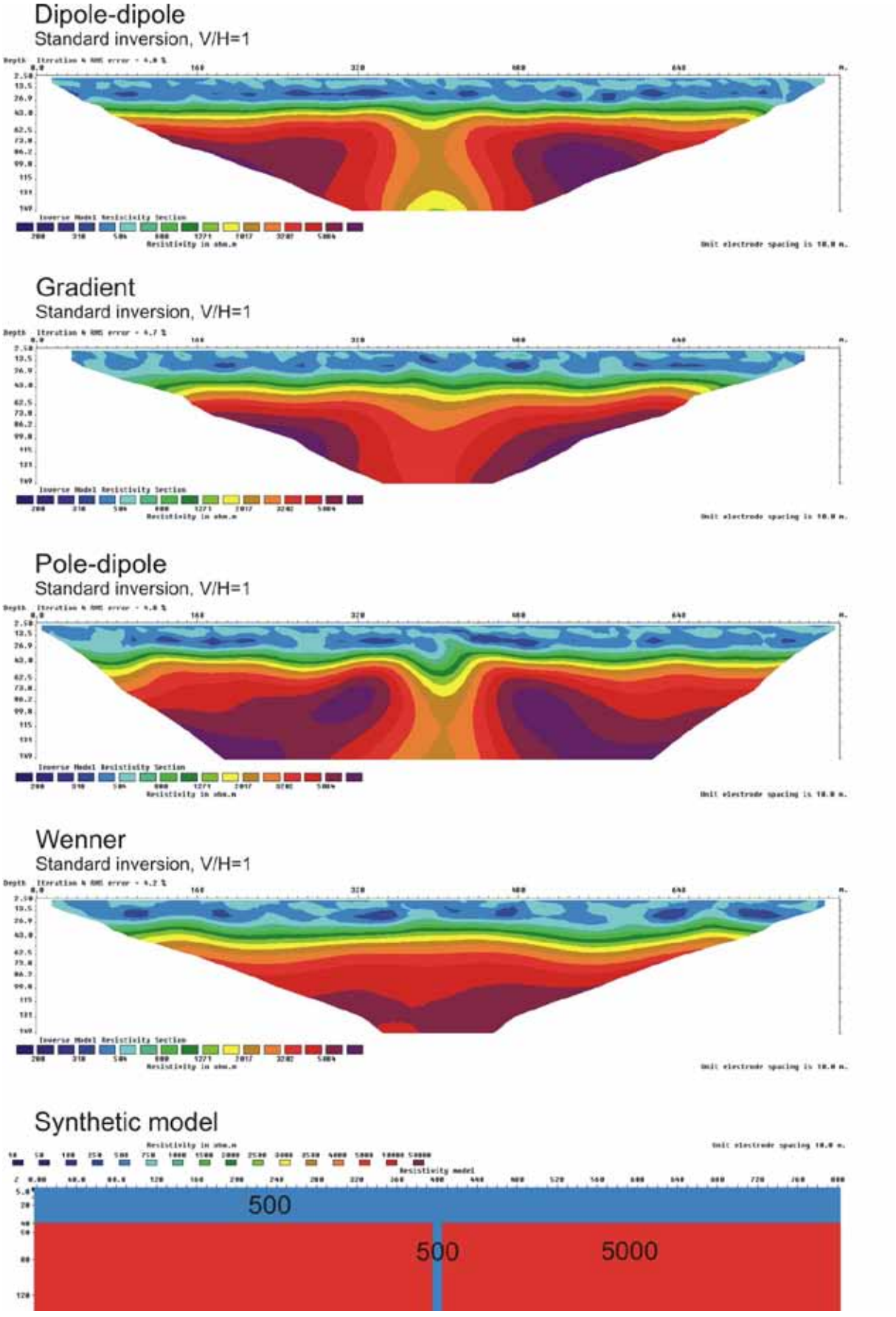

Figure 3.5.52: 10 m zone (500 ohmm) below a 40 m layer (500 ohmm), V/H=1

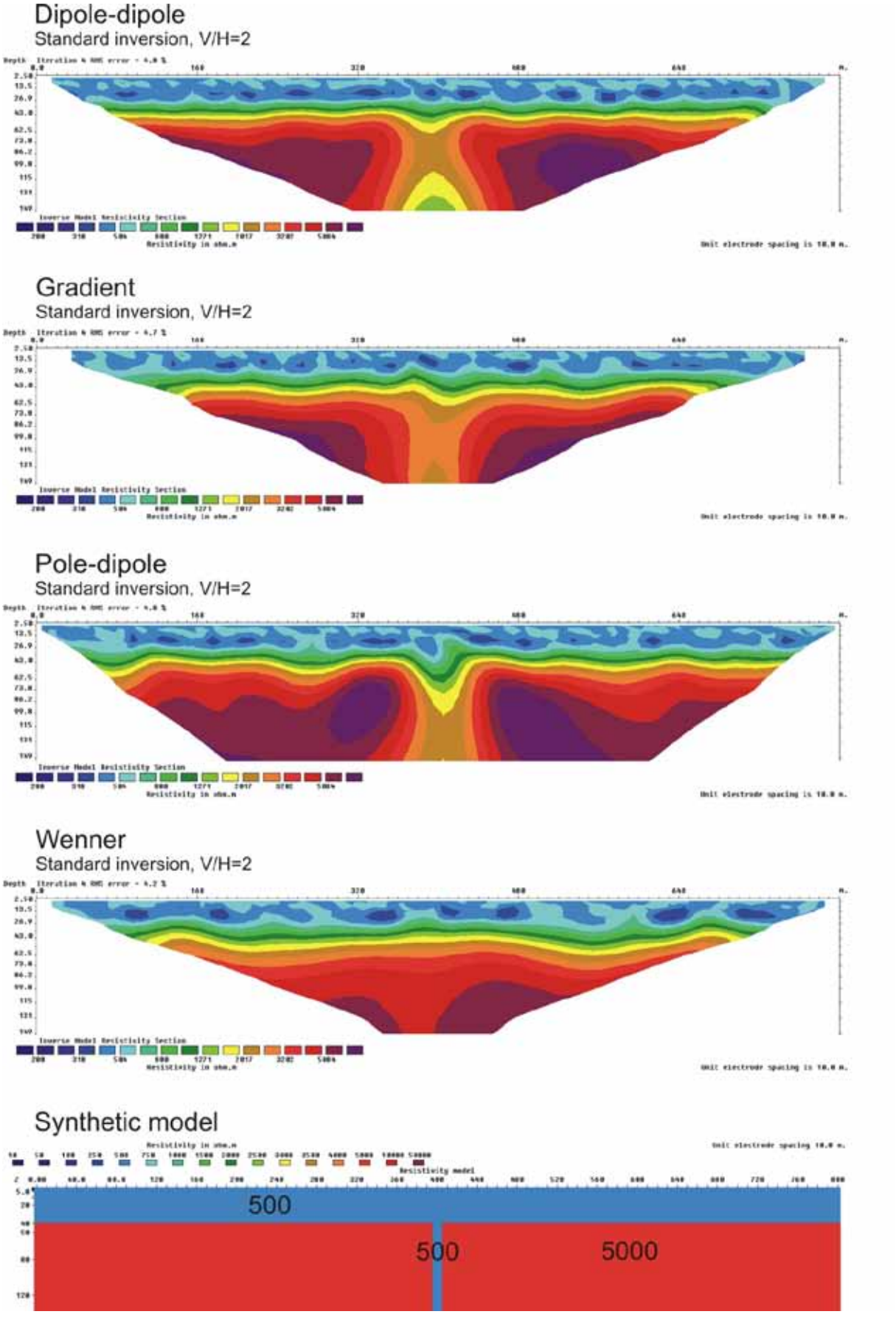

Figure 3.5.53: 10 m zone (500 ohmm) below a 40 m layer (500 ohmm), V/H=2

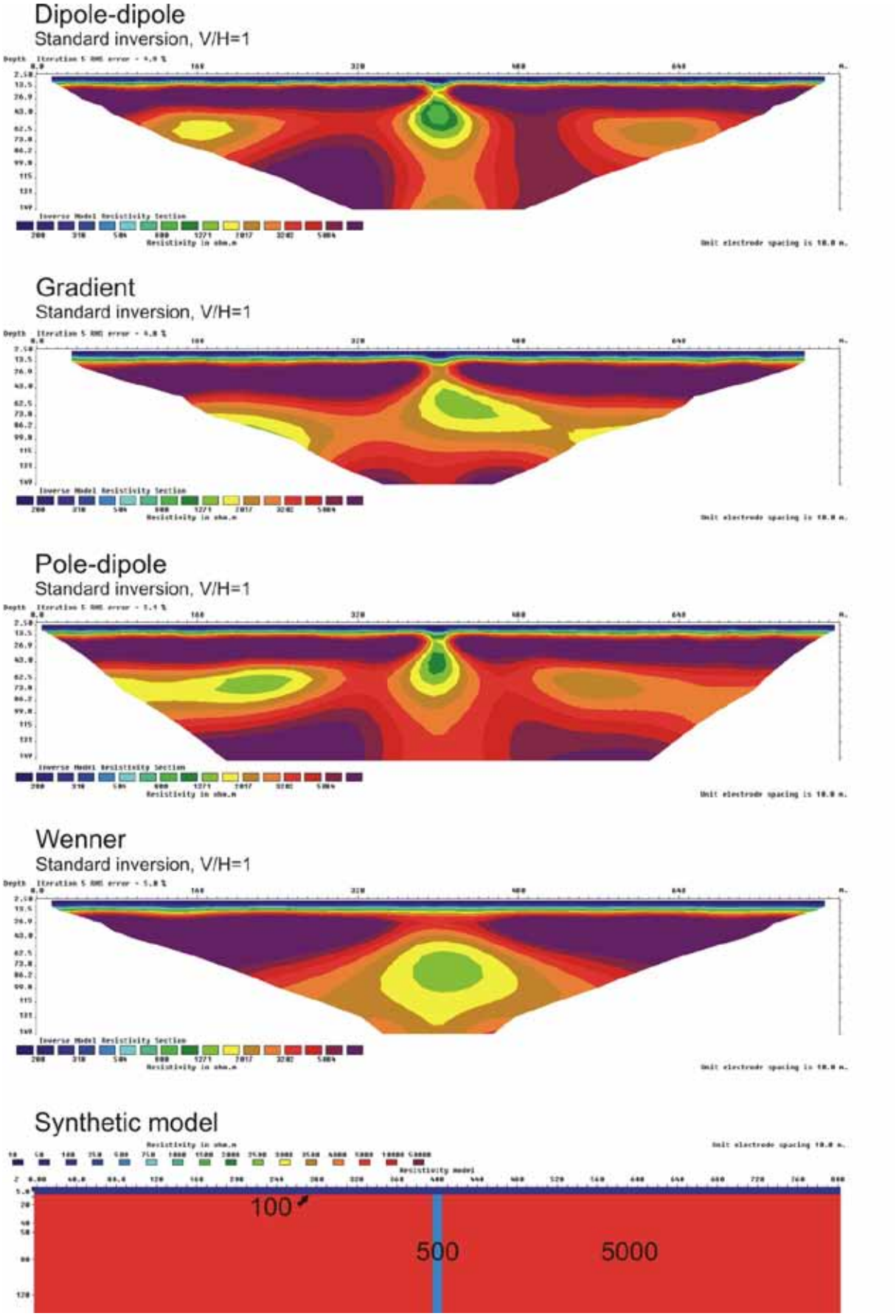

Figure 3.5.54: 10 m zone (500 ohmm) below a 5 m layer (100 ohmm), V/H=1

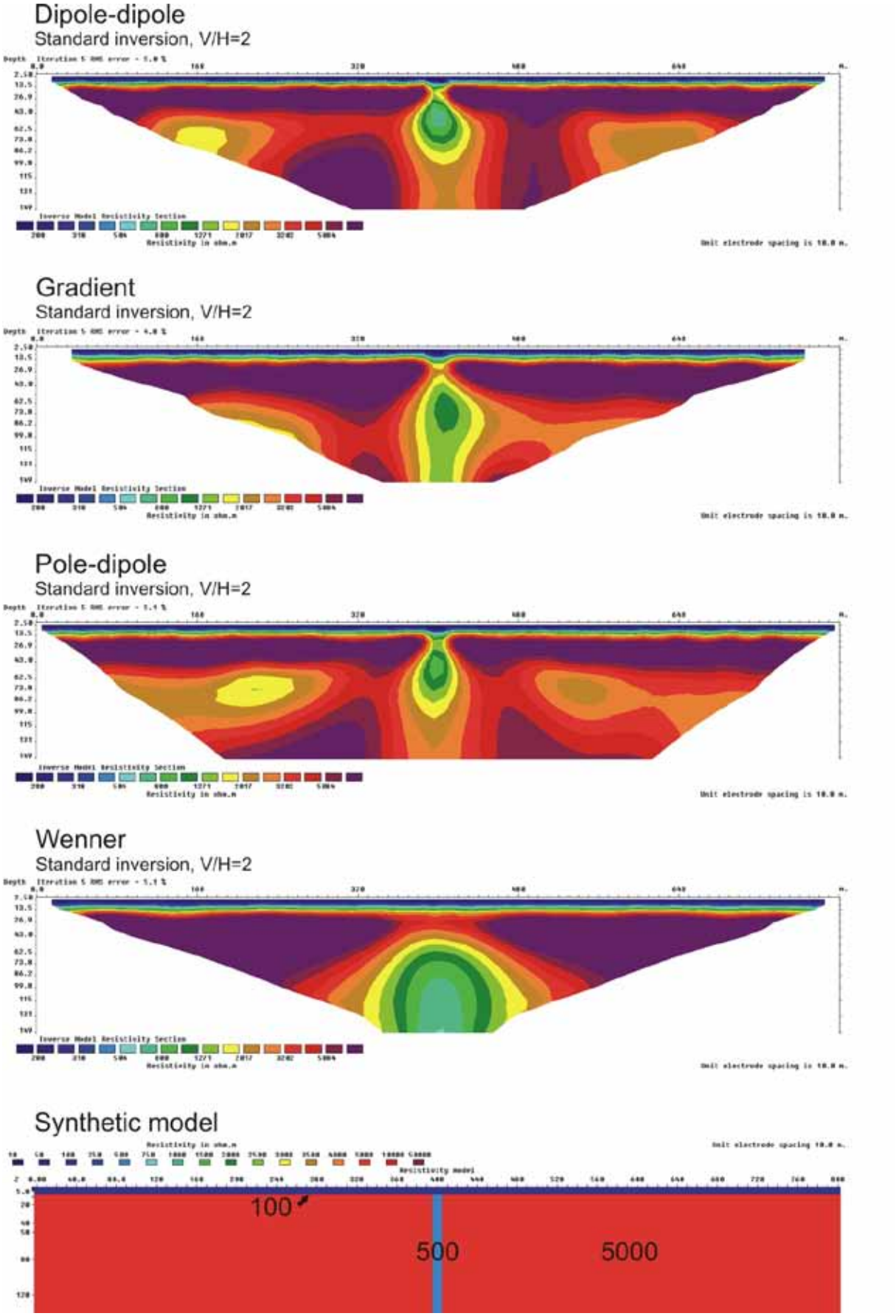

Figure 3.5.55: 10 m zone (500 ohmm) below a 5 m layer (100 ohmm), V/H=2

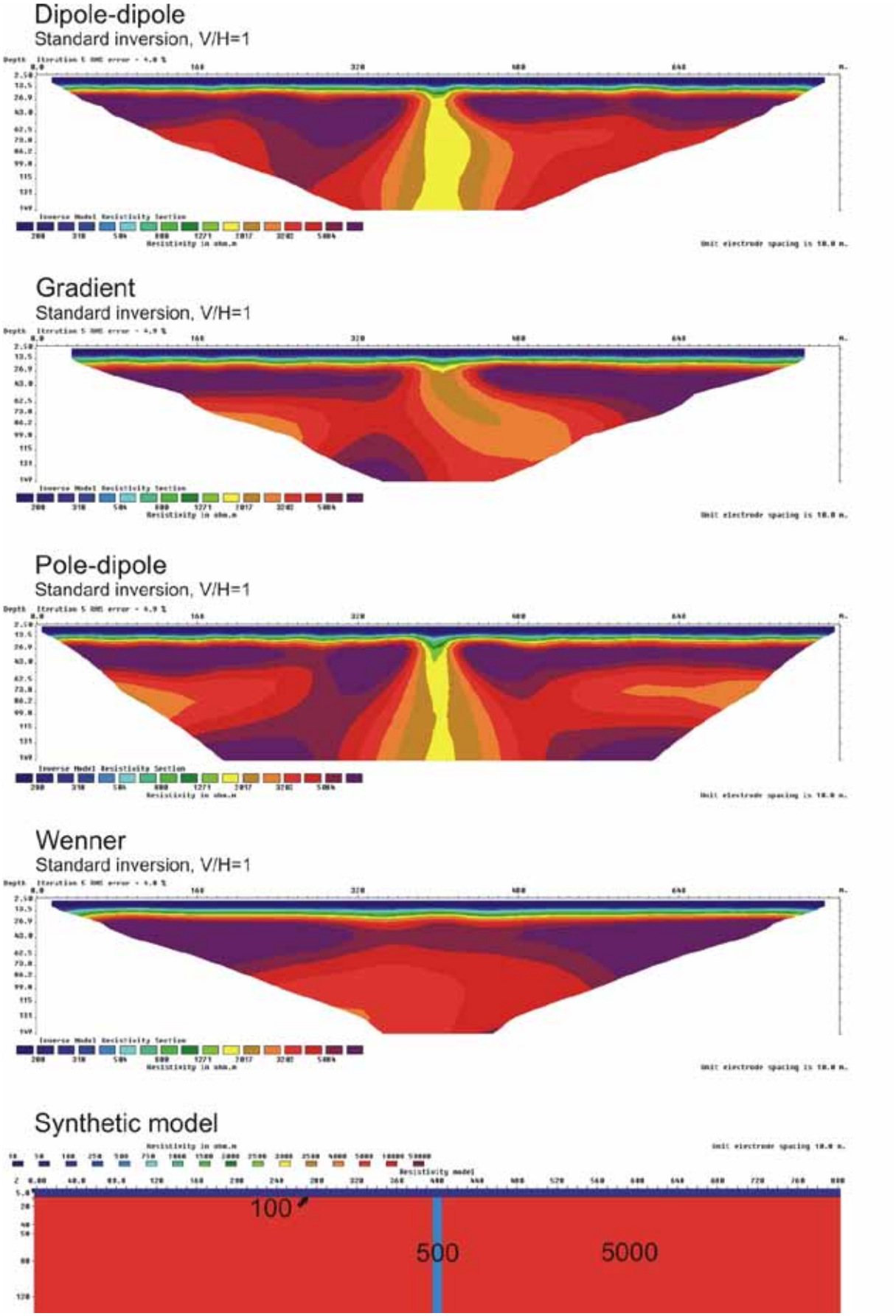

Figure 3.5.56: 10 m zone (500 ohmm) below a 10 m layer (100 ohmm), V/H=1

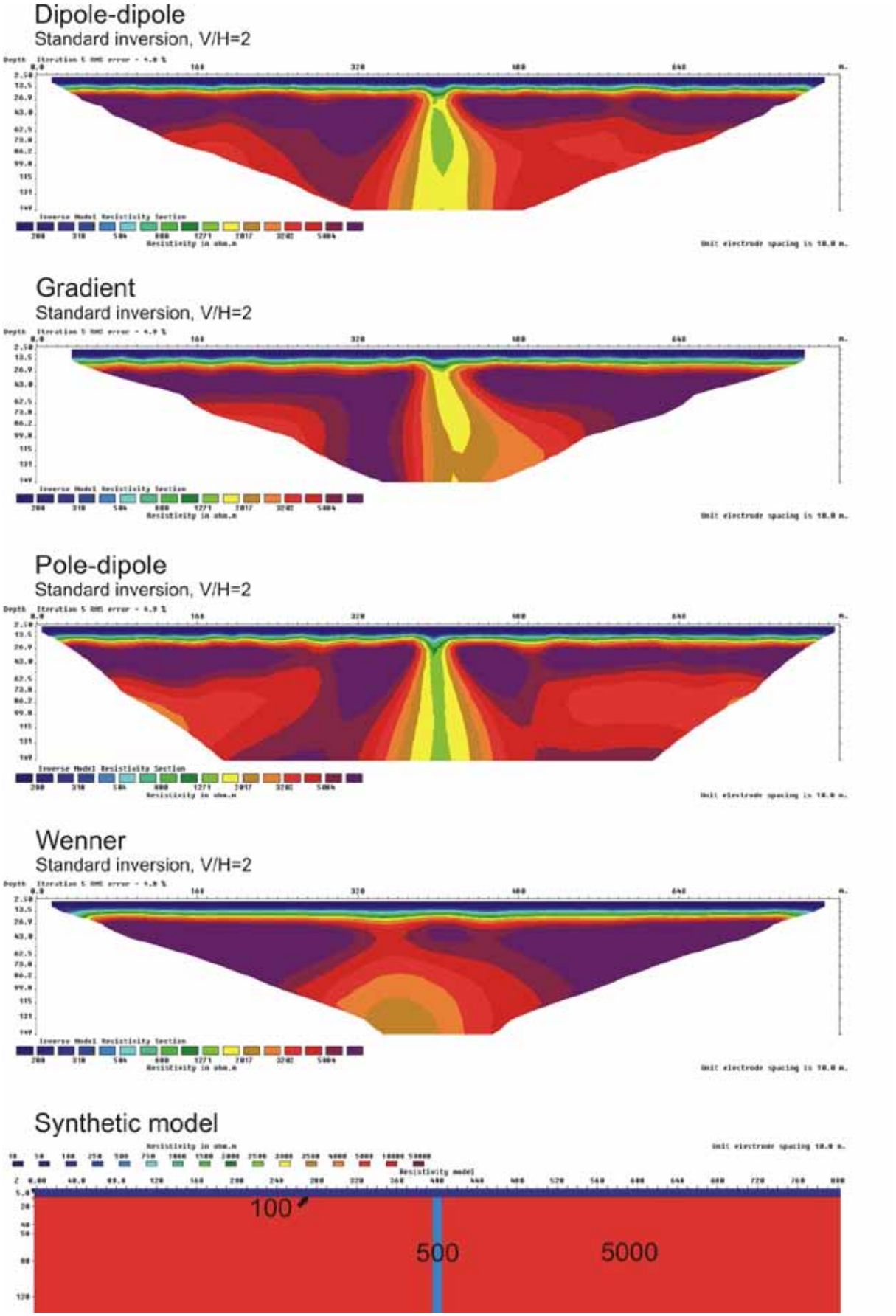

Figure 3.5.57: 10 m zone (500 ohmm) below a 10 m layer (100 ohmm), V/H=2

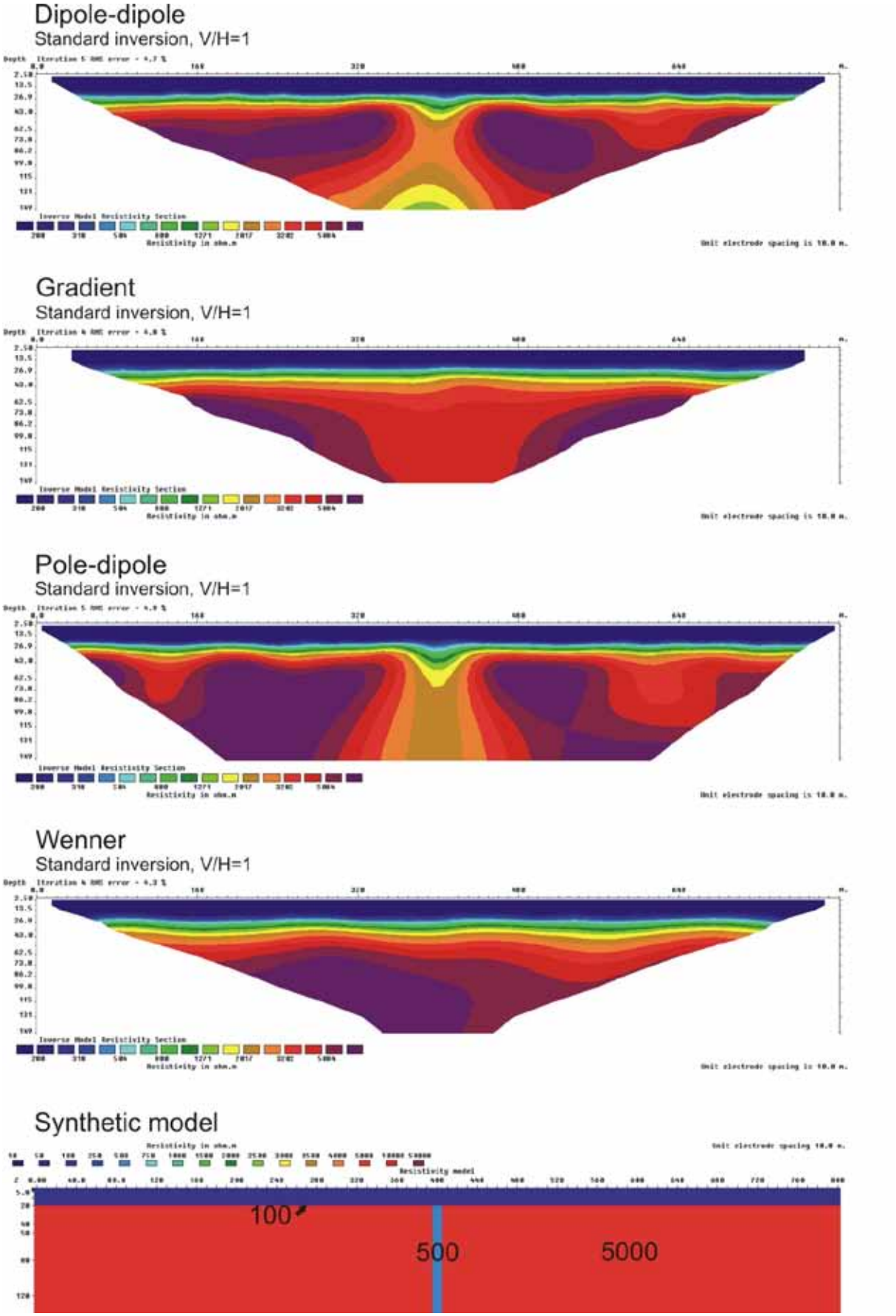

Figure 3.5.58: 10 m zone (500 ohmm) below a 20 m layer (100 ohmm), V/H=1

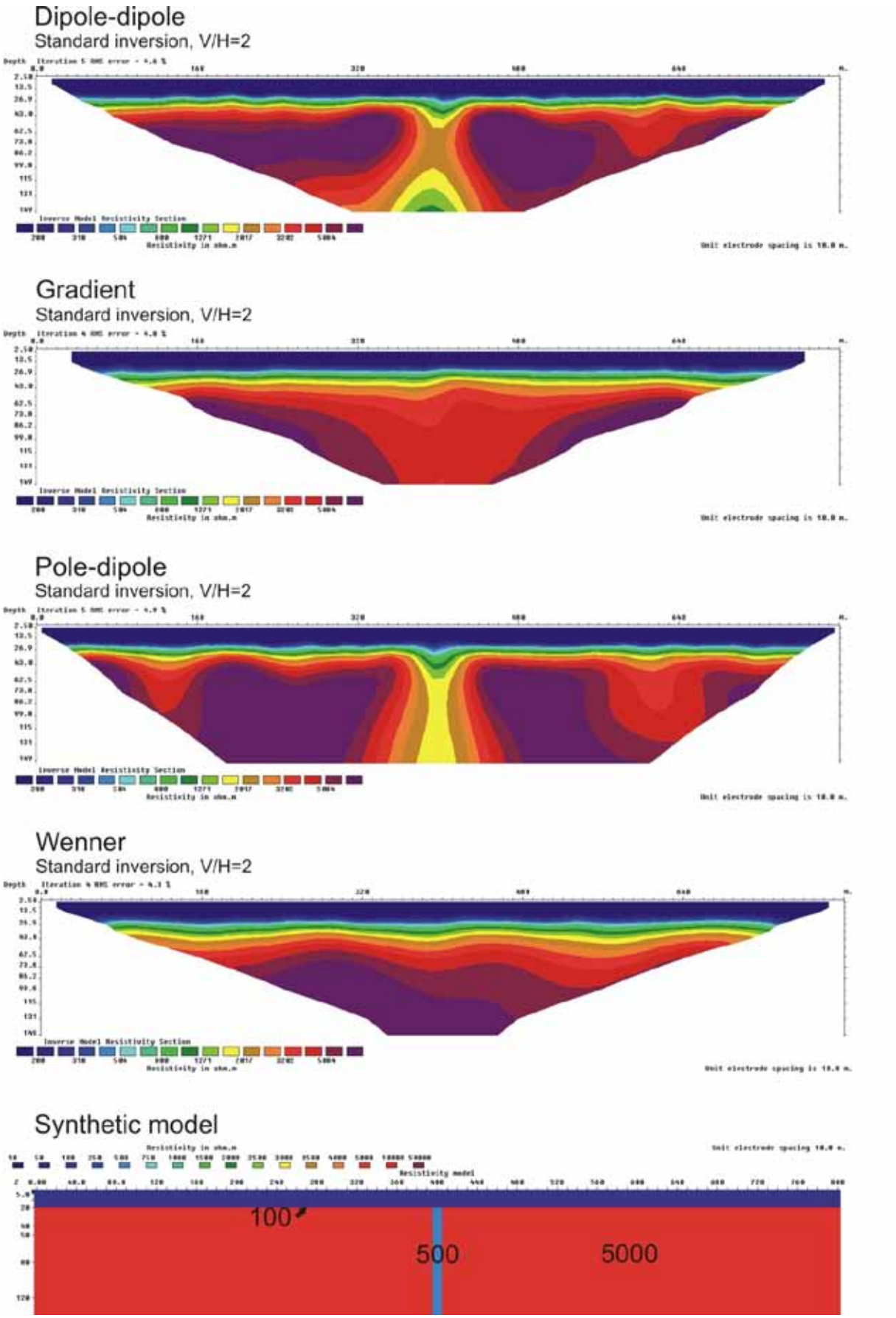

Figure 3.5.59: 10 m zone (500 ohmm) below a 20 m layer (100 ohmm), V/H=2

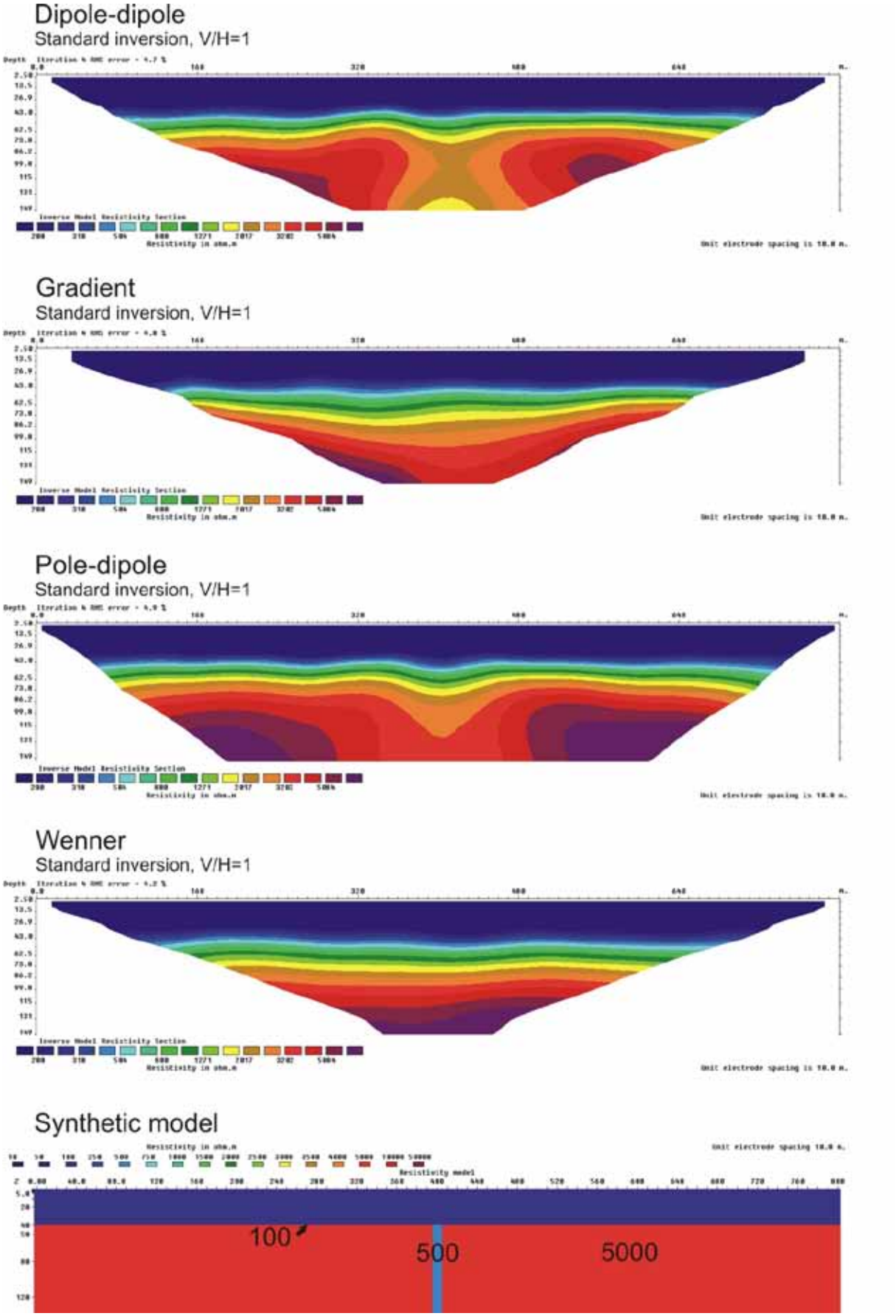

Figure 3.5.60: 10 m zone (500 ohmm) below a 40 m layer (100 ohmm), V/H=1

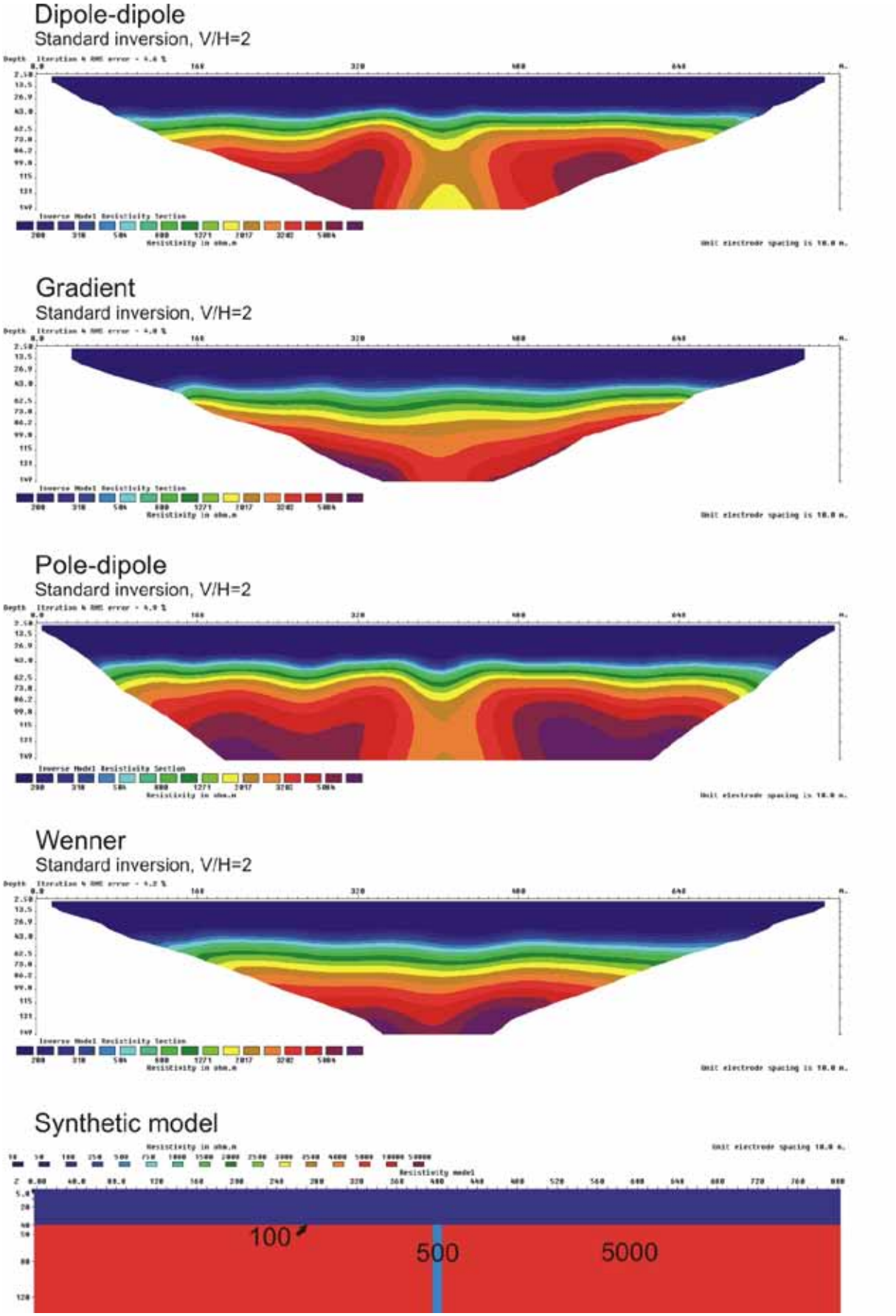

Figure 3.5.61: 10 m zone (500 ohmm) below a 40 m layer (100 ohmm), V/H=2

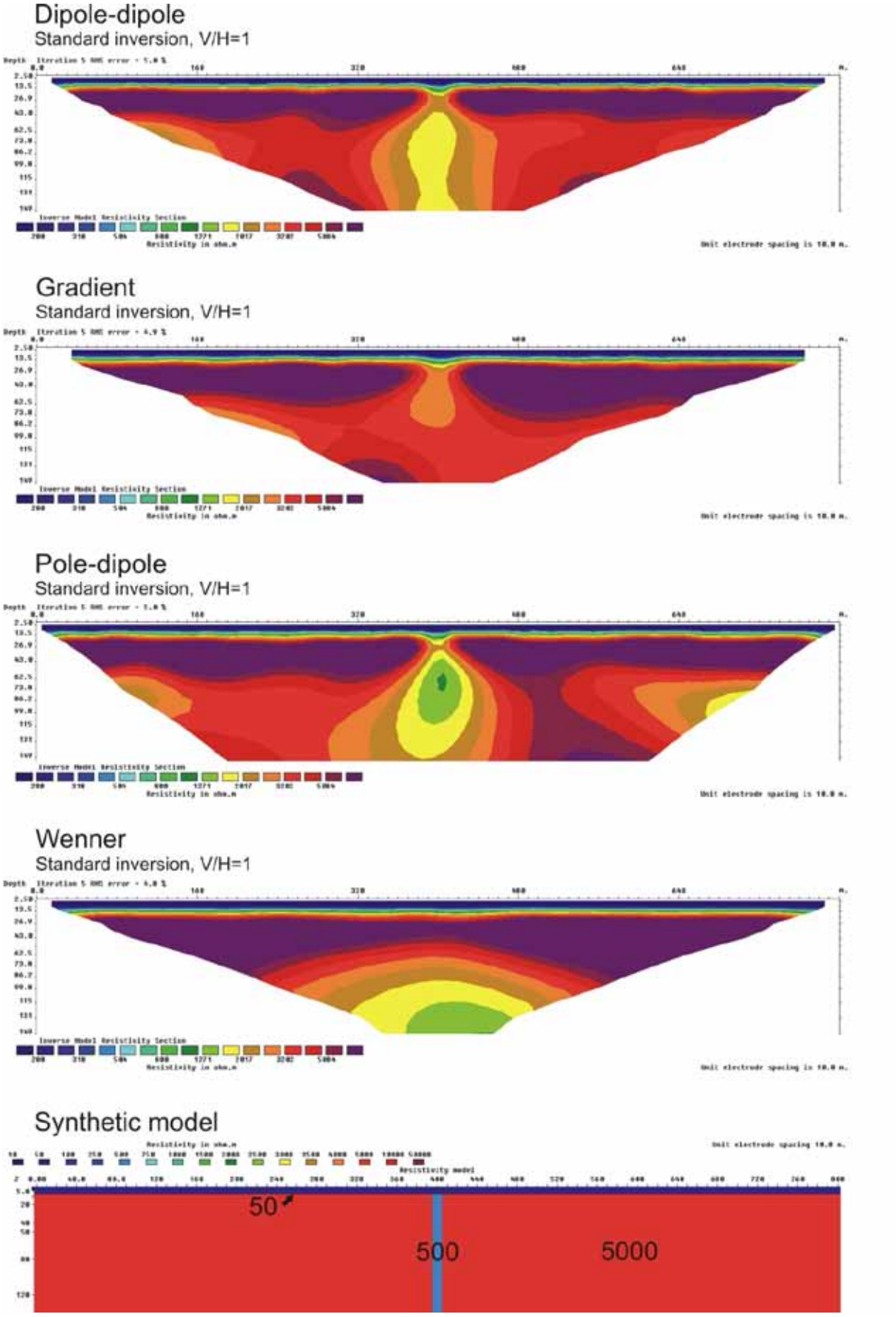

Figure 3.5.62: 10 m zone (500 ohmm) below a 5 m layer (50 ohmm), V/H=1

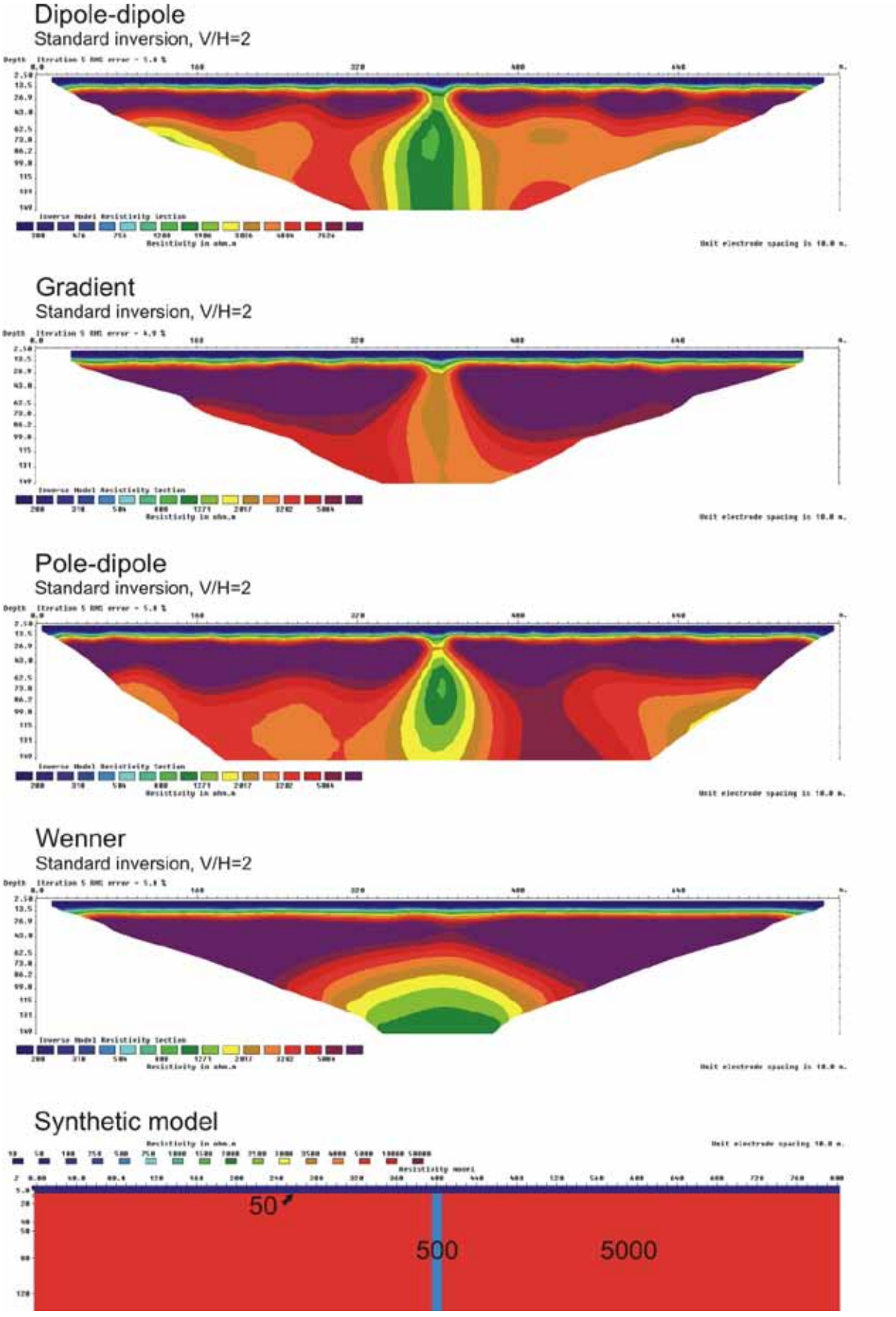

Figure 3.5.63: 10 m zone (500 ohmm) below a 5 m layer (50 ohmm), V/H=2

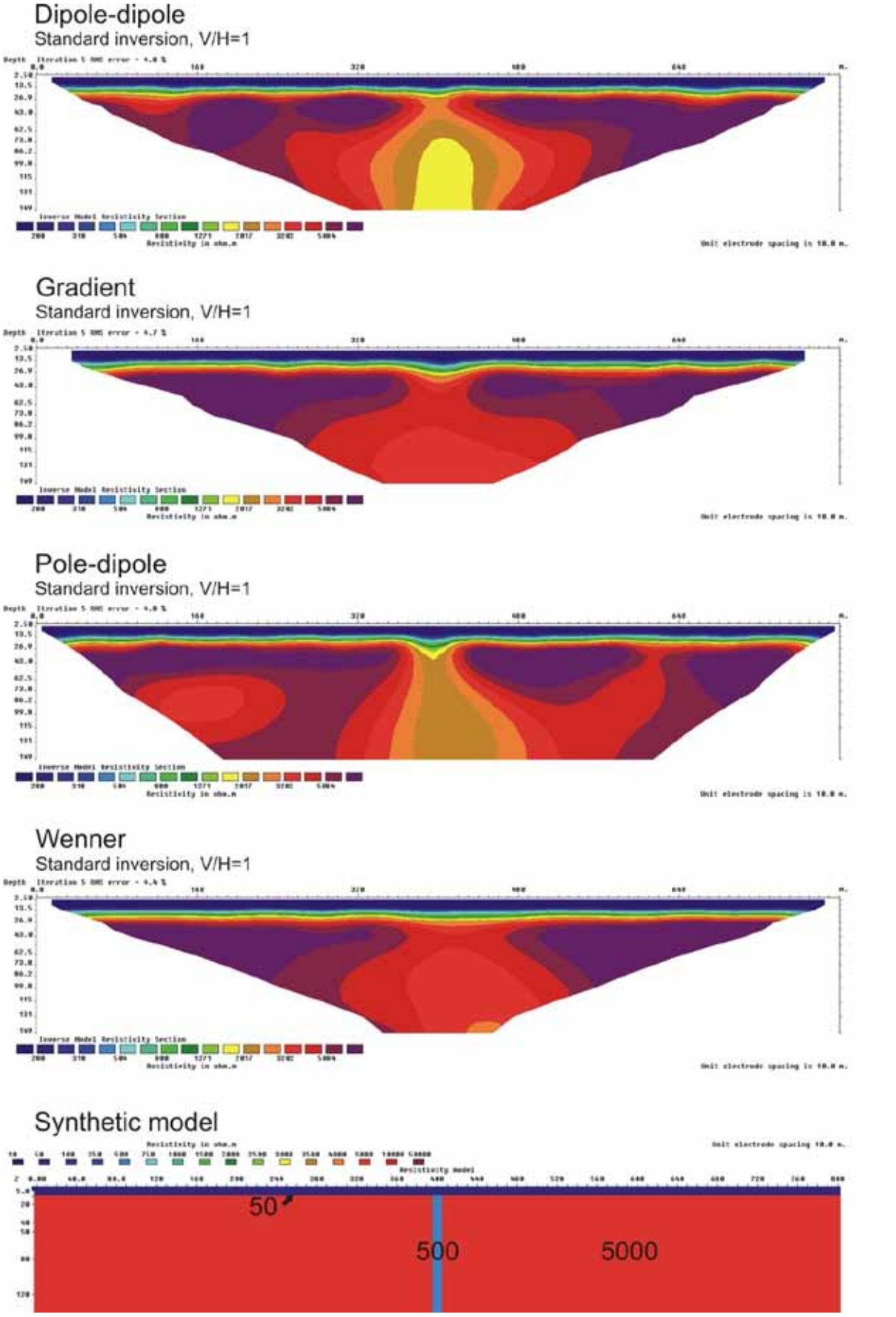

Figure 3.5.64: 10 m zone (500 ohmm) below a 10 m layer (50 ohmm), V/H=1

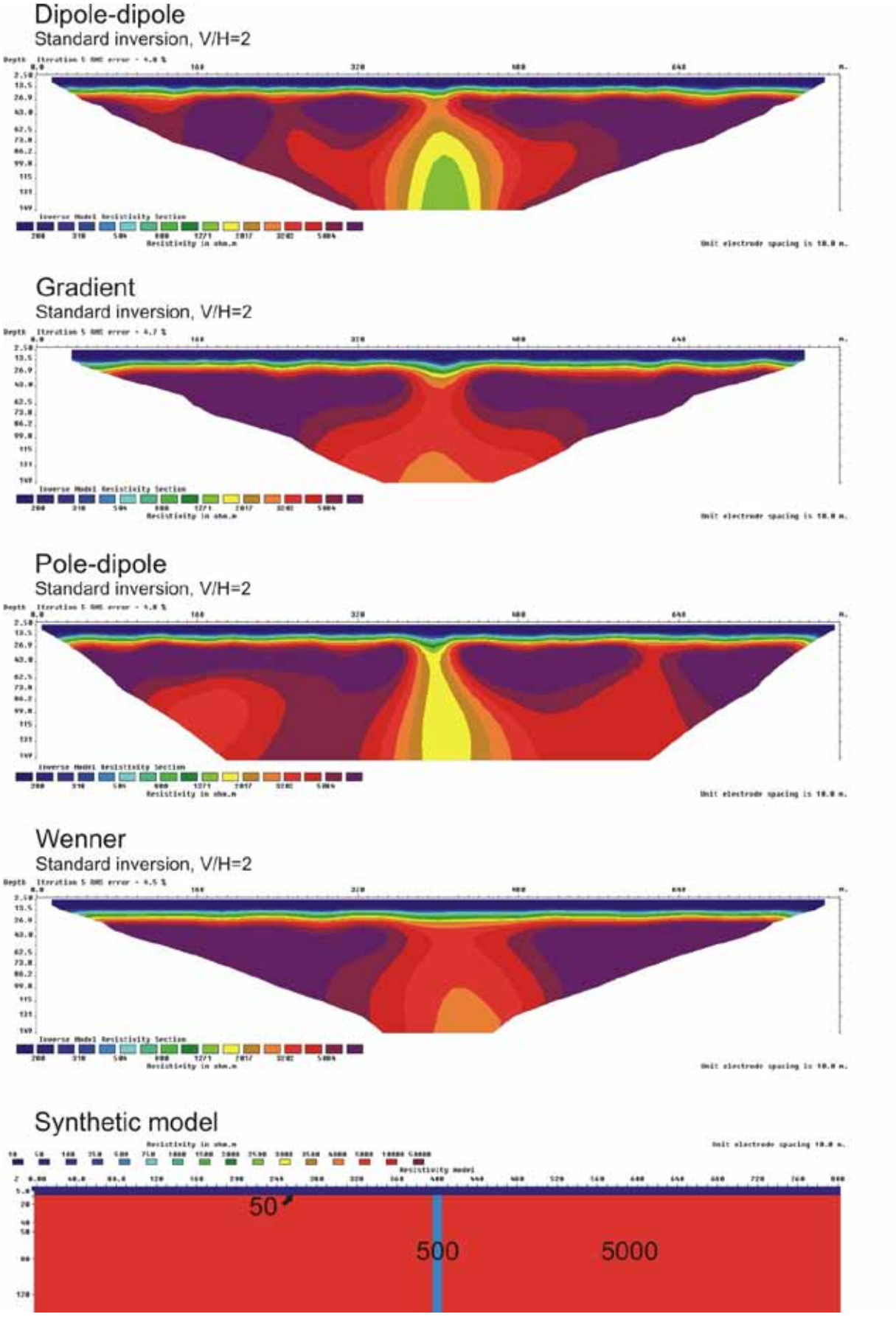

Figure 3.5.65: 10 m zone (500 ohmm) below a 10 m layer (50 ohmm), V/H=2

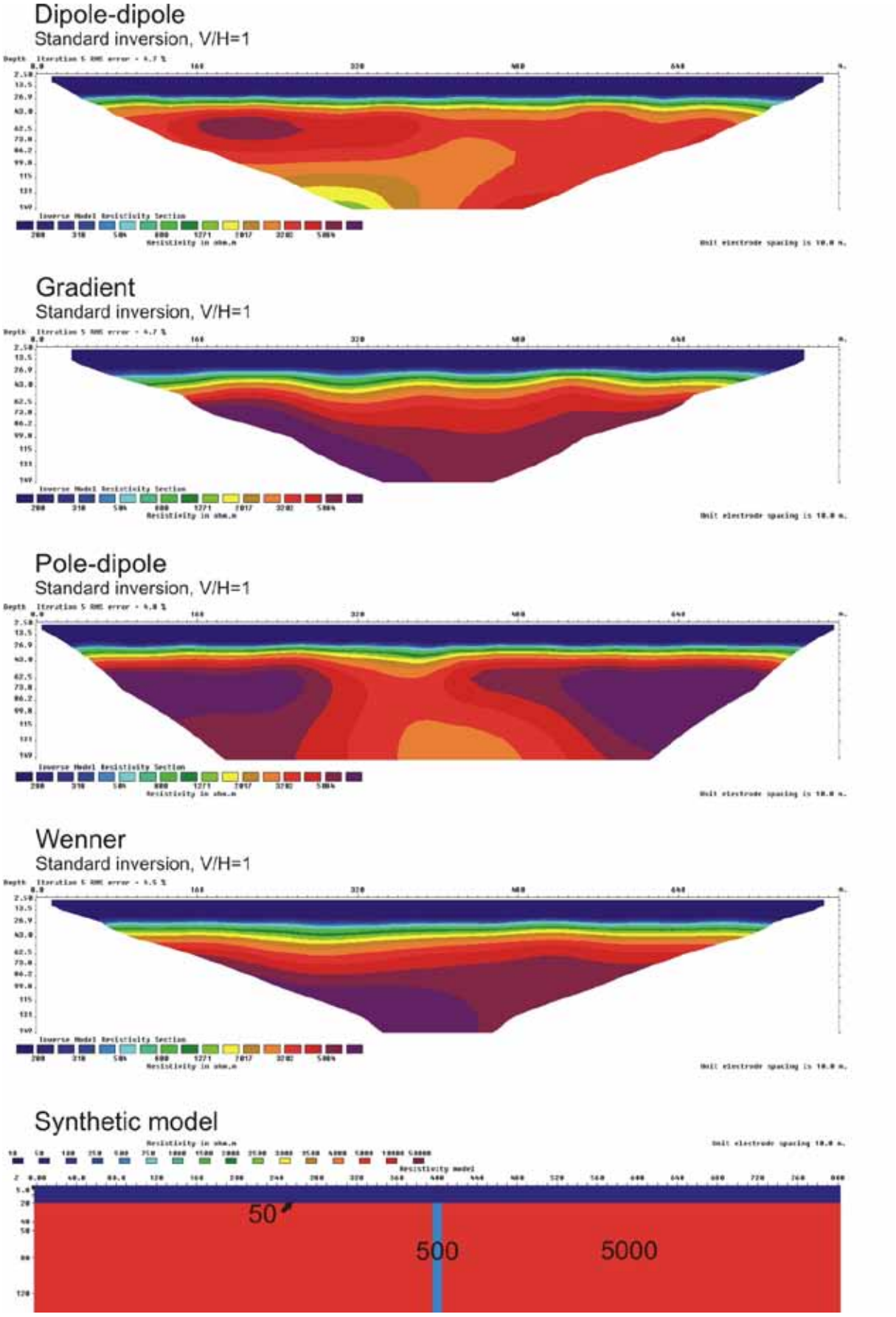

Figure 3.5.66: 10 m zone (500 ohmm) below a 20 m layer (50 ohmm), V/H=1

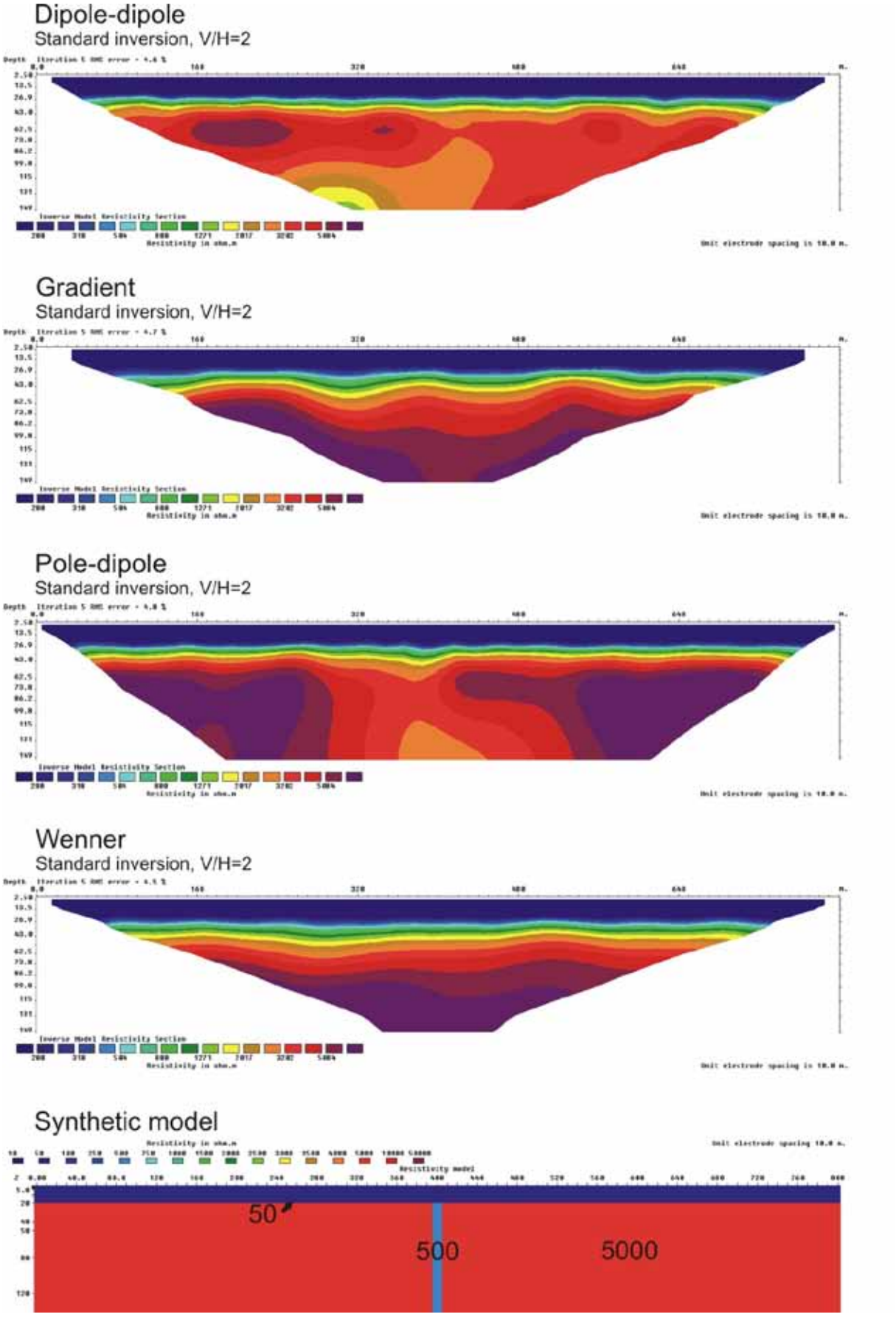

Figure 3.5.67: 10 m zone (500 ohmm) below a 20 m layer (50 ohmm), V/H=2

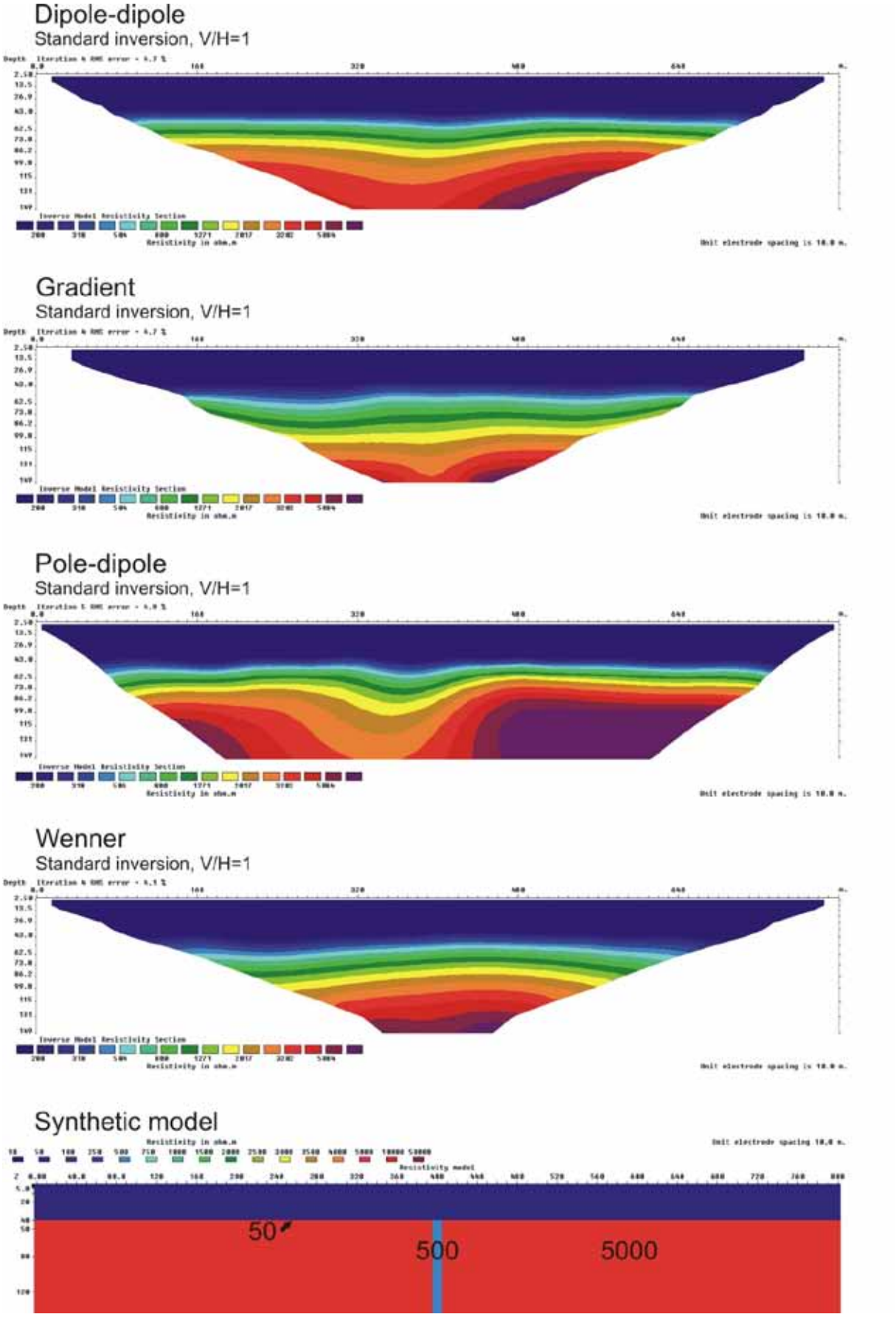

Figure 3.5.68: 10 m zone (500 ohmm) below a 40 m layer (50 ohmm), V/H=1

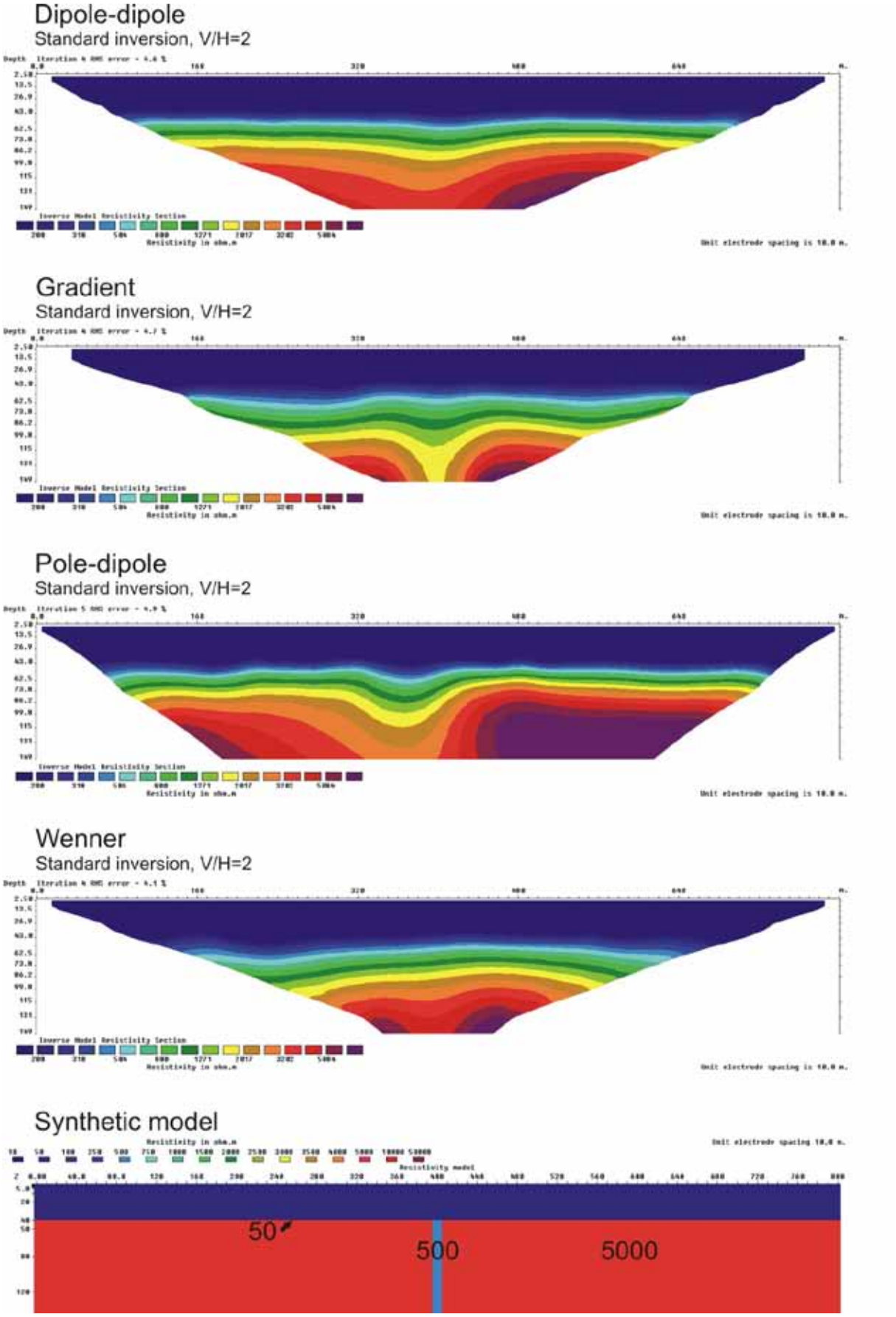

Figure 3.5.69: 10 m zone (500 ohmm) below a 40 m layer (50 ohmm), V/H=2

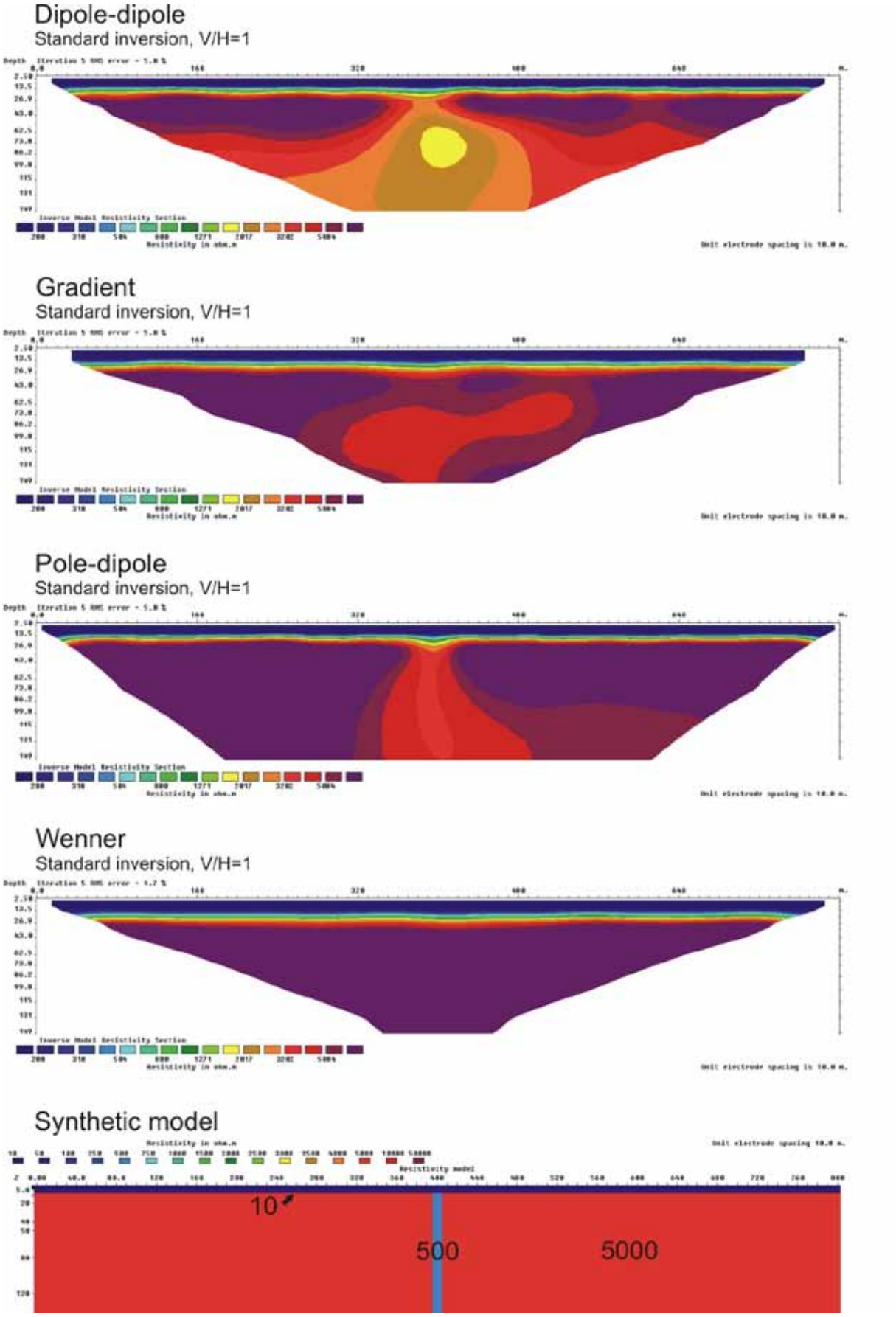

Figure 3.5.70: 10 m zone (500 ohmm) below a 5 m layer (10 ohmm), V/H=1

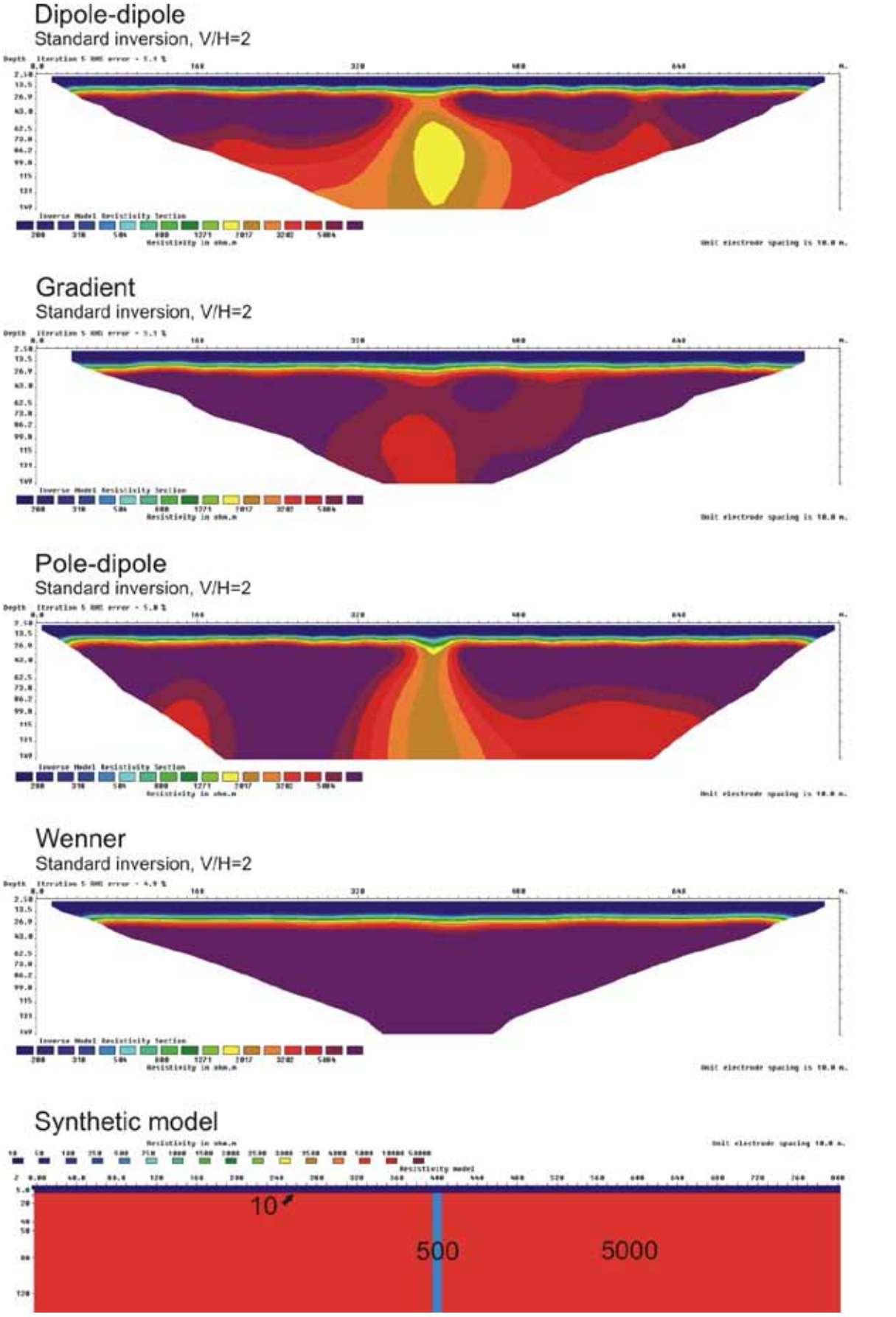

Figure 3.5.71: 10 m zone (500 ohmm) below a 5 m layer (10 ohmm), V/H=2

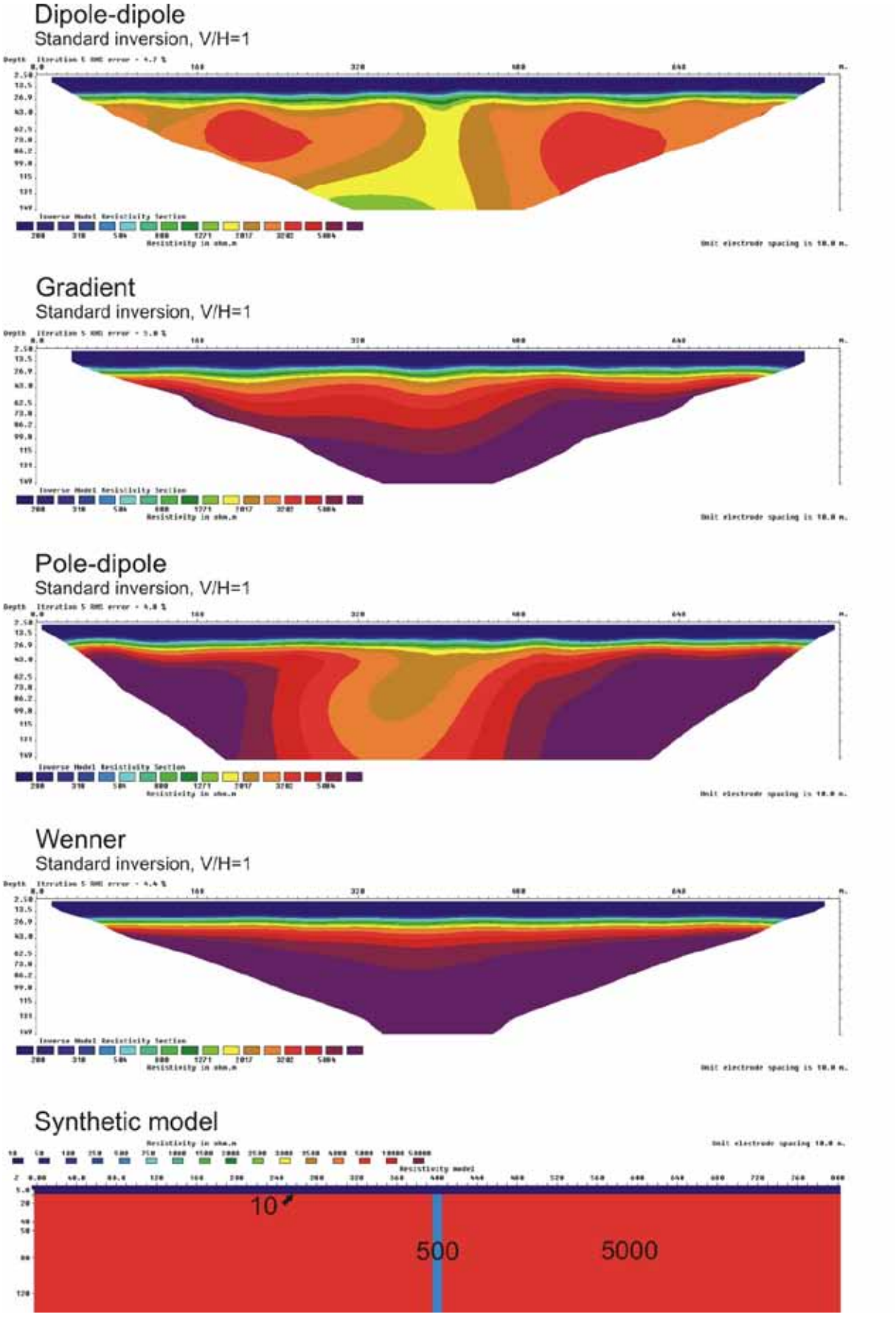

Figure 3.5.72: 10 m zone (500 ohmm) below a 10 m layer (10 ohmm), V/H=1

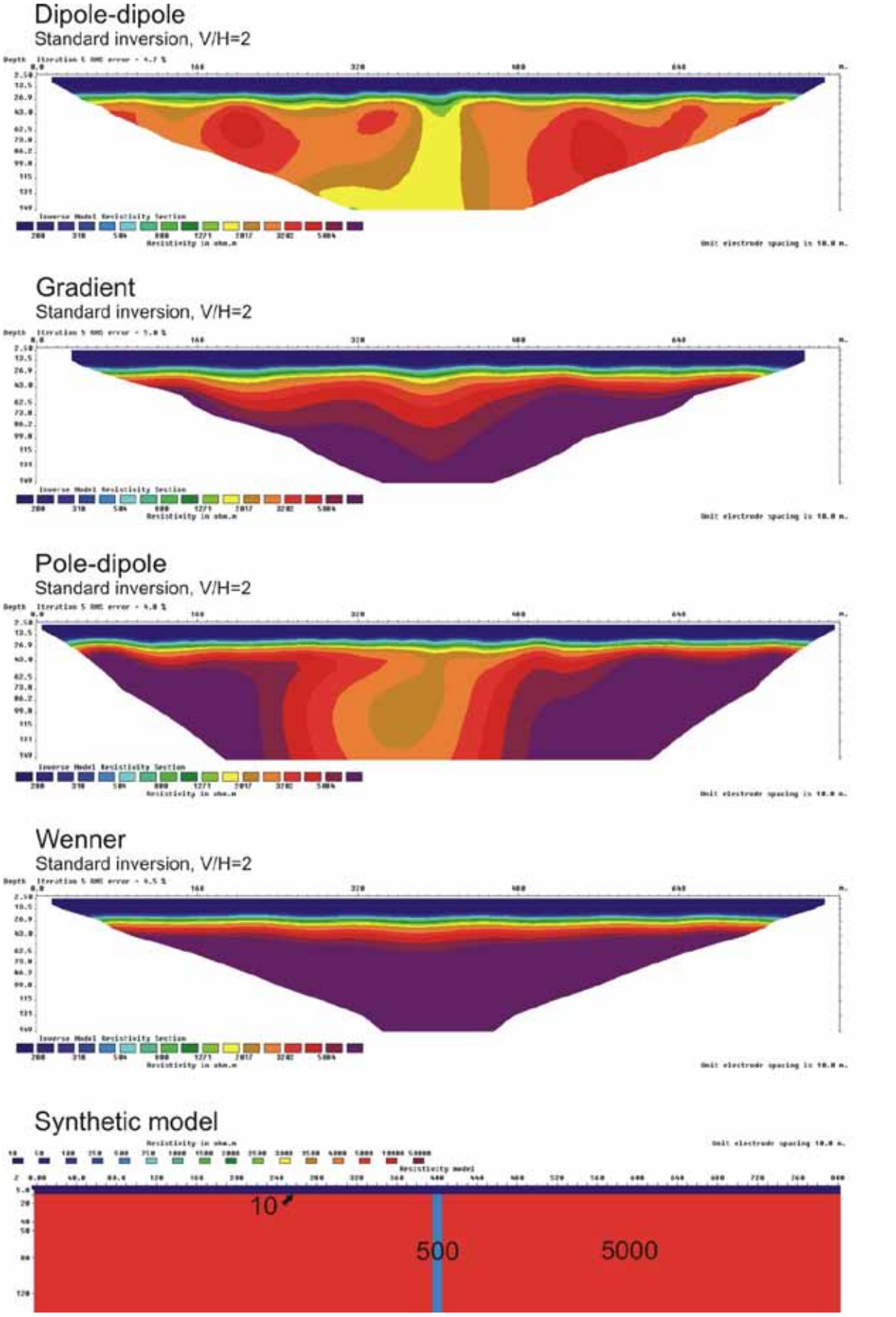

Figure 3.5.73: 10 m zone (500 ohmm) below a 10 m layer (10 ohmm), V/H=2

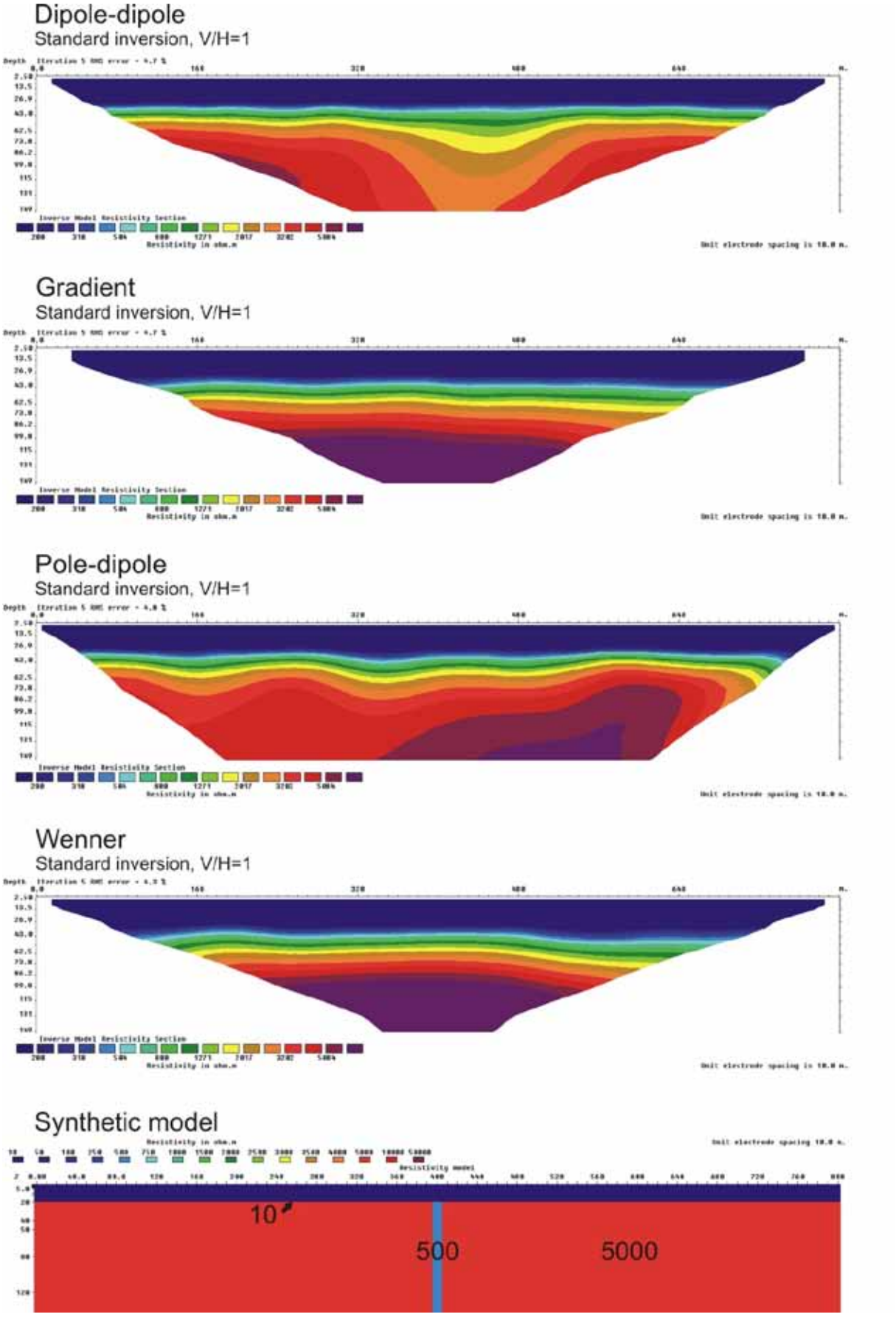

Figure 3.5.74: 10 m zone (500 ohmm) below a 20 m layer (10 ohmm), V/H=1

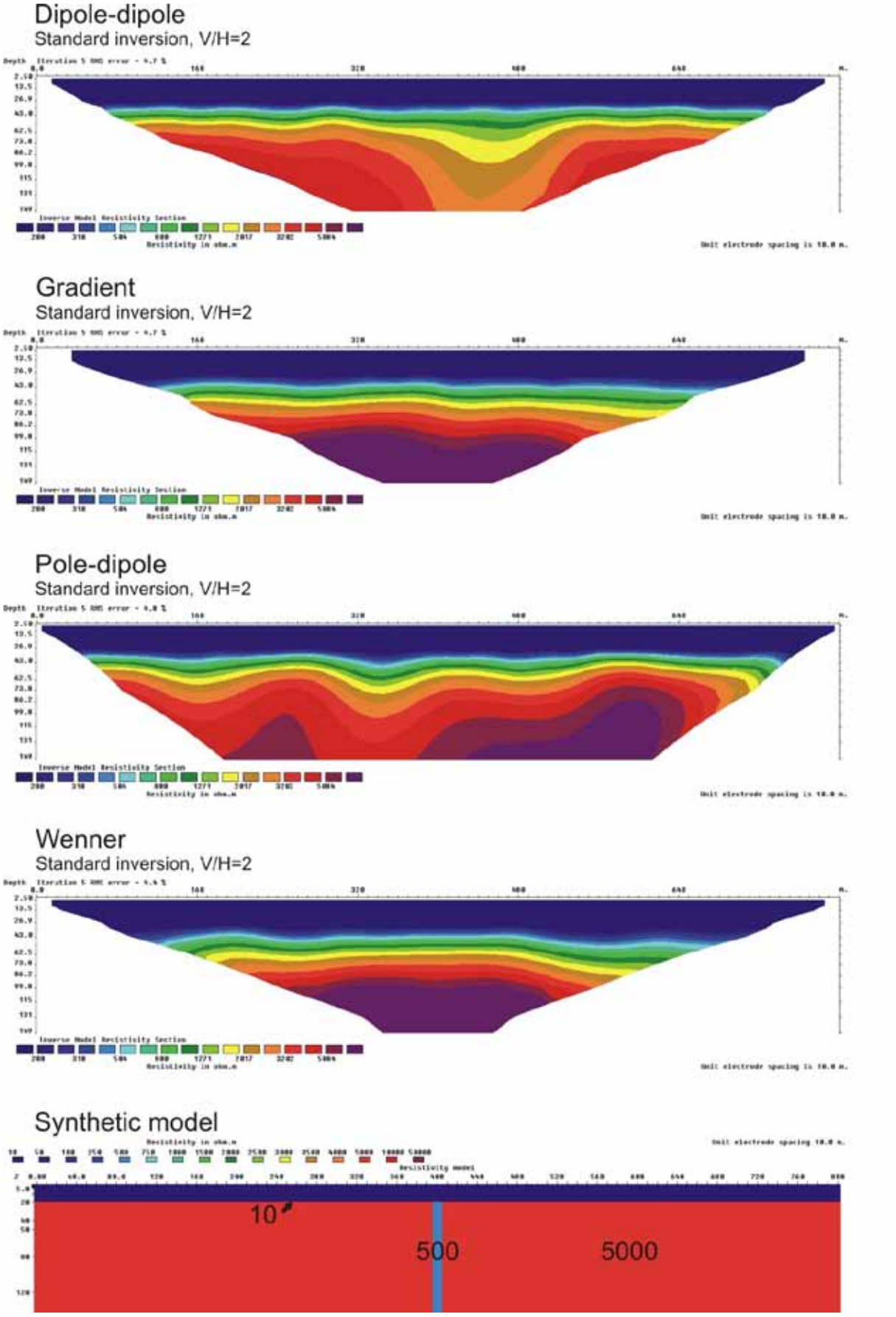

Figure 3.5.75: 10 m zone (500 ohmm) below a 20 m layer (10 ohmm), V/H=2

Modelling results: Horizontal Layers

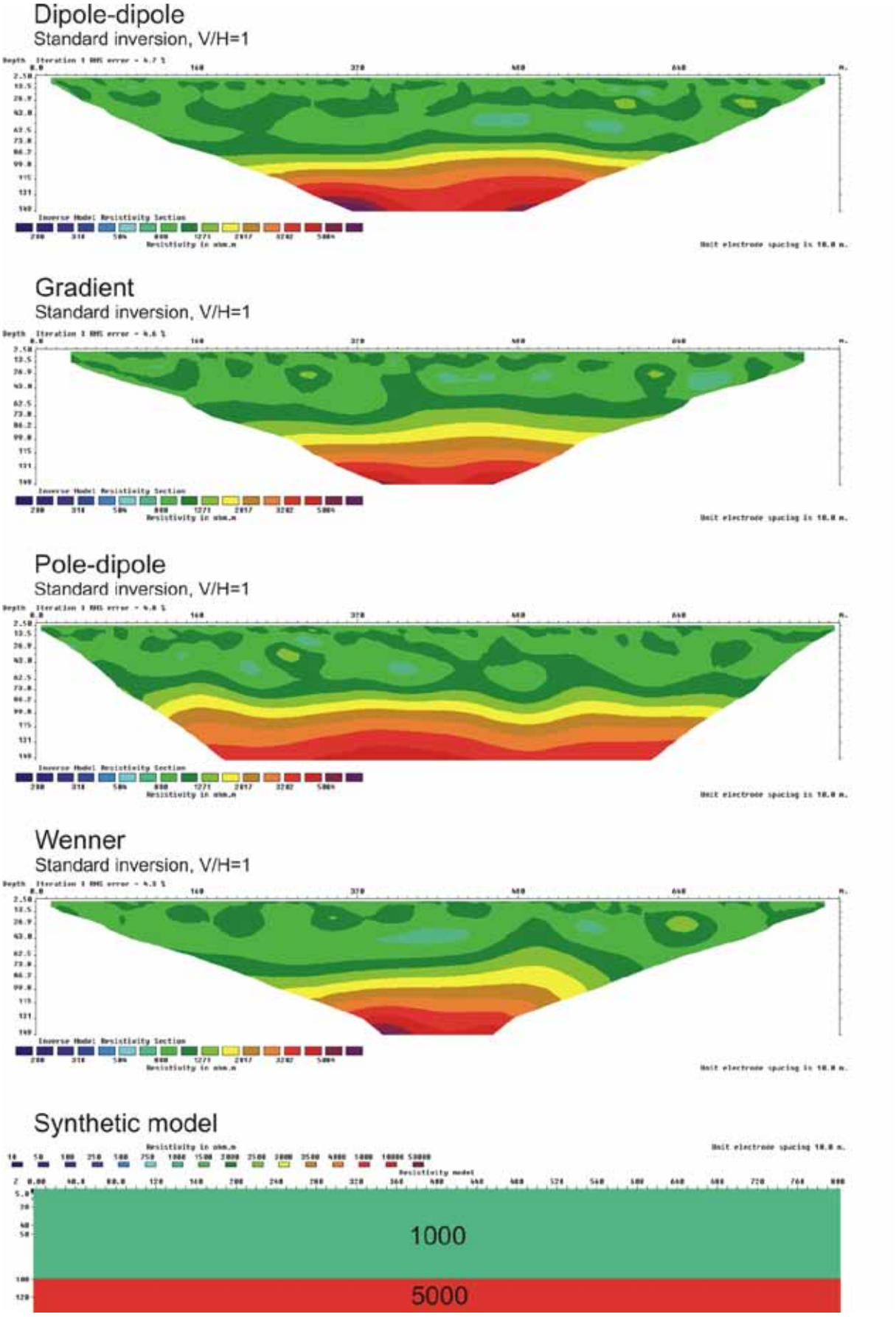

Figure 3.6.76: 2-layer model (1000 ohmm over 5000 ohmm), V/H=1

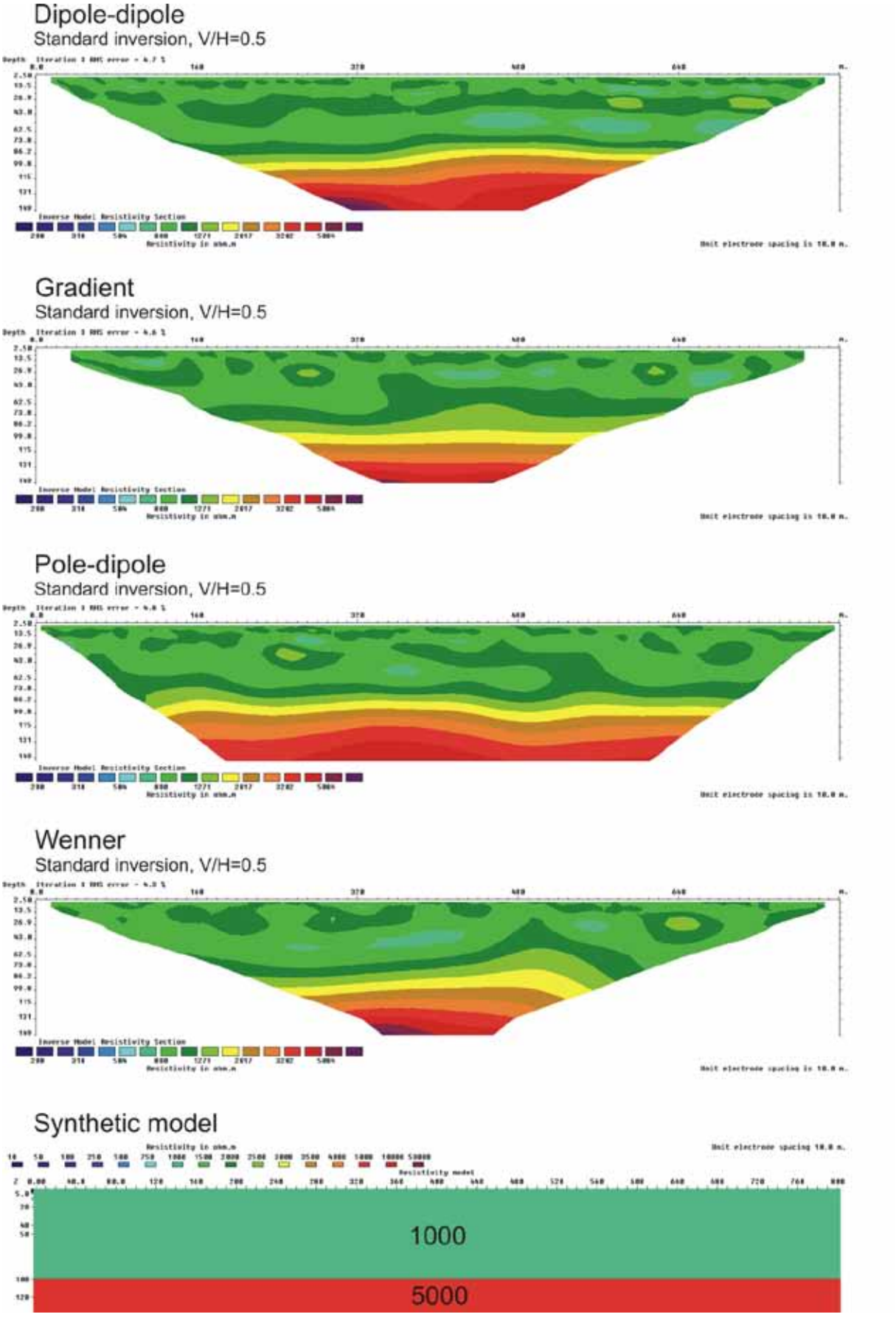

Figure 3.6.77: 2-layer model (1000 ohmm over 5000 ohmm), V/H=0.5

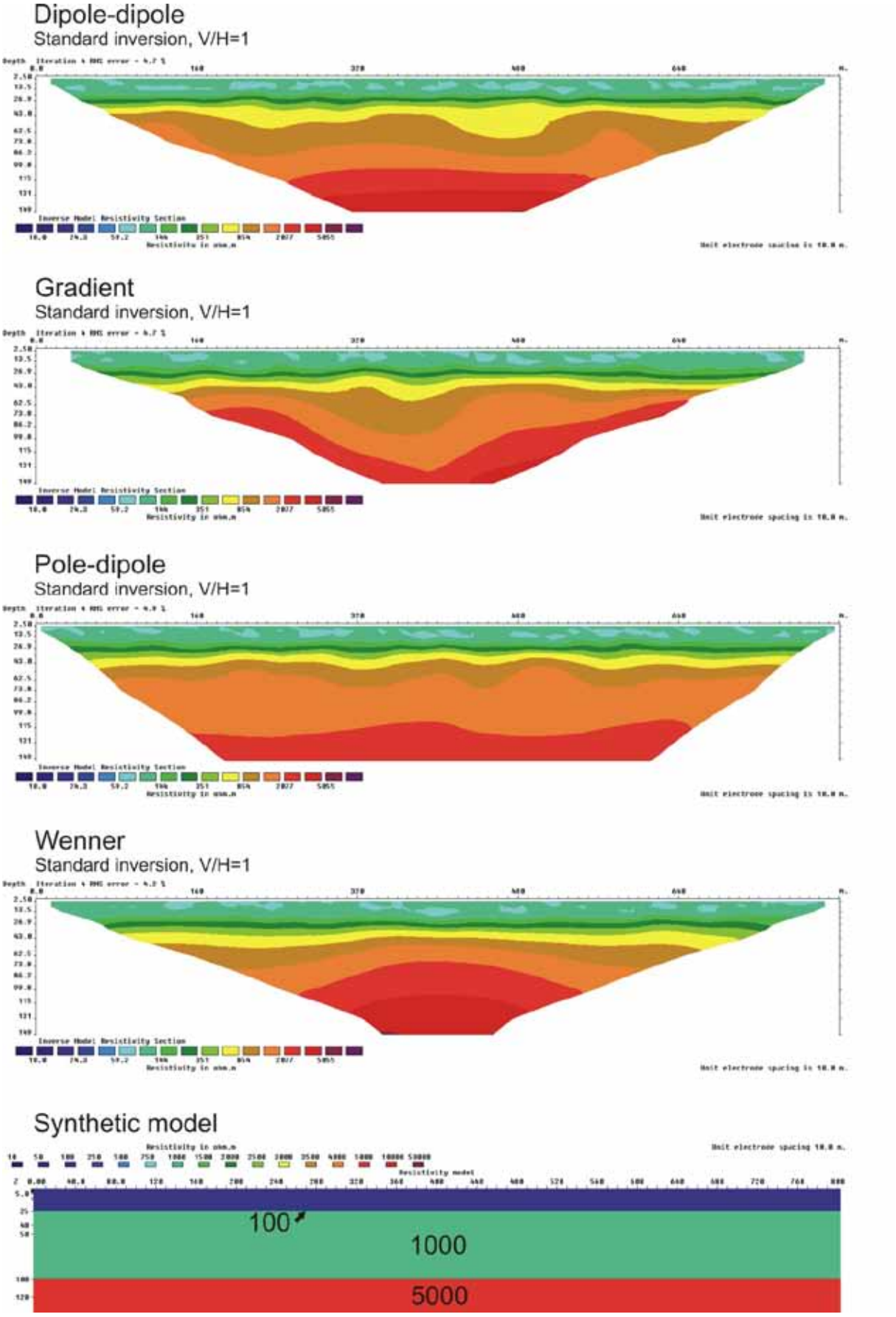

Figure 3.6.78: 3-layer model (100 ohmm, 1000 ohmm, 5000 ohmm), V/H=1

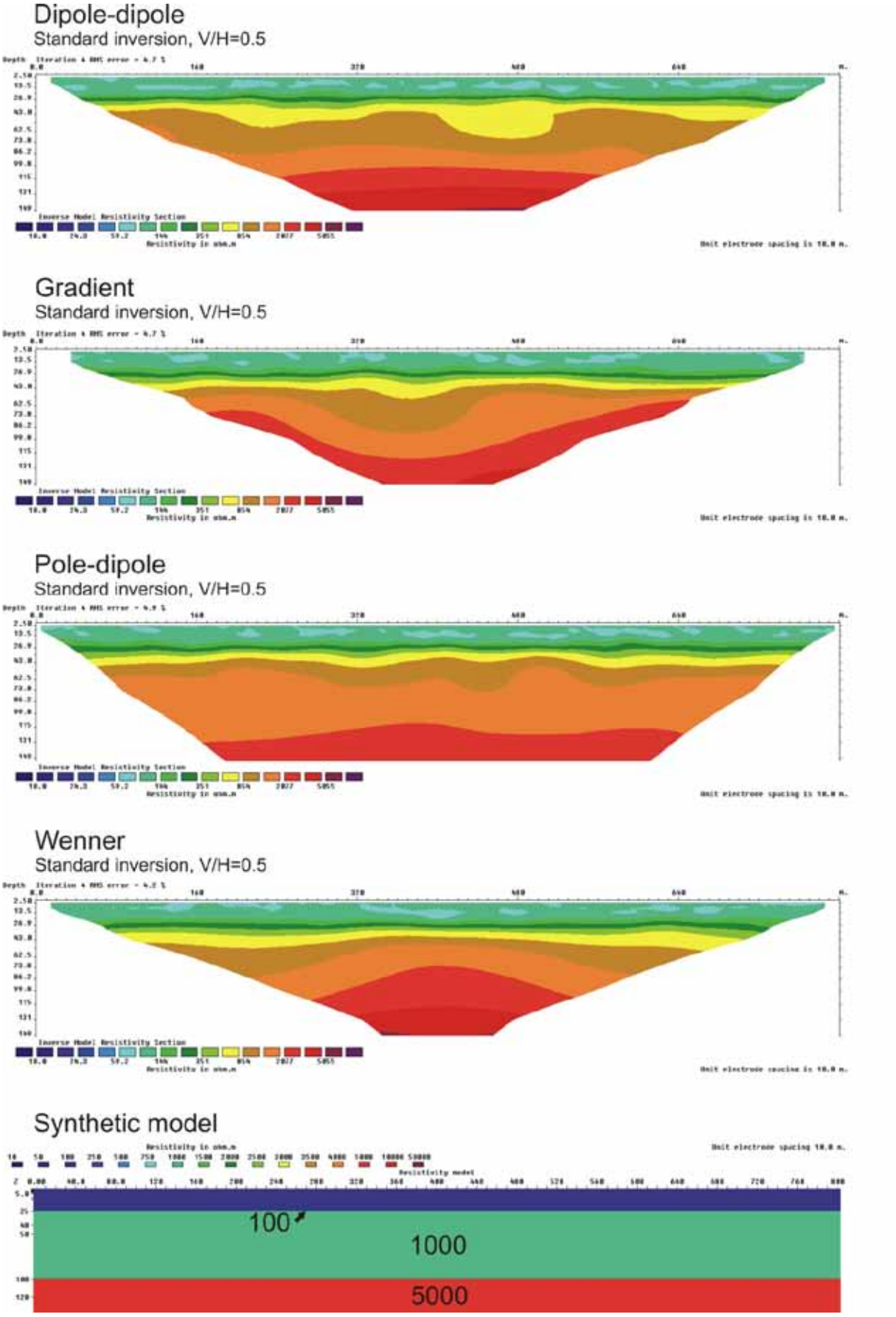

Figure 3.6.79: 3-layer model (100 ohmm, 1000 ohmm, 5000 ohmm), V/H=0.5

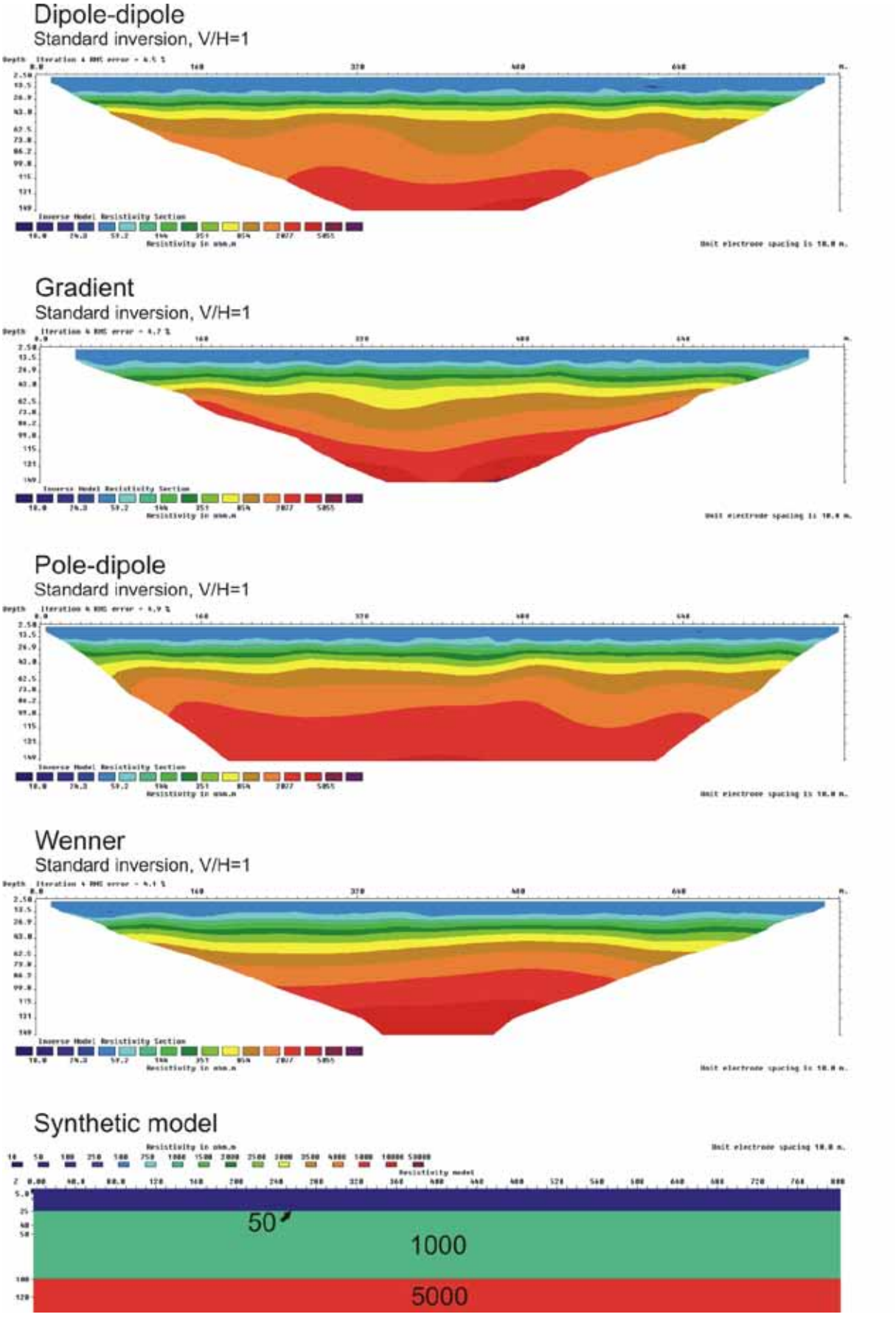

Figure 3.6.80: 3-layer model (50 ohmm, 1000 ohmm, 5000 ohmm), V/H=1

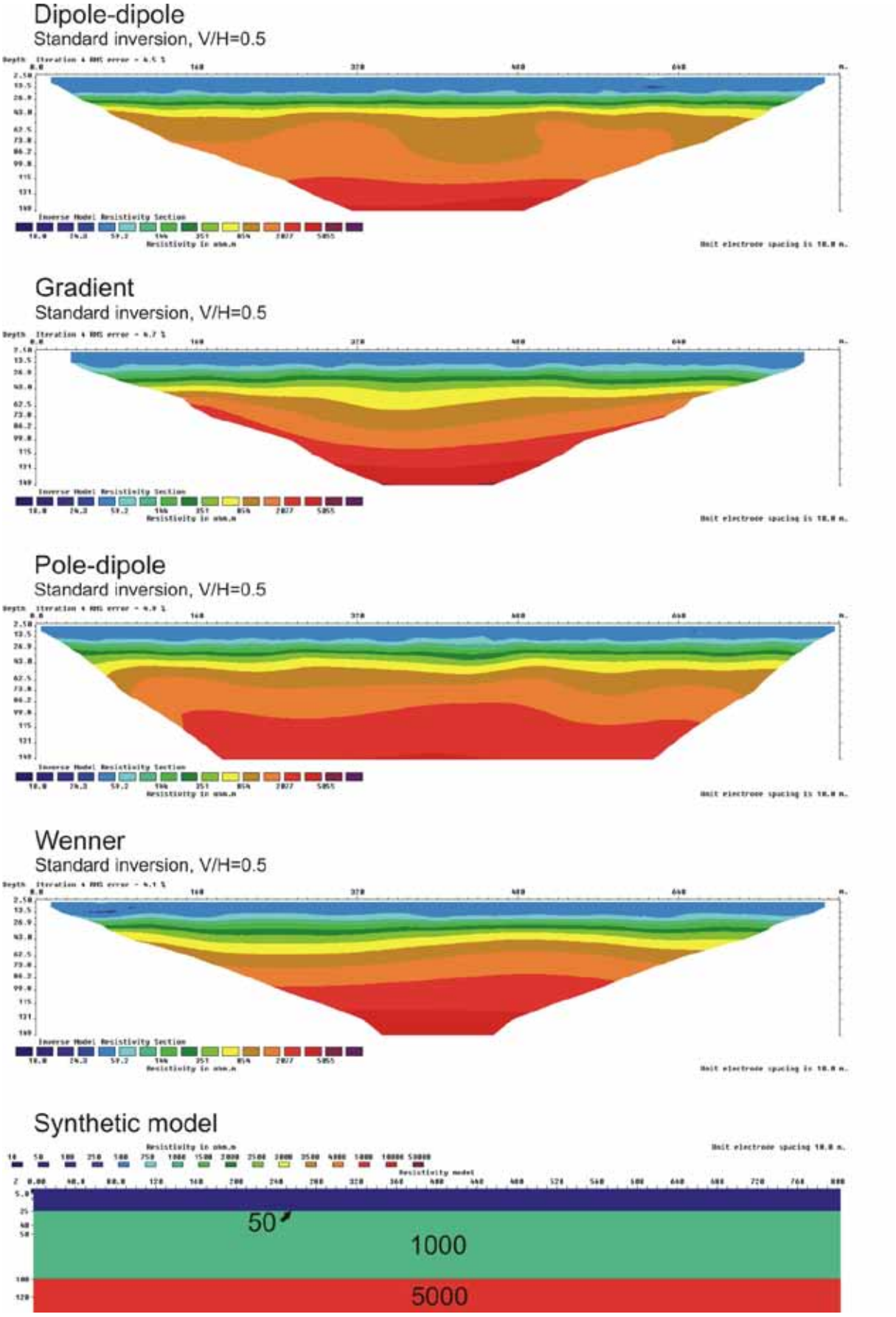

Figure 3.6.81: 3-layer model (50 ohmm, 1000 ohmm, 5000 ohmm), V/H=0.5

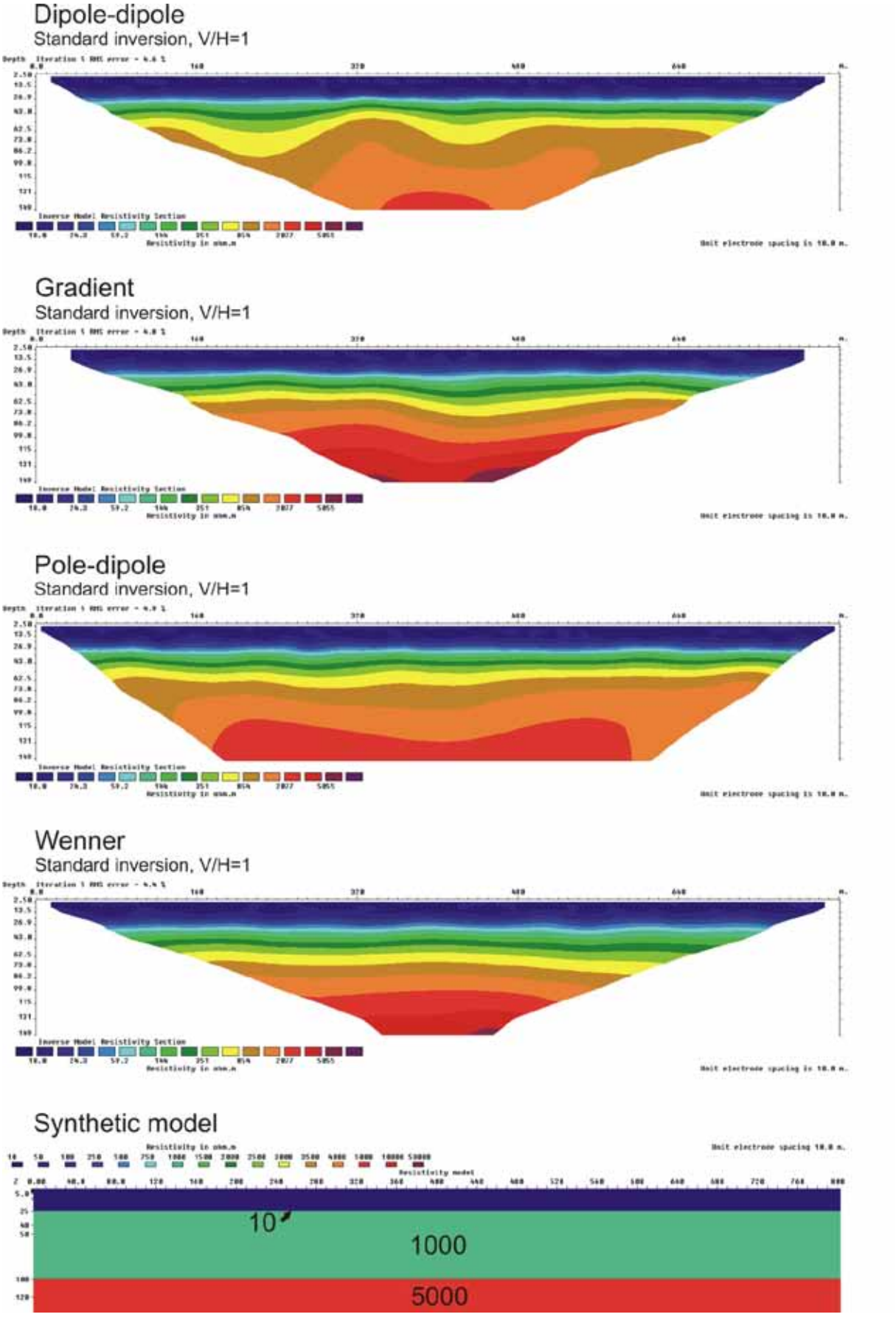

Figure 3.6.82: 3-layer model (10 ohmm, 1000 ohmm, 5000 ohmm), V/H=1

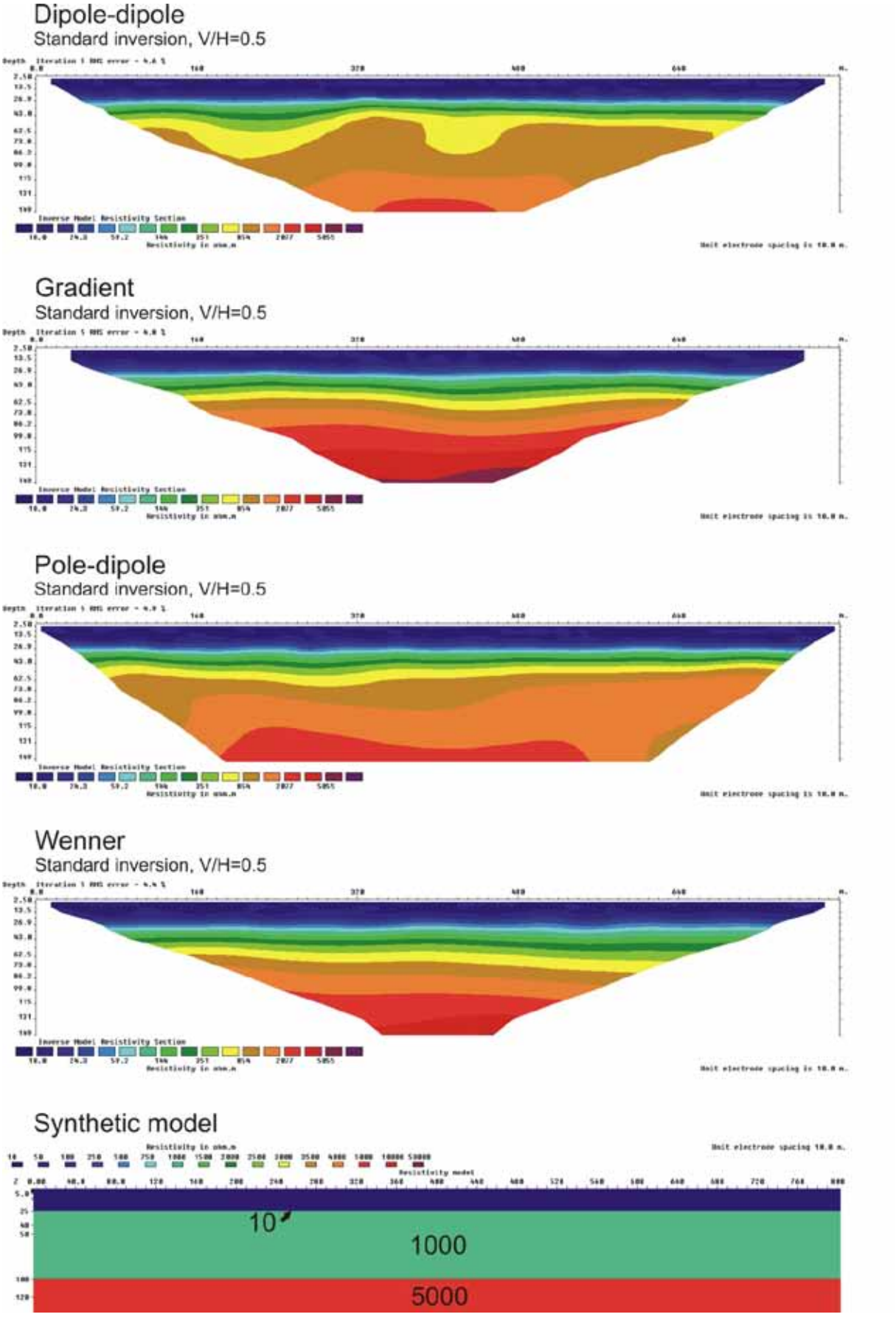

Figure 3.6.83: 3-layer model (10 ohmm, 1000 ohmm, 5000 ohmm), V/H=0.5

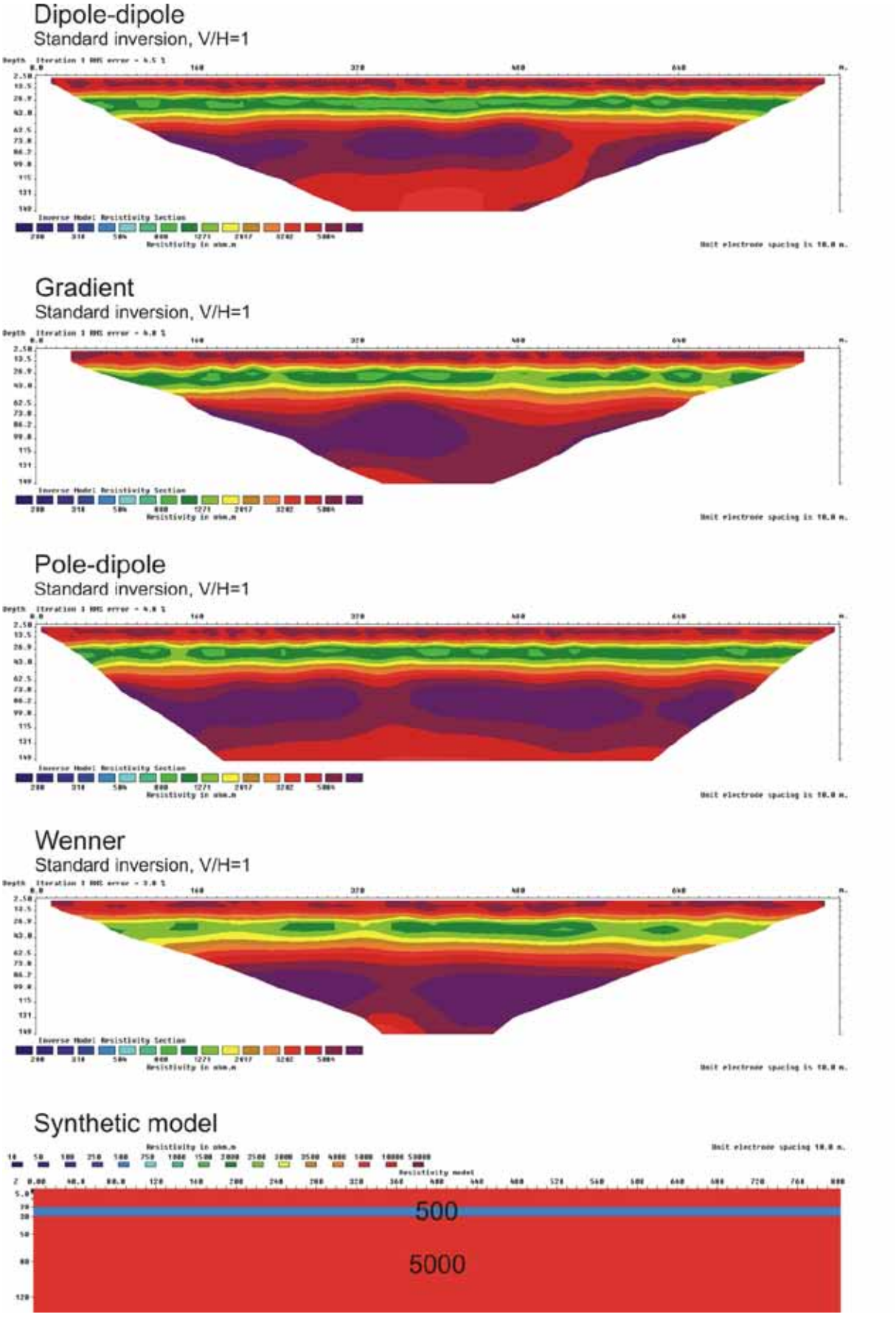

Figure 3.6.84: 10 m zone (500 ohmm) at a depth of 20m, V/H=1

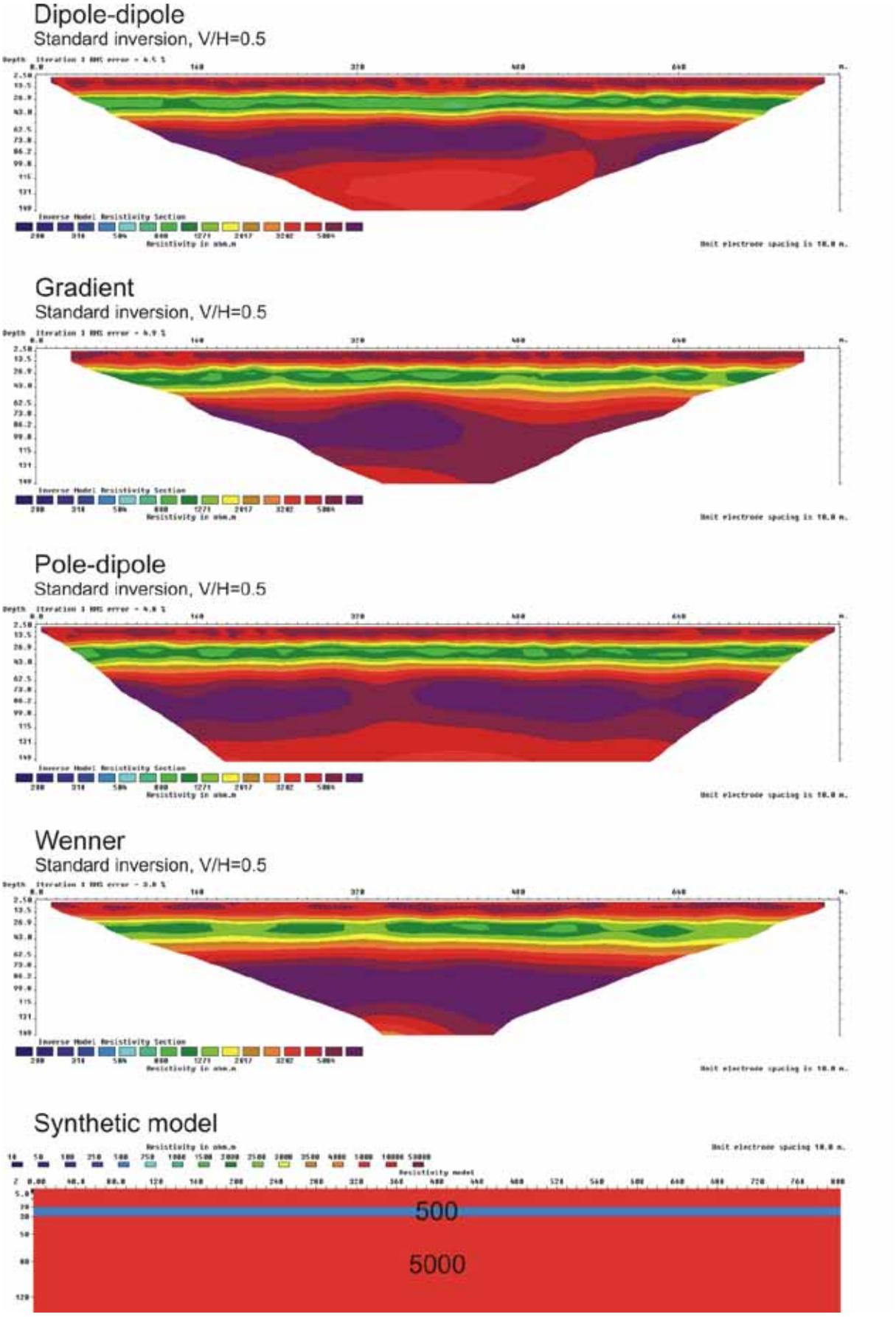

Figure 3.6.85: 10 m zone (500 ohmm) at a depth of 20m, V/H=0.5

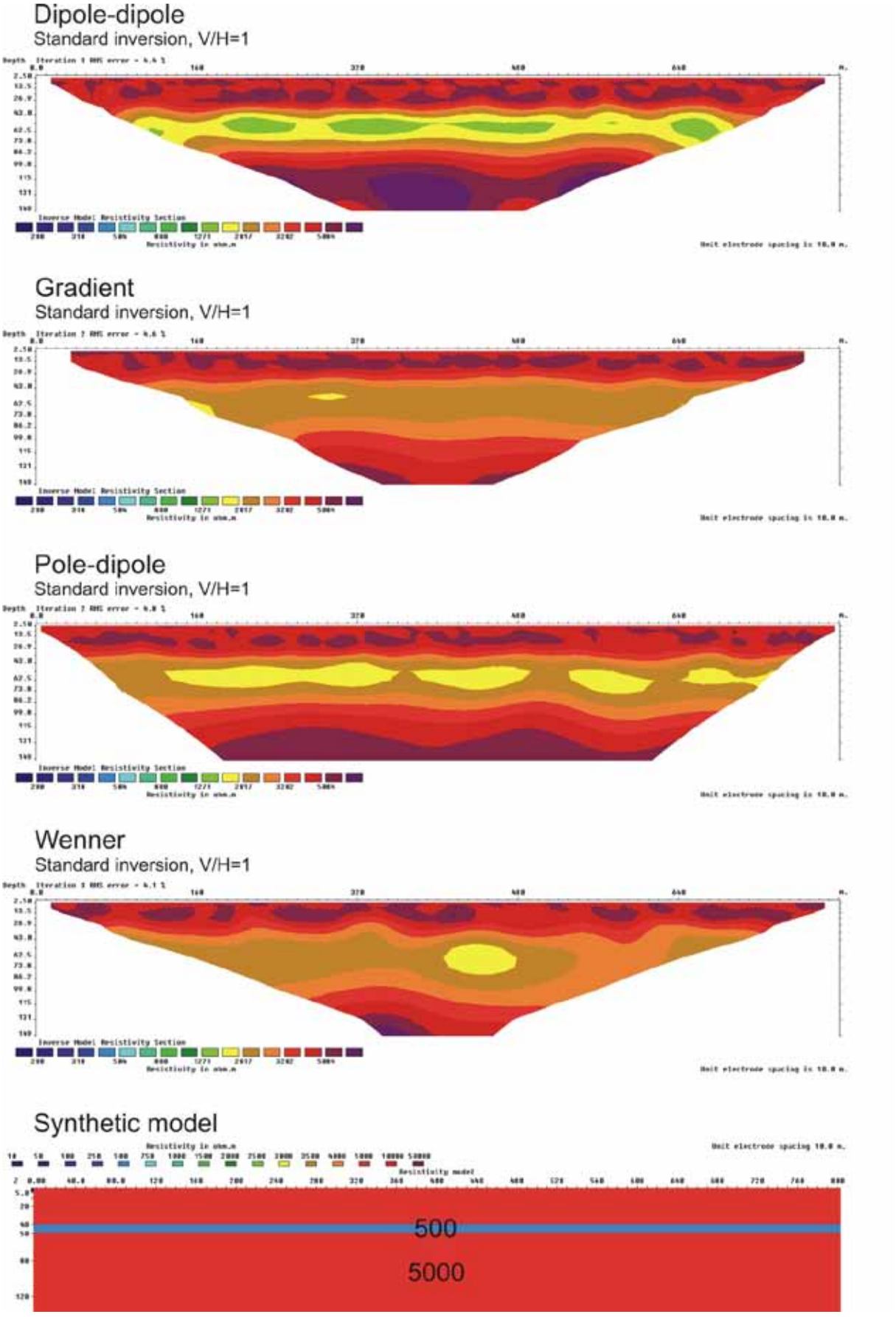

Figure 3.6.86: 10 m zone (500 ohmm) at a depth of 40m, V/H=1

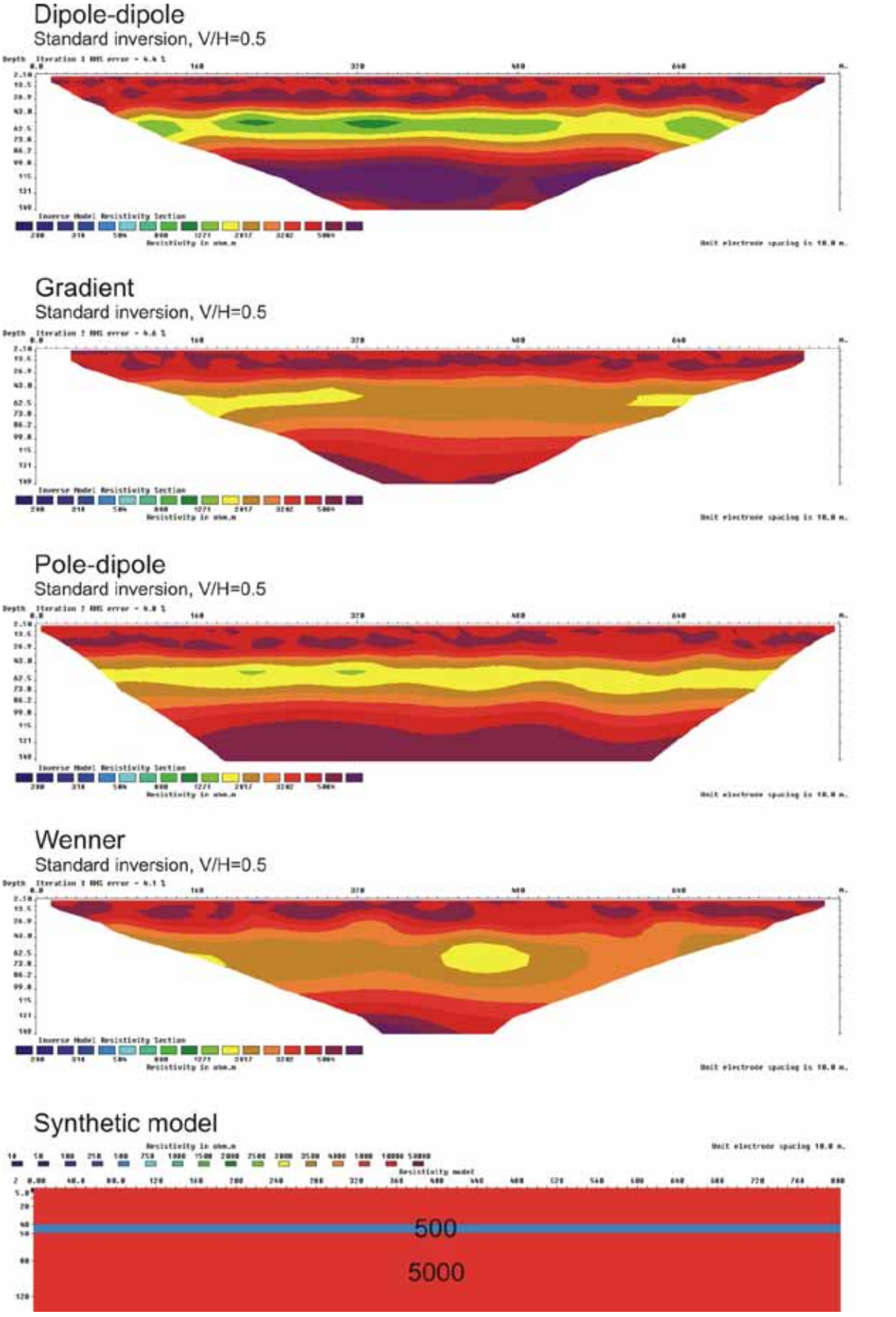

Figure 3.6.87: 10 m zone (500 ohmm) at a depth of 40m, V/H=0.5

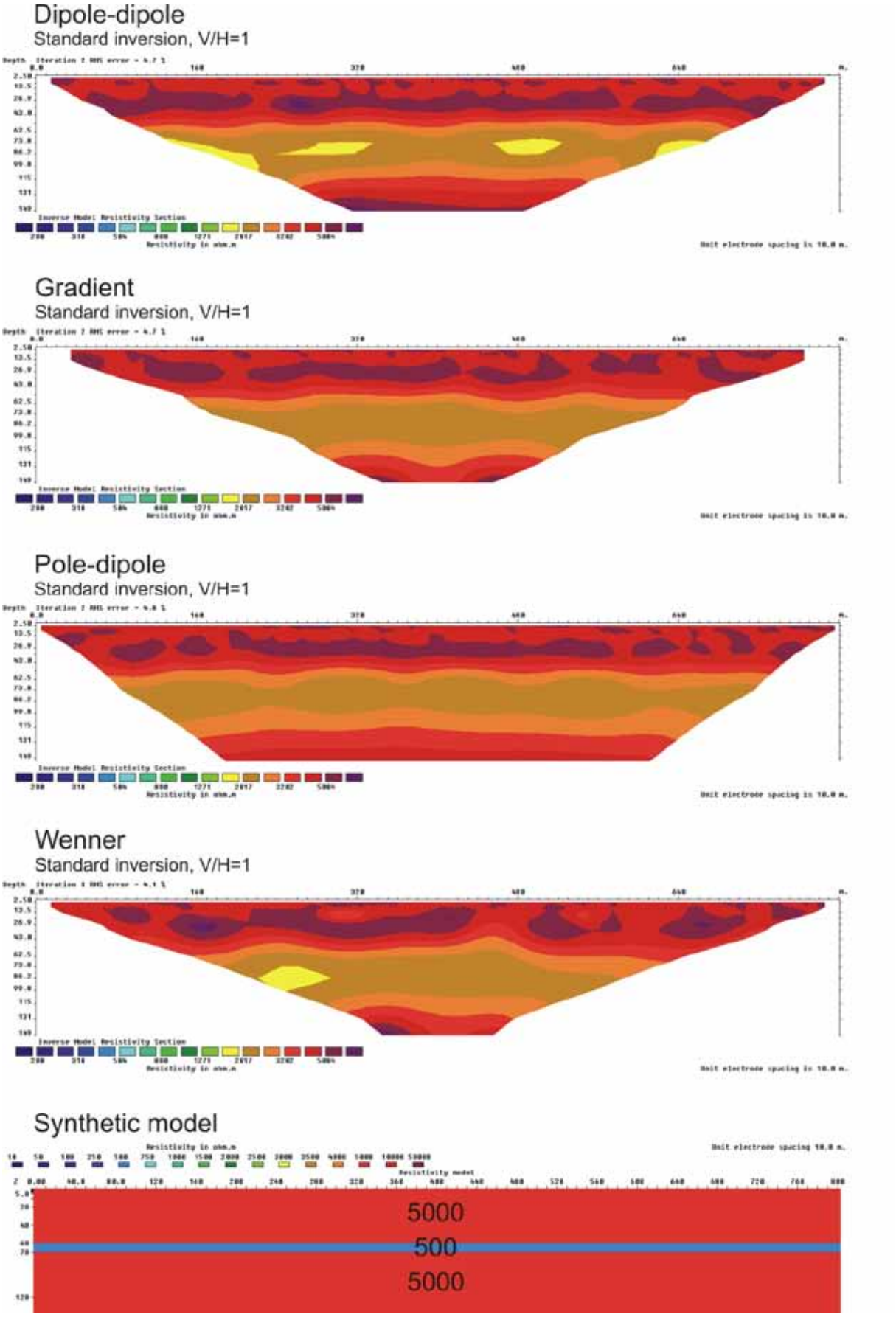

Figure 3.6.88: 10 m zone (500 ohmm) at a depth of 60m, V/H=1

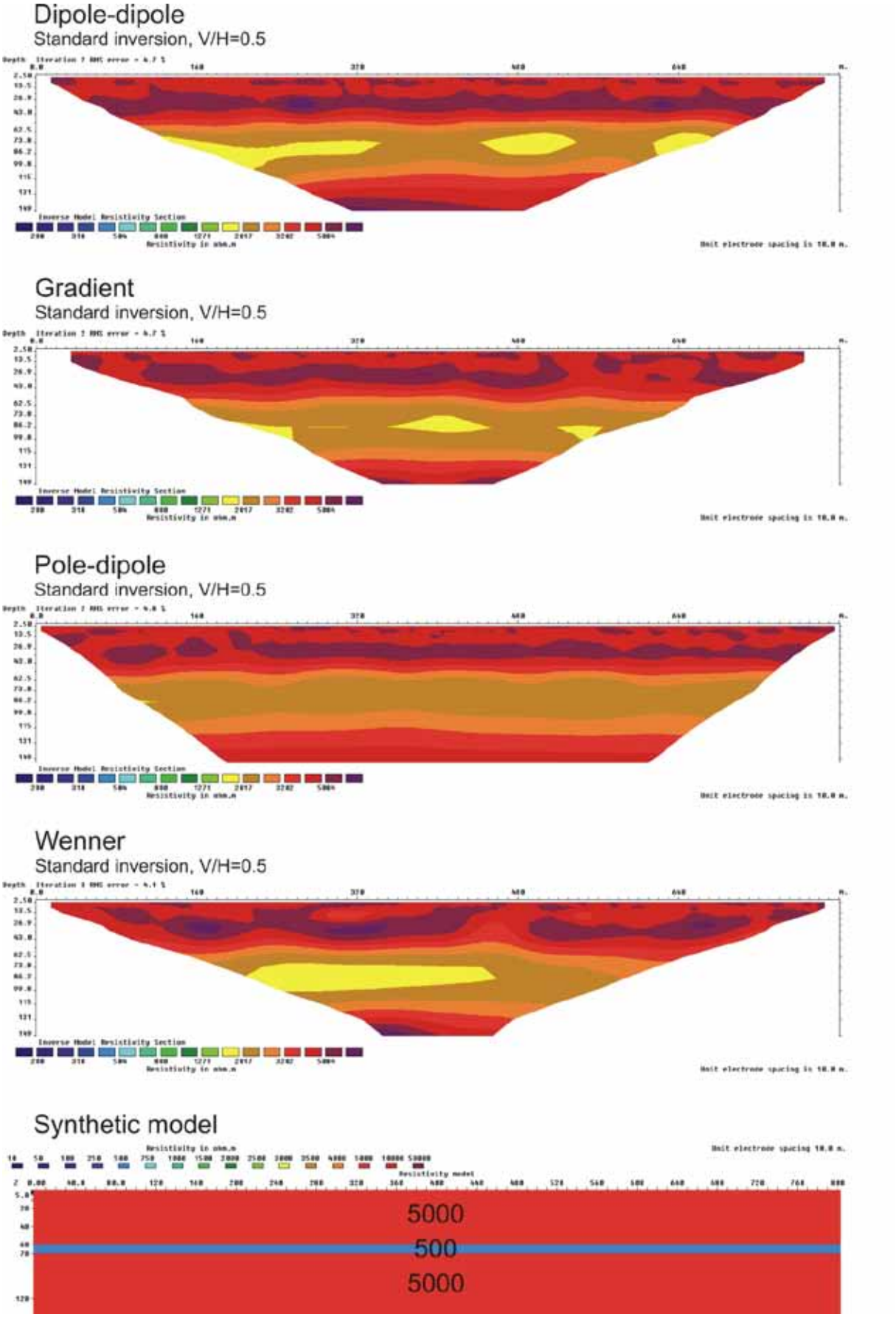

Figure 3.6.89: 10 m zone (500 ohmm) at a depth of 60m, V/H=0.5

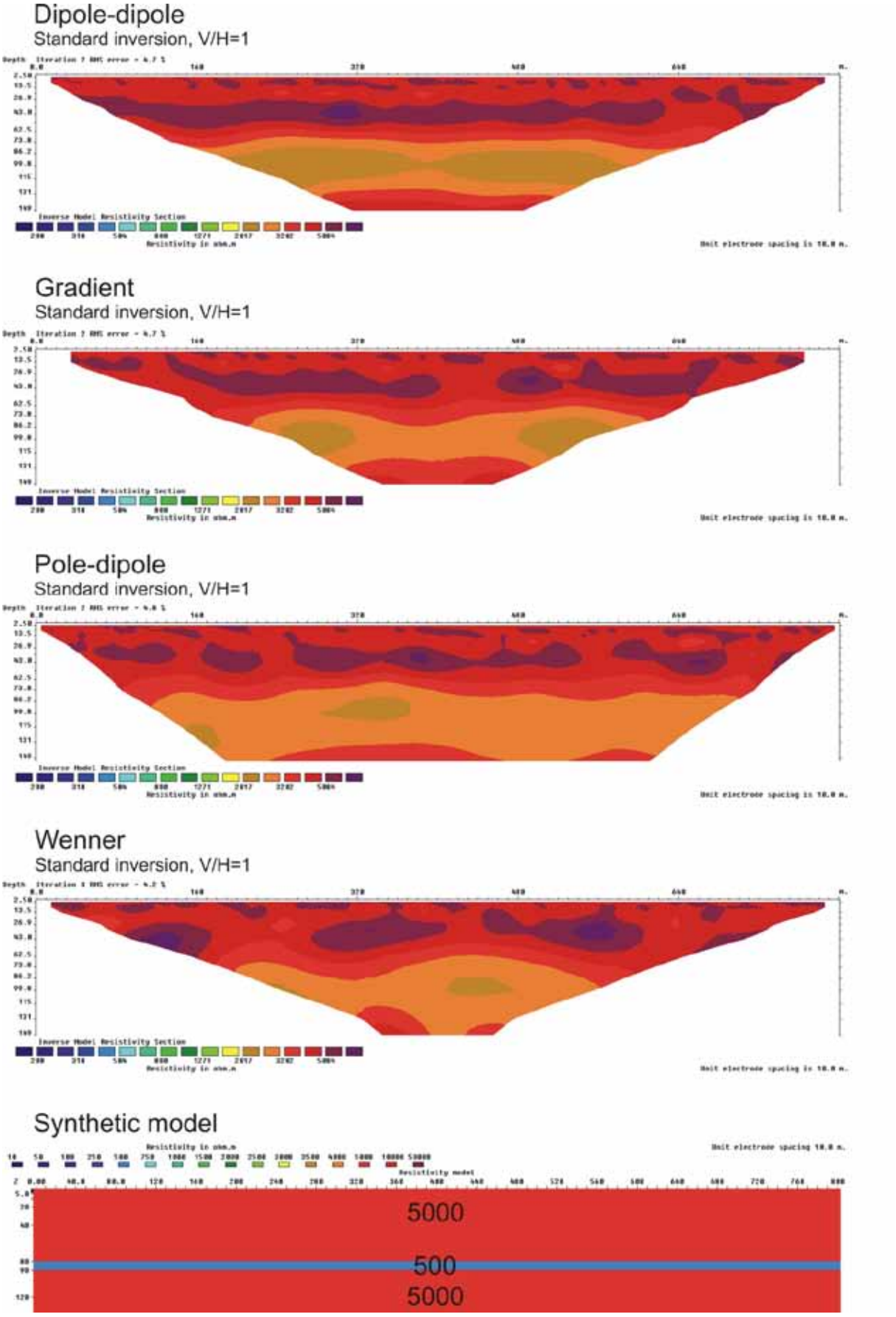

Figure 3.6.90: 10 m zone (500 ohmm) at a depth of 80m, V/H=1

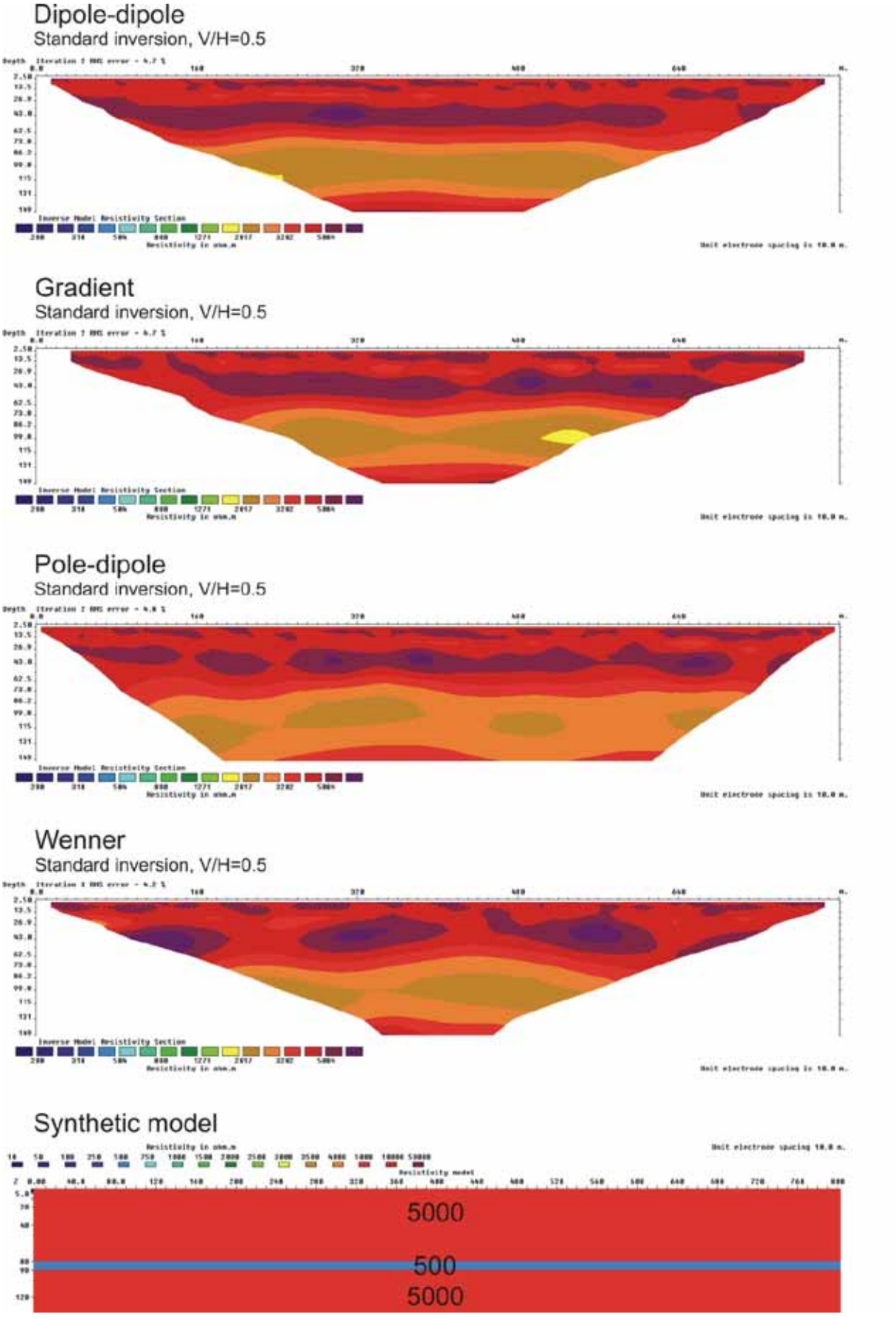

Figure 3.6.91: 10 m zone (500 ohmm) at a depth of 80m, V/H=0.5

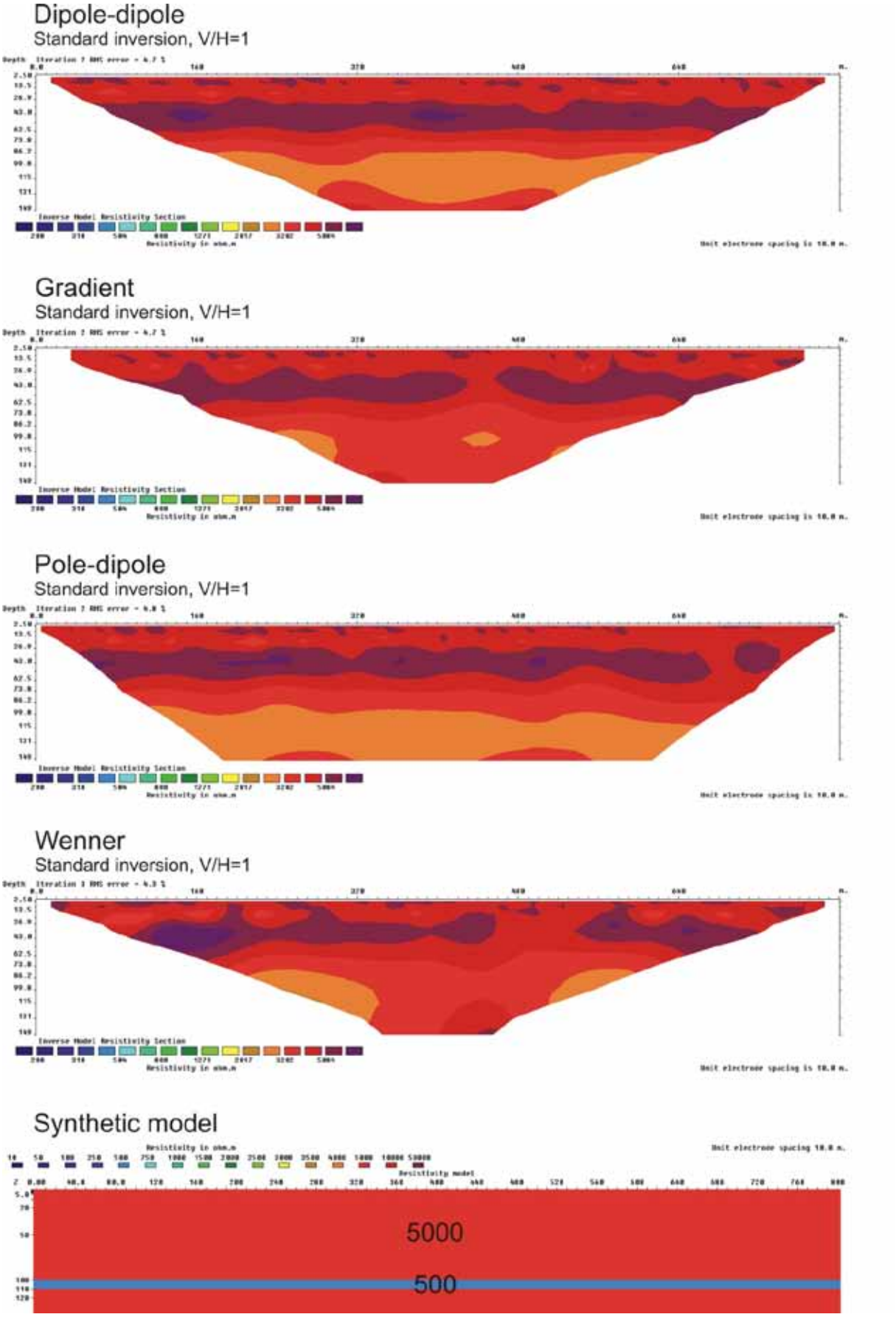

Figure 3.6.92: 10 m zone (500 ohmm) at a depth of 100m, V/H=1

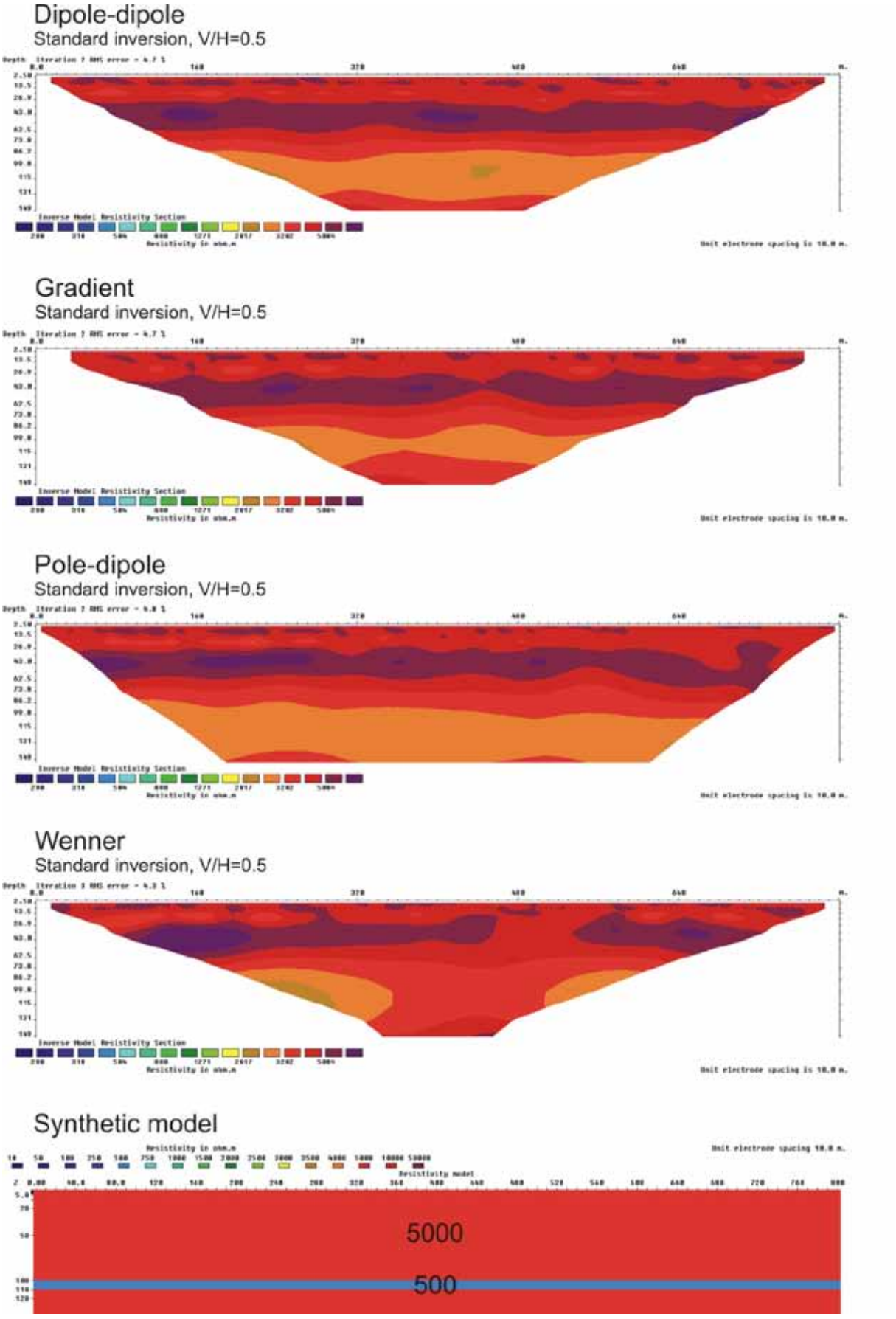

Figure 3.6.93: 10 m zone (500 ohmm) at a depth of 100m, V/H=0.5

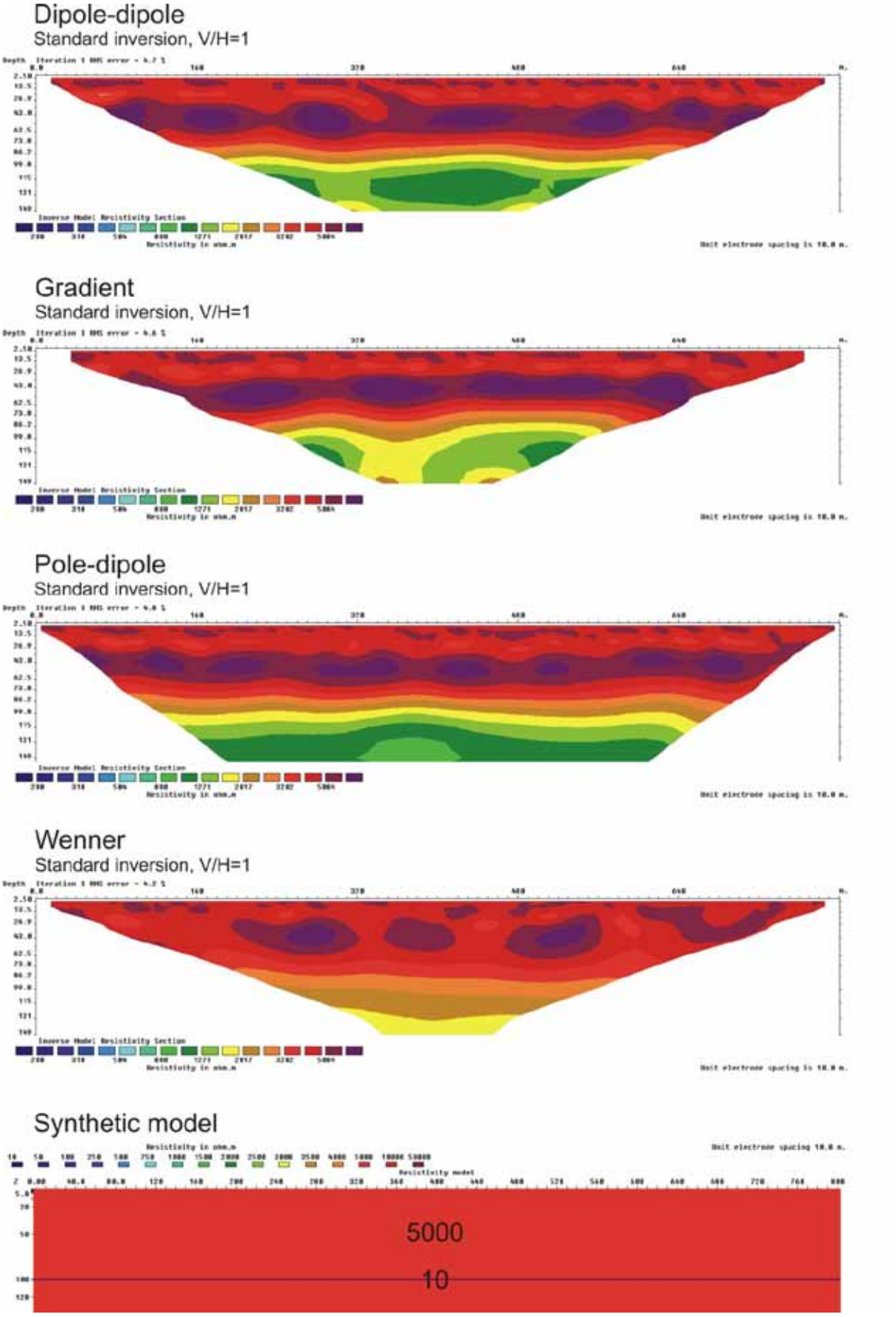

Figure 3.6.94: 1 m zone (10 ohmm) at a depth of 100m, V/H=1

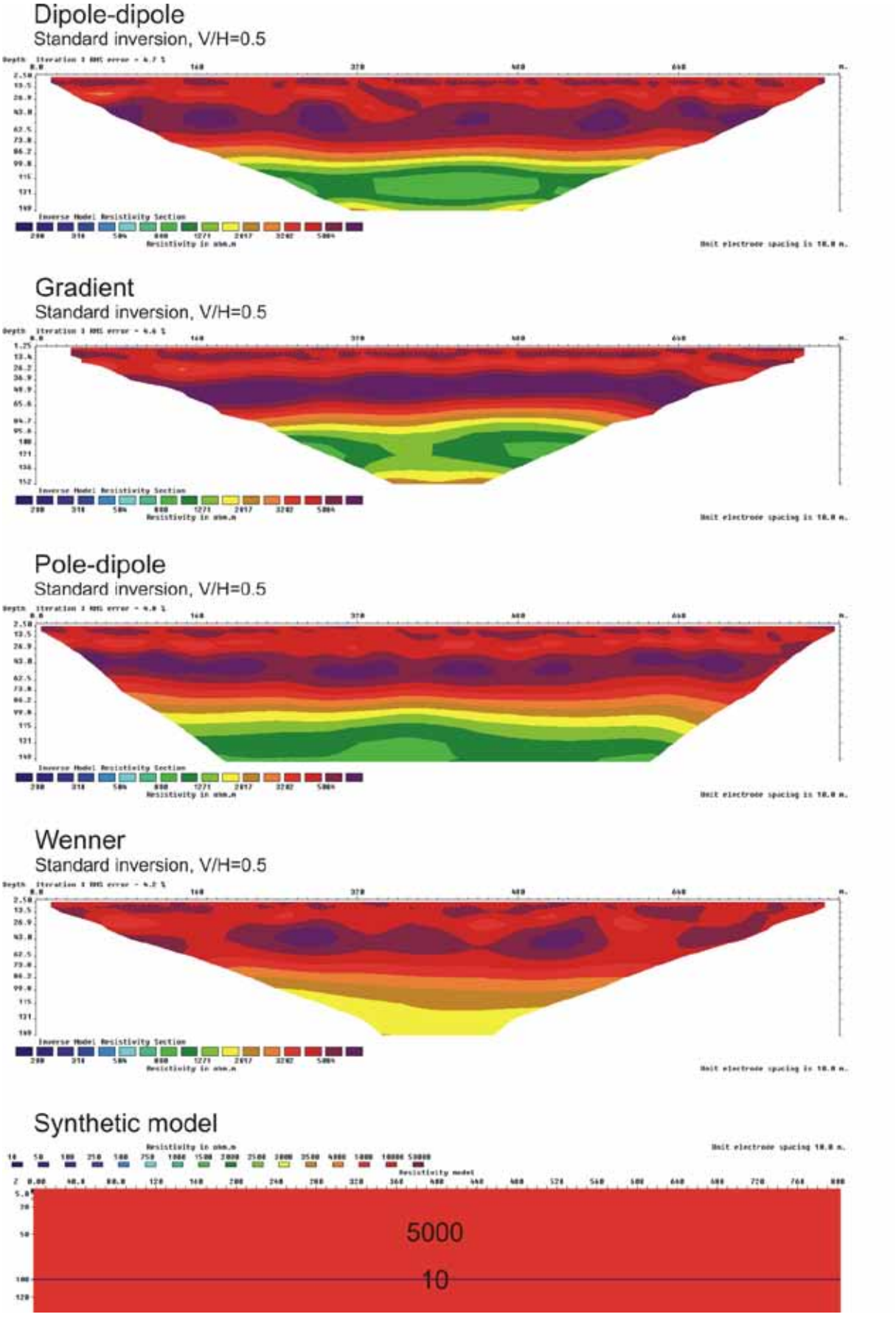

Figure 3.6.95: 1 m zone (10 ohmm) at a depth of 100m, V/H=0.5

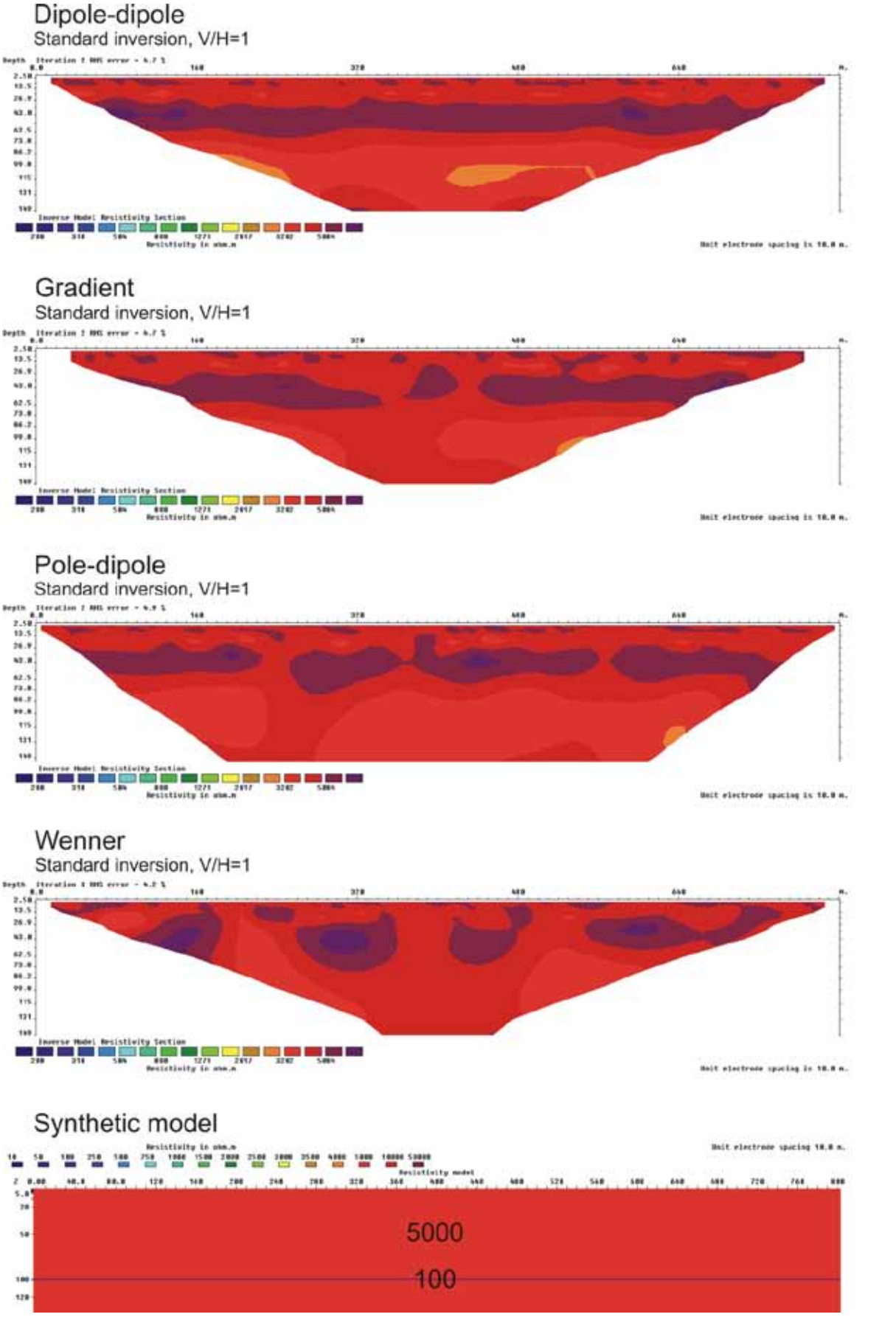

Figure 3.6.96: 1 m zone (100 ohmm) at a depth of 100m, V/H=1

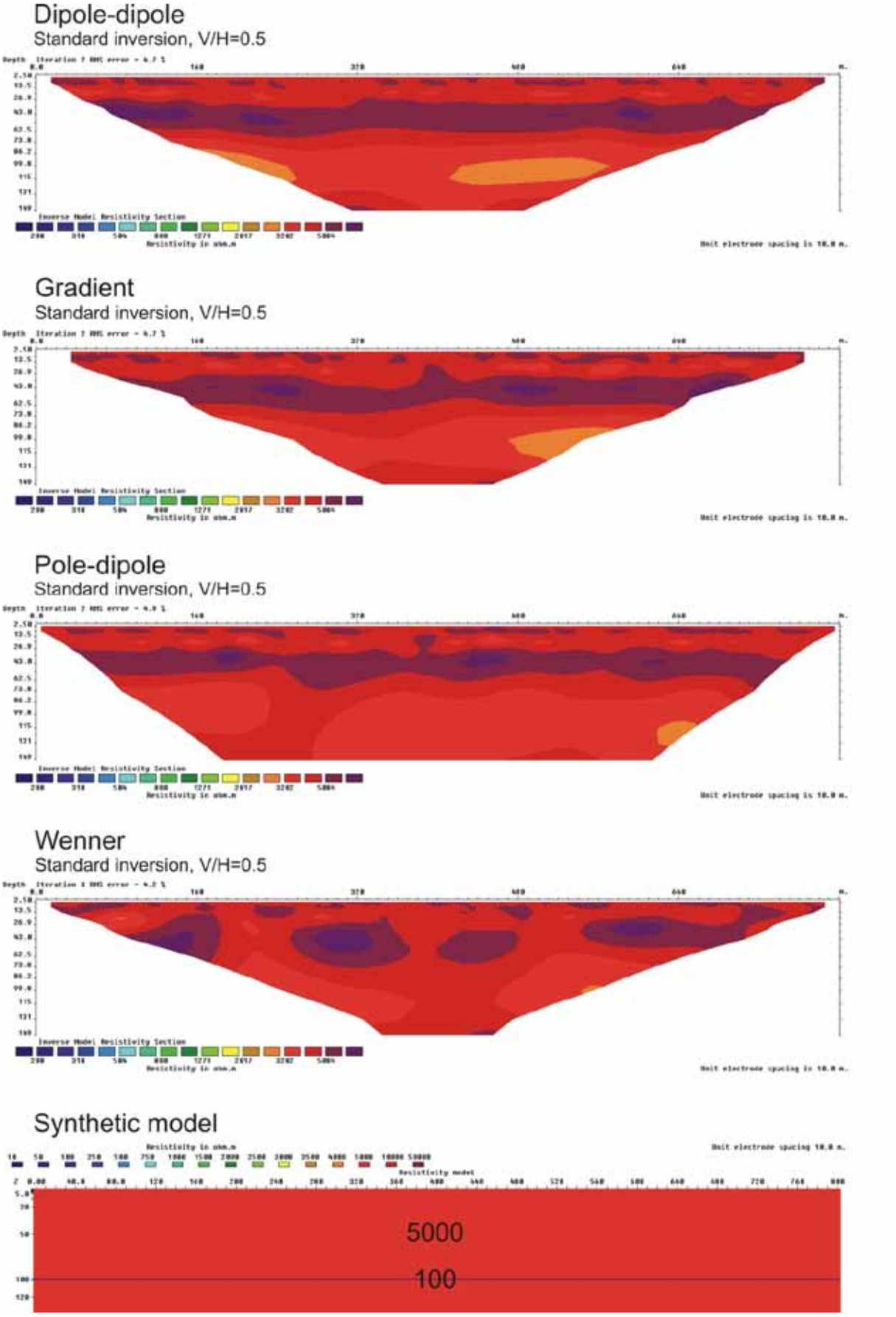

Figure 3.6.97: 1 m zone (100 ohmm) at a depth of 100m, V/H=0.5